Louisiana Transportation Research Center

Final Report 623

Analysis of Driven Pile Capacity within Pre-bored Soil

by

Shengli Chen, Ph.D.
Lin Li, Ph.D.

LSU

4101 Gourrier Avenue | Baton Rouge, Louisiana 70808
(225) 767-9131 | (225) 767-9108 fax | www.ltrc.lsu.edu

TECHNICAL REPORT STANDARD PAGE

1. Title and Subtitle
Analysis of Driven Pile Capacity within Pre-bored Soil

2. Author(s)
Shengli Chen, Ph.D. and Lin Li, Ph.D.

3. Performing Organization Name and Address
Department of Civil and Environmental Engineering
Louisiana State University
Baton Rouge, LA 70803

4. Sponsoring Agency Name and Address
Louisiana Department of Transportation and Development
P.O. Box 94245
Baton Rouge, LA 70804-9245

5. Report No.
FHWA/LA.17/623

6. Report Date
May 2020

7. Performing Organization Code
LTRC Project Number: 18-1GT
SIO Number: DOTLT1000208

8. Type of Report and Period Covered
Final Report
09/2017-08/2019

9. No. of Pages
144

10. Supplementary Notes
Conducted in Cooperation with the U.S. Department of Transportation, Federal Highway Administration

11. Distribution Statement
Unrestricted. This document is available through the National Technical Information Service, Springfield, VA 21161.

12. Key Words
Pre-bored pile; long-term shaft resistance; shaft resistance reduction factor; numerical modelling; practical design formulas

13. Abstract

In Louisiana and many other states in the U.S., pre-boring procedures are routine practice for large displacement piles driven through hard/stiff cohesive soils. At present, the analysis and design of pre-bored piles rely primarily on local experiences, since the effects of pre-boring on the driving force as well as on the setup and long-term shaft resistances within the pre-bored zone remain unclear. Due to the high cost and time involved with field instrumentation and testing on pre-bored piles, this numerical study is funded by the Louisiana Department of Transportation and Development (DOTD) as a first step to explore the impacts of pre-bore size on the drivability and long-term shaft resistance reduction of piles.

In this research, researchers developed simplified yet realistic numerical model, which considers a thin horizontal soil disc sufficiently far from the ground surface and the pile base using the ABAQUS package to investigate the effects of pre-boring on the pile behaviour over different installation and loading stages. Leveraging on the finite element model developed, the long-term shaft resistance reduction factor curves have been generated for typical Louisiana soil strata to provide guidelines for a

better design and construction of pre-bored piles in Louisiana. On the basis of the numerical calculation results, a preliminary protocol, including the site selection, soil properties investigation, and the testing procedure and data collection, is subsequently proposed for future instrumented pile field tests of pre-bored piles in Louisiana. Finally, to facilitate the design of pre-bored piles, a set of practical formulas are developed to predict/evaluate conveniently the driving force, setup and long-term shaft resistances of pre-bored piles. The current research work not only reveals the shaft resistance reduction mechanism of pre-bored piles, but also provides a simple and reliable approach to evaluate the driving force and shaft resistance of pre-bored piles, which will be helpful and beneficial for geotechnical and construction engineers involved with the design and installation of the pre-bored pile foundations in Louisiana.

Project Review Committee

Each research project will have an advisory committee appointed by the LTRC Director. The Project Review Committee is responsible for assisting the LTRC Administrator or Manager in the development of acceptable research problem statements, requests for proposals, review of research proposals, oversight of approved research projects, and implementation of findings.

LTRC appreciates the dedication of the following Project Review Committee Members in guiding this research study to fruition.

LTRC Administrator/Manager

Zhongjie "Doc" Zhang, Ph.D., P.E.
Pavement and Geotechnical Research Manager

Members

James Melton
Jesse Rauser
Chris Nickel
Jeffrey Lambert
Francisco Gudiel
Arturo Aguirre
Glynn Gautreau

Directorate Implementation Sponsor

Christopher P. Knotts, P.E.
DOTD Chief Engineer

Analysis of Driven Pile Capacity within Pre-bored Soil

By
Shengli Chen, Ph.D.
Lin Li, Ph.D.

Department of Civil and Environmental Engineering
Louisiana State University
Baton Rouge, LA 70803

LTRC Project No. 18-1GT
SIO No. DOTLT1000208

conducted for
Louisiana Department of Transportation and Development
Louisiana Transportation Research Center

May 2020

Abstract

In Louisiana and many other states in the U.S., pre-boring procedures are routine practice for large displacement piles driven through hard/stiff cohesive soils. At present, the analysis and design of pre-bored piles rely primarily on local experiences, since the effects of pre-boring on the driving force as well as on the setup and long-term shaft resistances within the pre-bored zone remain unclear. Due to the high cost and time involved with field instrumentation and testing on pre-bored piles, this numerical study is funded by the Louisiana Department of Transportation and Development (DOTD) as a first step to explore the impacts of pre-bore size on the drivability and long-term shaft resistance reduction of piles. The major contributions of this research work contain the following four aspects:

- A thorough literature review has been conducted on pre-bored piles to investigate the state of the art of design and analysis of pre-bored piles. The literature review, which involves the laboratory and field pile tests, the theoretical studies, and the numerical analyses of previous and on-going nationwide and worldwide research projects, summarizes the installation effects, setup and long-term load carrying capacity of both full displacement piles and pre-bored piles particularly in clayey soils. The literature review shows that currently no comprehensive research, either theoretical study or instrumented field testing, has been conducted to properly evaluate the capacity reduction of pre-bored piles (EOID, long-term, and setup) with different pilot hole sizes, thus indicating/emphasizing the significance of the present research.
- A finite element model (FEM) that integrates the entire process from pile installation through subsequent consolidation to pile loading is developed using the ABAQUS package to investigate the effects of pre-boring on the pile behaviour over different installation and loading stages. The FEM model basically sticks to a (representative) thin horizontal soil disc sufficiently far from the ground surface and the pile base, which simplifies the pre-bored pile problem, in each of the stages involved, to a one-dimensional situation yet still well captures the overall two-dimensional feature of the problem considered. The numerical model has been validated through comparisons with the analytical solution developed by Chen and Abousleiman [1] for the undrained cylindrical cavity expansion problem, i.e., corresponding to the radial expansion of the soil mass induced by the pile installation. On leverage of the developed numerical

model, the changes in the stress state of the surrounding soils due to the pile installation and loading are thoroughly investigated so as to reveal the long-term shaft resistance reduction of the pre-bored piles.

- The impacts of the size of pre-drilled hole on the long-term shaft resistance reduction of pre-bored piles in three representative Louisiana soils are explored by using the developed finite element model. Long-term shaft resistance factor curves and shaft resistance reduction factor curves are generated for these typical soil strata, which may provide guidelines for better design and construction of pre-bored piles in Louisiana. The reduction factor curve potentially can be implemented into the current pile analysis and design software, through directly lowering the α or β coefficient involved to determine the reduced pile capacity. On the basis of the numerical calculation results, a preliminary protocol, including the site selection, soil properties investigation and the testing procedure and data collection, is proposed for future instrumented pile field tests of pre-bored piles in Louisiana.
- Taking advantage of some essential findings from the numerical study, a set of simplified formulas have been developed for the practical purpose to predict/evaluate the driving force, setup, and long-term shaft resistances of pre-bored piles. The proposed practical formulas take proper account of the size of pre-drilled holes, the installation effects, and the soil consolidation, as well as the shearing of the soil around the pile, and hence capable of yielding satisfactory predictions when compared with the more comprehensive finite element numerical results. Extensive parametric studies are conducted to investigate the impacts of pre-drilled hole size, the overconsolidation ratio and the earth pressure coefficient at rest on the driving force, the setup and long-term shaft resistances reduction of pre-drilled piles. These formulas provide a relatively simple yet reliable approach to evaluate the driving force and shaft resistance of pre-bored piles, which will be helpful and beneficial for geotechnical and construction engineers involved with the design and installation of the pre-bored pile foundations in Louisiana.

Acknowledgments

The financial support of this research was provided by the Louisiana Department of Transportation and Development (DOTD) and the Louisiana Transportation Research Center (LTRC) under state project No. DOTLT1000208 and LTRC research project No. 18-1GT.

The authors would like to acknowledge the valuable comments provided by the following Project Review Committee members: Matt Melton (Chair); Doc Zhang (Project manager); Chris Nickel; Jeff Lambert; Jesse Rauser; Francisco Gudiel; Arturo Aguirre; and Glynn Gautreau. Especially, the great help, guidance, and administrative support from Dr. Doc Zhang, Pavement & Geotechnical Research Administrator of LTRC, are much appreciated. The authors are also grateful to Matt Melton and Michael Boudreaux for their constructive comments and suggestions made on this final report.

Implementation Statement

This research project consists of a comprehensive numerical study and analytical analysis to investigate the shaft resistance reduction mechanism of pre-bored piles. The implementation items of this study can be summarized as follows:

- The shaft resistance factor curves and shaft resistance factor reduction curves generated for the typical soil strata in Louisiana, after careful calibrations, can be readily implemented into the current pile analysis/design software to determine the reduced capacity of pre-bored piles installed in Louisiana.
- The simplified design formulas are developed for the practical purpose of predicting/evaluating the driving force, setup and long-term shaft resistances of pre-bored piles under different geological conditions, may be recommended to be incorporated into the Louisiana Standard Specifications for Roads and Bridges (LSSRB) as a first approximation to more rationally analyze/design the pre-bored piles in Louisiana.
- The LSSRB does not provide clear guidance on the diameter of square concrete piles. This ambiguity has caused confusion over whether the side dimension or cross dimension of the pile should be used when determining the allowable pre-boring diameter. The report presents a clear method of determining an equivalent circular diameter, D_{eq}, of a square concrete pile based on the equivalent volume principle. This definition should be adopted in practice for defining the diameter of a square pile and could be included in the next edition of the LSSRB.
- The study indicates that when the diameter of the prebored hole is less than 50% of the pile diameter the effect on the long term side resistance is negligible. Future editions of the LSSRB could allow for pre-boring up to 50% of the pile diameter without approval of the Engineer of Record.
- The study indicates that since the expansion and displacement of the soil due to pile driving reduces the side resistance to residual strength, the side resistance component of driving resistance is independent of prebored hole size. This suggests that the common practice of reducing the unit side resistance in the prebored zone when performing a GRLWEAP analysis to assess drivability is not necessary. Since the reduction of side resistance in the prebored zone should

be the same as no pre-boring, the same loss/gain factors can be used for both cases.

- Methods of calculating a driving force reduction factor, $R_{\mathrm{d,pre}}$ and long-term shaft resistance reduction factor, R_{qs} were presented. These methods can be used to optimize prebored hole size to provide the necessary reduction of driving resistance to install the pile while minimizing the effect on the long-term resistance. This optimization of pre-boring will allow for contractors to select the appropriate equipment to install the pile in the most efficient manner while still meeting the required nominal resistance. This in turn should benefit DOTD by reducing construction claims due to issues with pile installation.

Table of Contents

List of Tables

List of Figures

Introduction

In Louisiana and many other states in the U.S., pre-boring procedures are routine practice for large displacement piles driven through hard/stiff cohesive soils. By pre-boring a pilot hole, the end resistance and side friction within the pre-bored zone are reduced, thus aiding pile driving installation. However, pre-boring will in turn reduce the squeezing effects and the excess pore water pressures generated by pile installation, the effects of which will propagate to the subsequent consolidation and loading phases and hence impact the setup and long-term shaft resistance of the pile.

It has been widely recognized by engineers that the pre-drilled hole will result in a loss of skin friction and reduction in the axial load carrying capacity of the pile. However, there has been no unified recognition on the size of pre-bored hole to be drilled for aiding pile installation at present [2], let alone the reduction effect of pre-boring on the driving force, setup and long-term load carrying capacity of pre-bored pile. For pre-bored piles, the long-term end bearing of the pile will not be an issue, as it is recommended by Department of Transportation and Development (DOTD) Standard Specifications for Roads and Bridges [3] that “the maximum diameter of a pre-boring hole be 80% of the pile size” and “the depth of the pre-boring hole should stop within 3 ft. from the recommended pile tip elevation.” However, the pre-drilled pilot hole, although the size of which is generally smaller than the pile diameter, will significantly reduce the setup and long-term shaft resistance of the pile, which should be therefore taken into account when determining the load carrying capacity of the pile. At present, extensive research efforts in either instrumented pile load tests or numerical studies have been dedicated to the setup and long-term load carrying capacity of full displacement piles [4-13]. However, due to the extreme complexity of the reduction mechanism and the high cost involved in fully instrumented pile load tests for different sizes of pre-drilled bore hole, there is a dearth of research on the setup and the long-term load carrying capacity of pre-bored piles, although the reduction in shaft resistance over the pre-drilled depth has been well realized for a long period of time [14]. A comprehensive numerical study and practical formulas are still yet not available for assessing the setup and long-term shaft resistance of pre-bored piles, which motivates development of both feasible numerical model and analytical method to assess the reduction effects of pre-boring on the setup and long-term shaft resistance of pre-bored piles.

At present, the design and analysis of pre-bored piles primarily relies on the local experiences as the effects of pre-boring on the driving force, the setup and long-term shaft resistance within the pre-bored zone are still unclear. However, due to the high cost and time involved with field instrumentation and testing on pre-bored piles, it is impractical to conduct a large number of fully instrumented pile load tests to investigate the shaft resistance reduction effects of pre-bored piles. As an alternative to the field experimentation, this numerical study is funded by the DOTD as a first step to explore the impacts of pre-bore size on the drivability and long-term shaft resistance reduction of piles.

This research contains both numerical modeling and analytical study to investigate the shaft resistance reduction mechanism of pre-bored piles. A feasible finite element technique, using a one-dimensional disk to represent the soil around the pile, was developed with the ABAQUS program to explore the impacts of the size of pilot hole on the long-term shaft resistance of the pile within the pre-bored zone. The numerical model integrates the entire process from pile installation through subsequent consolidation to pile loading and hence is capable of reflecting the effects pre-boring on the behaviour of the pile at different stages. Leveraging on the numerical simulations, a set of reduction factor curves are generated for various combinations of pre-bore size and soil conditions, and specifically, are presented for the typical Louisiana soil strata. The produced reduction factor potentially can be implemented into the current pile analysis and design software, through directly lowering the α or β coefficient involved to determine the reduced pile capacity. To facilitate the design of pre-bored piles, researchers developed practical formulas based on some remarkable findings from the numerical results to assess the driving force, the setup and the long-term shaft resistance within the pre-bored zone. The proposed practical formulas are validated by comparing with the results generated from the finite element model, which shows satisfied agreements. Extensive parametric studies are conducted to investigate the impacts of pre-drilled hole size, the overconsolidation ratio and earth pressure coefficient at rest on the driving force, the setup and long-term shaft resistance reduction of pre-drilled piles. It is expected that the outcomes of this research could provide guidance for future instrumented field tests in in Louisiana. It is also expected that the proposed numerical model and practical formulas will serve as useful tools for design and construction of pre-bored piles in Louisiana.

Literature Review

Pile is usually used to transfer the structural loads to a firm stratum at some depth below the base of the structure. It provides reinforcement to the soil, increasing its load capacity and improving its deformation behavior. The axial strength, or ultimate load capacity, of a pile, Q_u, an important aspect in the pile design, can usually be estimated/expressed in a general form as follows [15, 16] (see Figure 1a):

$$Q_u = Q_b + Q_s,\ Q_b = q_b A_b, Q_s = \int_0^L q_s(z) C_d(z) dz \quad (1)$$

where, Q_u = total pile bearing capacity; Q_b = ultimate base resistance; Q_s = ultimate shaft resistance (or side friction); q_b is the ultimate unit point resistance (maximum stress that can be mobilized at the pile base); A_b is the area of pile base; q_s = ultimate skin resistance per unit area of shaft; C_d = perimeter of pile; and L = pile length.

Figure 1. Pile driven (a) without pre-boring; (b) with pre-boring method

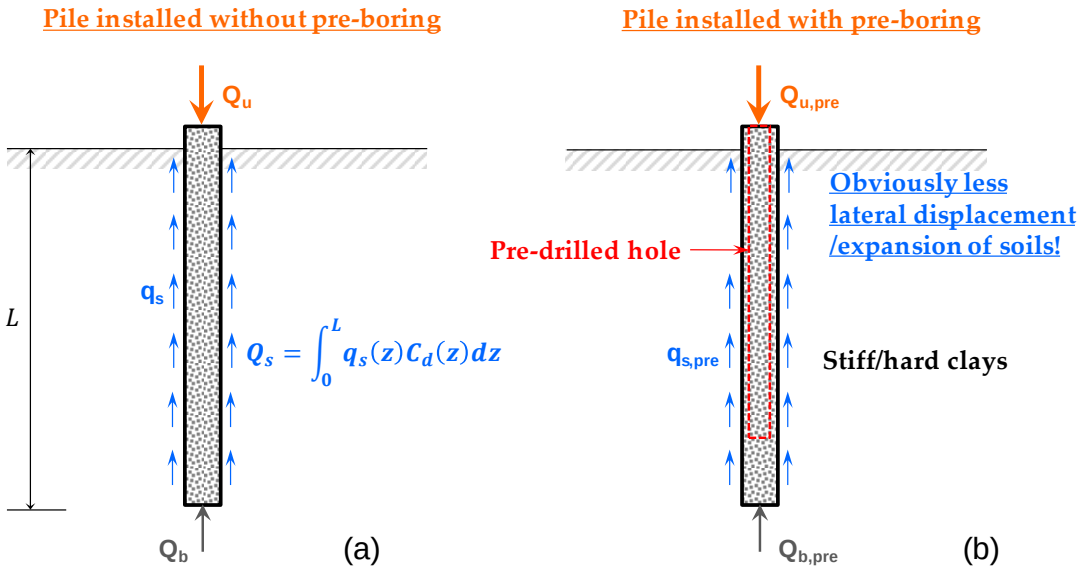

The ultimate unit point resistance q_b is commonly evaluated from the well-established bearing capacity theory in terms of the soil properties such as the cohesion and/or friction angle of the soil [17]. While for the estimation of ultimate unit shaft resistance q_s, both "α method" and "β method" have been recommended by FHWA [18]. The former

assesses the shaft resistance through an empirical coefficient α with the in-situ undrained strength s_u [19], i.e.,

$$q_s = \alpha \cdot s_u \tag{2}$$

so it basically corresponds to an undrained strength, usually for piles in clays and known as the total stress method. The latter one of β method is based on Coulomb's friction law in terms of the effective stresses [15]. With this approach, the value of q_s may be related to the local effective radial stress at failure σ'_{hf} and to the in-situ vertical effective stress σ'_{v0} by [7, 20]

$$q_s = \sigma'_{hf} \cdot \tan\delta' = K_s \cdot \sigma'_{v0} \cdot \tan\delta' = \beta \cdot \sigma'_{v0} \tag{3}$$

where, δ' represents the peak mobilized angle of friction acting parallel to the pile shaft; σ'_{hf} has been taken as some ratio K_s of the vertical effective stress σ'_{v0}, thus resulting in the second form of the above expression; and β as shown is a lumped parameter equal to $K_s \cdot \tan\delta'$.

Pre-boring is a method used to facilitate the driving of large displacement piles in hard/dense soils. It is generally recommended for pile penetrating through stiff clays, as the pre-bored hole may not be able to stay open without a casing for cohesionless soils [2]. For piles driven in clay, it is natural and necessary to calculate the pile bearing capacity both at the end-of-initial driving (EOID), i.e., "pile drivability", and in the long term after full consolidation of the soil, since the dissipation of excess pore water pressure generated during the pile installation will significantly affect the pile capacity, i.e., the well-known effect of "setup" [5]. According to the request for proposals, the long-term end bearing within the pre-bored zone will not be an issue, as specifications prohibit predrilling to the tip elevation [21]. However, it is anticipated that pre-boring may profoundly reduce the pile shaft resistance and thus has an impact on pile drivability and its long term capacity.

In the current practice when using pre-boring technique to facilitate pile driving, a pilot hole, generally smaller in size than the pile to be installed, is first bored to a specified depth. Figure 1b shows the schematic diagram for a pile driven with the pre-boring method. In comparison with the pile without pre-boring (Figure 1a), it is intuitively apparent that the major impact of pre-boring on the pile capacity shall be attributed to the reduced amount of soil volume being laterally displaced during the installation, through the size of the zone of remoulded soil surrounding the pile as well as the magnitudes of

the stresses to which the soil is subjected [22]. Such an impact is conceived to further propagate in the subsequent consolidation and loading phases via the changes of mobilized unit shaft resistance q_s, and therefore deemed to contribute to the pile setup effect as well.

Pre-bored piles belong to the partial displacement pile group. It is useful to note that, on one hand, a pre-bored pile becomes a full displacement pile when the pre-boring radius reduce to zero, but on the other hand, it degenerates to a non-displacement pile (i.e., drilled shaft) if the pre-boring size approaches that of the pile itself. From this viewpoint, both the full displacement pile and non-displacement pile can be regarded as particular cases of the pre-bored pile. It is expected that, by leveraging the respective advantages of the full-displacement and non-displacement piles, an optimized analysis and design for the pre-bored pile may be achieved through the adjustment of the pilot hole radius, so as to considerably improve the pile drivability yet without greatly affecting its bearing capacity. Given the fact that the pre-bored piles essentially encompass the conventional full displacement piles as a special case of no pre-bore, they must bear significant similarities between each other as far as the important impacts of pile installation and setup effect are concerned on the pile capacity. For this reason, in this review report the literature search will be conducted in a parallel way for both the full displacement piles and pre-bore piles, to gain a better understanding of the state-of-the-art of research and practice on the subject of pre-bore piles.

To date, extensive research efforts, including laboratory and field tests, analytic models, and numerical analyses, have been performed to investigate the bearing capacity of piles with different installation methods and the behaviour of piles under various loading conditions. This literature review is therefore presented in terms of these three main aspects, with the specific emphasis on the examination of pile installation and setup effects.

Laboratory Model and Field Testing

Displacement Piles

Carefully designed laboratory and field tests of instrumented piles provide the key to understanding the mechanisms that govern pile behaviour [23]. From the laboratory model/prototype field testing, not only the complex changes of stresses, strains, and excess pore water pressure of the surrounding soils can be consecutively traced, but the

driving force or resistance and the performance of piles at different loading stages may also be directly measured/captured. Especially in the field pile tests, the in situ soil conditions can be properly taken into account, so the effects of pile installation and setup may be truly assessed from the test results. Over the last few decades, the influences that the installation and setup of full displacement piles might have on the soil and pile behaviour have been well explored in the literature [24-33]. As summarized in Poulos and Davis [15], these effects include mainly: (a) Remolding the soil surrounding the pile; (b) Alteration of the stress state in the soil in the vicinity of the pile; and (c) Dissipation of the excess pore pressures developed around the pile.

Early investigations into the effects of pile driving on the properties of clays were made by Housel and Burkey [34] and Cummings et al. [35]. Based on the evidence from load tests to failure carried out on piles at different times after their installation, it can be inferred that the undrained strength of a clay is initially decreased considerably because of driving, but that a significant regain of strength occurs with elapsed time between driving and pile testing. In earlier contribution on the measurement and analysis of soil disturbance from pile driving, Bozozuk et al. [36] conducted the field tests of concrete piles installed in sensitive marine clay in eastern Canada, and found that the pile installation had little effect on the compressibility of the surrounding clay soils. However, it was observed that the in situ shear strength and cone penetration resistance were greatly reduced due to the pile installation effect and that the induced excess pore water pressure was much higher than the overburden pressure, which took around 8 months to dissipate after the completion of piling. Roy et al. [27] and Konrad and Roy [8] also reported full scale studies of six instrumented test piles in the Saint-Alban test site located about 80 km west of Quebec City, Canada, concerned again with the disturbance caused to the soft sensitive clay by pile driving and with the setup and dissipation of driving pressure. Their findings from the test results are quantitatively similar to the previous ones and can be summarized as follows: the vane shear strength of the soil around the pile was temporarily reduced by a maximum of 30%-40%; the pile in sensitive clayey soils exhibited apparent setup effects after pile installation; and the shaft bearing capacity increased significantly with time and the capacity after full dissipation of excess pore water pressure was about 12 times of the capacity immediately after pile installation. Furthermore, Azzouz, and Morrison [26] adopted the Piezo-Lateral Stress (PLS) cells, a device introduced by the Massachusetts Institute of Technology (MIT) that is capable of measuring and recording simultaneously the total horizontal stress and pore pressure acting on pile shafts throughout the various stages from pile installation to loading, to investigate in situ the effects of pile installation in slightly overconsolidated Boston Blue

Clay. According to the test results, the authors concluded, as would be expected, that pile installation reduces the effective horizontal stress on the shaft; the horizontal stress acting on the pile shaft increases during the phase of soil consolidation that follows the pile installation; and that the clay sensitivity has an important effect on the pile shaft behaviour.

To remedy the situation of still lacking of reliable data regarding the physical processes that govern displacement-pile behaviour, a number of research groups, notably Oxford University and Imperial College, have been attract and involved with the field experiments of comprehensively instrumented piles since the late 1980s. Coop and Wroth [37] developed an instrumented model pile at Oxford University with the intention of investigating the fundamental behaviour of piles in both heavily overconsolidated and normally consolidated clays. Several interesting conclusions relating to the three phases of the performance of a pile (installation, reconsolidation and loading) were given from the site investigation data. For example, the stress relief immediately behind the pile tip during installation gave rise to total radial stress and pore pressure measurements on the shaft which were lower than the simple cavity expansion model predictions; during reconsolidation (pile setup), the radial effective stress drops initially, followed by a slow recovery, which was insufficient in the two clays investigated for the final value to reach that during installation. The work reported by Bond and Jardine [29] involved a series of field experiments using extensively instrumented closed-ended steel piles installed in heavily overconsolidated London clay. It was concluded that the penetration rate had a marked influence on the mobilized skin friction during installation and subsequent loading; negative pore water pressures were developed at the pile wall during installation; and that the load capacity of pile in heavily overconsolidated London clay showed no increase with time after installation but instead fell slightly.

Given the important role the full scale tests may play in understanding the performance of piles in soils, it is not surprising that this subject has been repeatedly revisited by various researchers throughout the 1990s and continues so today. Matsumoto et al. [38] presented the performance of axially loaded, open-ended steel pipe piles driven in soft rock, and demonstrated remarkable setup from the re-driving and the static load tests. Hwang et al. [39] investigated the changes in pore water pressure and ground deformations generated by pile installation from a series of large-scale pile tests performed at the Chiayi-Taipo area. The test site and the three test piles were instrumented with a network of piezometers, inclinometers, level posts, and velocity sensors for monitoring the variations of the dynamic soil pore water pressure, lateral ground deformations, vertical surface

displacements, and ground vibrations induced by the pile driving. They found that the excess pore water pressure decreased rapidly with an increase in distance from the pile and that such a decrease was faster in a clayey layer than a sandy layer. An approximate relation between the pile-driving resistance and the geological condition of the test site was finally suggested by the authors based on the test results. Most recently, Haque et al. [40] performed a comprehensive field study on two instrumented test piles to evaluate the effects of pile installation sequence on pile setup behaviour. A number of dynamic load tests and one static load test were undertaken on the piles to measure the increase in piles resistances with time. One of the main conclusions from this work was that clayey soil layers exhibited a larger amount of setup compared to sandy-silty soil layers.

As an alternative to full-scale field tests, well-designed laboratory experiments may also provide valuable insight into fundamental mechanisms affecting soil-pile interaction. Chandler and Martins [41]; Rojas [22]; and Al-Mhaidib [42]. Chandler and Martins [41] reported an experimental study of skin friction mobilization around model piles installed in Speswhite kaolin with attention focused more on the pile loading stage. The model pile tests were performed in a modified form of large hydraulic triaxial (stress path) cell in which the axial stresses and cell pressure can be varied independently. Based on the test results on nine normally consolidated and one overconsolidated samples, the authors showed that the angle of shaft friction is independent of the stress ratio in the soil before loading (for a range of stress ratios K), and is only just less than ϕ'_{triaxial} for normally and overconsolidated kaolin. The effects of disturbance caused by most pile installation techniques were highlighted by the differences between adhesion factor α back-calculated from the model tests and those normally encountered in practice. Al-Mhaidib [42] investigated the effects of the loading rate on the bearing capacity and behaviour of a model pile in clay and observed that increase in the loading rate results in a significant increase of the pile capacity; nevertheless, the loading rate has a negligible influence on the magnitude of the pile head displacement at failure for both the compression and uplift tests.

Pre-bored Piles

In contrast to the full displacement piles, the experimental investigations into the behaviour of pre-bored piles are much less extensive. An early yet essential paper related to the pre-bored piles probably should be attributed to Rojas [22], who conducted a series of model tests on concrete piles and reported that pre-boring has a major influence on the bearing capacity of friction piles, reducing the capacity as the pre-boring diameter

increases. The author also proposed a simple formula to describe such an effect. Recently, Carniero and Jardine [43] performed laboratory experiments by developing a very small scale model to find out how pile capacity (both tip capacity and shaft resistance) will change with respect to the ratio of section area of pre-bored hole to section area of pile. From the model test results, they concluded that overall soil resistance to installation for the specific soil properties considered was reduced by a factor of up to 2, and that the reduction factor grew systematically with the ratio of pre-bored hole to pile cross section which is fairly obvious.

Complementing the work by Rojas [22] and Carniero and Jardine [43] was the case study by Shong et al. [44], who investigated the pile capacity reduction of jack-in piles with empty pre-bored holes (the hole size equal to the diameter of piles) in meta-sedimentary formation at central part of Peninsular Malaysia which suffered pile capacity reduction problem with time. It was noted that the inherent softening behaviour of the meta-sedimentary formation with localized stress relaxation condition in empty pre-boring hole can significantly reduce soil strength, thus directly affecting the carrying capacity of mostly end bearing jack-in pile. The authors also stressed that the amount of pile capacity reduction is dependent on the subsoil material at the pile tip founding level and pile penetration (embedment) below the base of pre-bored hole.

Analytical Studies

Displacement Piles

The analytical approach for estimating the pile capacity can be divided into two broad categories, depending on the level of sophistication and rigor. The relatively simple category I procedures account for most pile design for bearing capacity done throughout the world, which involve basically the use of "α method" or "β method" (as described in the introduction section), with the appropriate adoption of the values of the empirical parameters to reflect the effects of pile installation and soil conditions. The typical examples of this category of procedures include Tomlinson [45], Skempton [46], Burland [47], and especially well illustrated in the two Terzaghi Lectures delivered by Meyerhof [17] and O'Neill [48]. The DrivenPiles design software (MDSC)[49] and FHWA [18] recommended "α method" for cohesive soils uses the empirical adhesion factor/coefficient α originally proposed by Tomlinson [19], while their recommended "β

method" for cohesionless soils is based on the Nordlund Method [50] for which the unit frictional resistance of the soil around the pile is computed as follows [18]:

$$q_s = \beta \cdot \sigma'_{v0} = K_\delta C_F \frac{\sin(\delta' + \omega)}{\cos(\delta')} \cdot \sigma'_{v0} \quad (4)$$

where $\delta' =$ friction angle between pile and soil and $\sigma'_{v0} =$ effective overburden pressure, both of which have been defined in the "Introduction" section; $K_\delta =$ coefficient of lateral earth stress at certain depth; $C_F =$ correction factor for K_δ when δ' is not equal to the frictional angle of soil; and $\omega =$ angle of pile taper from vertical.

In contrast to "α method", the "β method" of equation (3) proves to be theoretically more robust [16, 47]. The method is related directly to the fundamental effective stress parameters K_s and δ' and therefore can deal with the EOID and long-term capacity of piles, with or without pre-boring, in a consistent way. However, to estimate the maximum shear stress mobilized using equation (3), both the radial effective stress and the angle of shaft friction acting at peak conditions must be determined. As both these quantities are heavily dependent of the soil type and its stress history, the type of the pile, and the method of pile installation, it is not surprising that selection of appropriate values for these two parameters would be a difficult task [7]. This would be particularly challenging when the pre-bore piles are concerned.

The category II procedures are based on a much sounder theoretical basis, in which the soil behaviour is usually modelled with realistic elastoplastic constitutive models and in general the complex stress changes in the soil around the pile that occur during installation, equilibration of excess pore pressures, and loading of the pile need to be properly considered. It should be remarked that the development of rigorous analytical theories of pile behaviour has largely concentrated on the first phase of installation, based primarily on the cavity expansion theory [5, 51, 52] or on Baligh's strain path method [53, 54], as will be described below.

The central assumption of the cavity expansion method is that pile installation has the same overall effect on the ground as the monotonic expansion of a long cylindrical cavity under undrained plane strain conditions. From this simple hypothesis, detailed predictions can be made (using a variety of elasto-plastic soil models) of the changes of stresses and pore water pressure in the soil at the end of pile installation, thus enable the parameters involved in the "β method" be determined in a more accurate way. The first detailed study of the installation of piles using large-strain cylindrical cavity expansion theory was

given by Randolph et al. [5], where the widely used modified Cam Clay model had been adopted to describe the behaviour of clay. The authors argued that the maximum excess pore pressure generated at the pile wall, Δu_{max}, is related to clay's original undrained shear strength s_u by the equation

$$\Delta u_{max} = \left(p_0' - p_f'\right) + s_u \ln\left(\frac{G}{s_u}\right) \tag{5}$$

where, G/s_u is well known as the rigidity index of the soil; p_0' and p_f' denote the mean effective stress at the in-situ and failure conditions, respectively. Using an earlier general solution of the cavity expansion problem originally presented by Vesic [51], Roy et al. [27] predicted the generation of pore pressure around the shafts of piles installed in Quebec silt clay, which has been shown to be in satisfactory agreement with the field measurements.

There is an abundance of analytical cavity expansion solutions existing in the literature, much of which has been developed by considering the soil to obey the Mohr-Coulomb yield criterion or more advanced critical state model of Cam Clay [1, 51, 55-58]. Among these, however, it is the analysis of Chen and Abousleiman [1], which for the first time proposed an exact solution for the undrained expansion of a cylindrical finite cavity in a modified Cam Clay soil without any approximation imposed on the mean and deviatoric stresses. These important analytical solutions based on the large deformation and Lagrangian framework have of course provided further insights into the mechanism of the development of earth pressure acting on the pile shaft. As advocated by Randolph [59] in his Rankine lecture devoted to piling, despite the approximations involved in the cylindrical cavity analogue to model the installation of displacement piles, it appears that the general pattern of excess pore pressure, and the consolidation response, can be predicted reasonably by the cavity expansion method for the driven piles.

The strain path method, pioneered by Baligh [53] at MIT, is capable of accounting for the two-dimensional aspect of the pile installation, which possesses an obvious advantage over the one-dimensional nature of cavity expansion method. According to the stress path method, the soil deformations/strains in the soil are estimated by means of (known) velocities of an ideal fluid moving around an object having the shape of a pile. The stresses and pore pressure therefore can be determined by considering appropriate constitutive relations for the soils. By using the strain path method, Azzouz and Morrison [26] provided the analytical predictions of the effective horizontal stress and pore pressure development on the pile shaft that was driven in Empire, Louisiana. Both the

modified Cam Clay model and MIT-E2 constitutive model have been incorporated into the framework of strain path method in carrying out the installation predictions. The authors found that the strain path method can yield a reasonable prediction for the build-up of excess pore water pressure, which compares favourably with the cavity expansion method that tended to significantly overestimate the pore pressure dissipation rate. Nevertheless, none of these two approaches can provide consistently accurate predictions for all important aspects of the shaft behaviour.

As regards to the setup effect of displacement piles, analytical solutions for the rate of dissipation of excess pore pressures around a driven pile (and hence the changes of effective stresses acting on it) are usually obtained by assuming simple consolidation theory that dissipation occurs radially only [4, 60-64]. Randolph and Wroth [4] derived a closed-form solution for the radial consolidation of the soil around a driven pile, where the excess pore water pressure immediately after pile installation was calculated from the cylindrical cavity expansion theory. They concluded that the final stress state after consolidation is similar to that in an oedometer (K_0) test, and that the proposed radial consolidation solution in combination with the cavity expansion theory provided a rational approach to estimate the time needed for a displacement pile to achieve its maximum loading capacity. In a similar way, Heydinger and O'Neill [61] modelled the radial dissipation of installation excess pore pressures during the reconsolidation phase, with due consideration given to the increase of the soil modulus with the radial distance from the pile to reflect the relaxation effects of the surrounding soils during consolidation. The developed method was verified by comparing the predicted results with the data from two pile tests, and an expression was proposed to assess the setup effects of displacement piles.

Some recent advances made on the topic of pile setup effect include the contributions by Wang et al. [65], Zheng et al. [63], and Gong et al. [64]. In Wang et al. [65], a new growth-rate-based model for pile setup prediction has been established, based largely on the pile testing database provided by DOTD for southern Louisiana clayey soils. At around the same time, Zheng et al. [63] analyzed the dissipation of the excess pore water pressure again by the radial consolidation theory, but with the coefficient of consolidation assumed to be a variable. In their work, the variation of the consolidation coefficient during consolidation was determined through the relationships $e - \ln(p')$ and $e - \ln(k)$, while the governing equation was solved by the variable separation method along with a simple numerical technique. The effects of the compressibility and permeability on the setup effects of displacement piles were explored and discussed based on the proposed

semi-analytical solution. Whereas in the most recent analytical contribution by Gong et al. [64], a more advanced yet realistic model, i.e., the K_0 based anisotropic modified Cam Clay, has been adopted in the cylindrical cavity expansion analysis to analytically examine the pile installation and setup effects of jacked piles in clayey soils.

Pre-bored Piles

A review of literature reveals that an analytical approach for estimating the load capacity of piles is very scarce for piles with pre-boring methods. In respect to the simple "α" or "β" method, the following explicit expression suggested by Rojas [22]

$$\frac{P_u}{P_{u0}} = 1 - 0.5A_{pp}/A_{tp} \tag{6}$$

where, P_u and P_{u0} denote pile loading capacity with and without pre-boring, respectively; A_{pp} is the pre-bored area and A_{tp} the total pile area, should be considered as the first effort to quantitatively characterize the reduction of pile capacity due to the pre-boring operations. Note that equation (6) is proposed from the approximate curve fitting of small scale model test data [22], and that the formula is general enough to be applicable with either "α method" or "β method" in relevance to the calculation of pile loading capacity P_{u0}. It should be pointed out that, although in Louisiana and many other states in the U.S., pre-boring procedure has become a common practice/recommendation to facilitate large displacement pile driving in dense cohesive soils [3], the currently available specifications exclude any quantifications in regards to the potential reduction of pile capacity as a result of using pre-boring technique. This is in fact due to the very lack of analytical modelling that is capable of featuring the influences of pre-boring and relating the reduction of bearing capacity to the size of pre-bored hole. For example, according to the DOTD *Standard Specifications for Roads and Bridges* [3], only qualitative information is provided as a practical guidance for the pre-bored piles design and operations. To quote:

- Maximum diameter of pre-boring hole is 80% of the pile size.
- The depth of the pre-boring hole should stop within 3 ft. from the recommended pile tip elevation.

On the other hand, with reference to the second category of (more sophisticated) analytical modelling, barely any progress has been made pertaining to the pre-bored piles in the literature. Nevertheless, if the most general formulation of one-dimensional

cylindrical cavity expansion is to be adopted to model the important phase of pile installation and its subsequent effects on the stress disturbances of the surrounding soils, then technically there should be no difficulty at all to extend such an analytical approach for estimating pile capacity from conventional displacement piles to the desired ones of pre-bored piles. The only difference between the piles with and without pre-boring, in terms of the installation effects, is that for the pre-bored case the knowledge of the initial cavity radius representing the size of pilot hole is required in the cavity expansion analysis. For the finite expansion (i.e., with initial cavity radius) of cylindrical cavity in modified Cam Clay soil under undrained condition, actually an exact analytical solution now has been available, which was developed recently by Chen and Abousleiman [1] based on large deformations and Lagrangian description. Once the pile installation analysis is completed, the subsequent analytical modelling for the stages of soil consolidation and pile loading basically can go through the same processes for both piles with and without pre-boring, as will be described in details in the main body of the final research report.

Numerical Analyses

Displacement Piles

Modern numerical analysis, here particularly referring to the finite element method (FEM), has the ability to account for sophisticated constitutive models and coupled behaviour between the soil deformation and pore fluid diffusion processes, the complex issues which are specific to geotechnical engineering. This method essentially involves a computer simulation of the history of the geotechnical engineering boundary value problem from greenfield conditions, through construction and into the long term, and therefore in many respects is superior to the previous simple analytical method [66]. With the rapid advances in both computer hardware and commercial finite element software, the past 40 years have seen much application of fully numerical analysis to real pile driving problems [5, 12, 67-71]. However, this by no means indicates that performing a thorough numerical modelling of pile installation and subsequent consolidation and loading processes is an easy task. As a matter of fact, owing to the complicated elasto-plastic soil constitutive models involved, as well as the non-linearity and mesh distortion caused by large deformations associated with the pile installation and the high computational requirement pertinent to the adjustment of pile-soil frictional contact [12], development of a credible finite element model for pile-driving analysis has never been

cheap and oftentimes one may encounter the relevant limitations and pitfalls of this type of analysis.

The major advantage of numerical analysis approach is that it can logically and accurately predict the stress history of the soils around the pile from the in situ conditions to the conditions at failure, i.e., the pile problem may be broken down and analyzed step by step through the following three stages:

- Pile installation (an undrained analysis);
- Dissipation of excess pore pressures induced by installation (consolidation analysis); and
- Pile loading process (undrained or drained conditions depending on the loading rate)

Note that the radial effective stress at the pile-soil interface σ_r', which is known to have a significant contribution to the shaft resistance q_s, varies at each of the above three stages. For the EOID pile capacity, it can be predicted by combining the two stages of (a) and (c), both under undrained conditions as a restrike test for the EOID capacity (WEAP analysis) is usually performed in a short period of time. On the other hand, the long term capacity corresponding to the static loading test may be obtained straightforwardly by taking into account, in sequence, stage (a), stage (b) with $t \to \infty$, and stage (c) under drained condition. The pile setup effect can also be evaluated in a similar way by considering stage (a) + stage (b) $[0 < t < \infty]$ + stage (c) [drained].

The earliest finite element simulations and rigorous analyses of the stress changes, excess pore pressures, and subsequent consolidation around a driven pile were presented by Carter et al. [72] and Randolph et al. [5]. In their key contributions, the pile-driving process was modelled as the creation of a long cylindrical cavity by radial soil movement, i.e. using the cavity expansion theory [73]. The authors conducted extensive finite element numerical research into the prediction of stress disturbance after installing the pile, although no attention has been given to the effects of pile loading after installation. This particular obstacle was later removed by Potts and Martins [7], who extended the work of Randolph et al. [5] and presented an important numerical investigation into the mobilization of shear resistance along the pile shaft, based on a 1-D FEM (finite element method) analysis. Potts and Martins [7] made some important observations, including that the evolution of the stress state near the pile is significant and not simple as a result of loading, potentially leading to substantial changes in the

coefficient of lateral stress at the pile/soil interface as well as considerable shear strain localization near the pile. The authors also found that slip may occur before the generation of the largest theoretical pore pressures during the undrained pile loading process, and that the generated excess pore water pressures dissipated fairly rapidly, which well explained the phenomenon that significant pore pressures have seldom been measured in practice.

The simplified finite element calculations in combination with the cavity expansion method discussed above could effectively avoid the mesh distortion and greatly reduce the computational efforts required in the pile installation simulation. However, they cannot take the vertical shearing effect inherently accompanying with the installing of pile into consideration, a significant influence on the behaviour of the surrounding soils. To account for this issue, Basu et al. [11, 71] modelled driven pile installation and its effects on subsequent bearing performance indirectly through the following two separate technique sequences: (a) undrained expanding a cylindrical cavity to pile diameter by pushing the soil away to simulate the squeezing effect of pile installation; and then (b) applying a vertical shearing to the adjacent soil element to simulate the shearing effects of pile installation. In their simulation work, a two-surface plasticity-based constitutive model suitable for clay has been incorporated into the finite element code, and the entire stress path of a soil element undergone during the pile installation and subsequent consolidation and loading processes been traced. An important finding was that the shearing reduces the normal stress on the pile shaft from the very large value predicted by cavity expansion alone. The authors hence stressed that shearing plays a significant role in the changes in soil state around a driven pile. They also proposed useful equations, which only require initial state and intrinsic shear strength parameters of the soil as input parameters, to predict the short and long-term bearing capacity as well as the setup factors for driven piles in clay.

Along similar lines, numerical simulations on the pile installation effect have been further conducted recently by Mascarucci et al. [20] and Abu-Farsakh et al. [12]. In Mascarucci et al. [20], a new approach was proposed to model the increase of shaft friction associated with the increase of horizontal stresses during the pile loading phase, by means of FLAC 2D program and on account of the soil dilatancy in the shear band. While the latter paper modelled pile installation by the combination of a volumetric cavity expansion phase followed by a vertical penetration, and investigated the subsequent thixotropic and consolidation effects on pile setup. An anisotropic modified Cam Clay model has been adopted to describe the nonlinear soil behaviour. Abu-Farsakh et al. [74] also investigated

the pile set-up phenomenon for clayey soils through field tests and develop empirical models to predict pile set-up resistance at certain time after the end of driving.

Pre-bored Piles

Insight into the impacts of a pilot hole on the installation effect and bearing performance of pre-bored piles, through advanced numerical analysis, received much less attention than the case of full displacement piles. The literature search reveals that only a few attempts have been offered by Mabsout et al. [75] and then by Mabsout and Sadek [67]. In the former publication, the authors investigated and presented the results of computational driving of a pile (i.e., drivability) with the emphasis on examining the response of the pile-soil system. The state of stresses, pore water pressure, and deformations in the soils were monitored, and the total soil resistance to pile penetration, were computed. In the latter publication, the authors further developed a sophisticated 3-D finite element model for pile-driving analysis, utilizing the advanced bounding surface plasticity model for soils. The numerical model is capable of tracing the penetration of the pile into the soil starting from a pre-bored depth.

However, it should be noted that only one size of fully pre-bored hole, i.e., 100% to the design diameter of pile, has been covered in Mabsout and Sadek's [67] contribution. While according to the DOTD *Standard Specifications for Roads and Bridges* [3], the radius of the pilot hole is suggested not exceed 80% of the pile diameter and also, as a practice guideline, the pilot hole is prohibited to be drilled down to the tip elevation. The depth of the pilot hole, though being able to influence the drivability of piles, might not as intensively as the hole size in terms of the impacts on the long-term bearing performance of pre-bored piles.

Summary

The above literature review shows that relatively few data have been reported concerning the installation and setup effects of pre-bored piles, and especially very little quantitative information regarding the impacts of the size of pilot hole on the drivability and long-term bearing performance of pre-bored piles. An exception is the fairly recent research effort made by Ghose-Hajra and Tavera [2]. In their pilot research on this subject, the state-of-the-art and best practice results nationwide available were compiled for pre-bored piles, accompanied by the recommendation of multiple pile driving sites for future testing of piles in Louisiana as well as the development of an instrumentation testing plan

for field data collection with different sizes of pre-bored hole. They further proposed a protocol for evaluating the effects of pre-boring on the EOID and long-term pile capacity. It should, however, be pointed out that Ghose-Hajra and Tavera [2] provided merely a rough guideline for the examination of driven pile capacity within pre-bored soils, yet without any experimental results for quantifying the pre-boring effect on pile capacity.

Given the fact that currently no comprehensive research has been conducted to properly evaluate the capacity reduction of pre-bored piles (EOID, long-term, and setup) with different pilot hole size, the objective of this research aims to develop a feasible protocol that determines the reduction factors of side friction for the design and installation of pre-bore piles in Louisiana. The widely accepted method of one-dimensional cylindrical cavity expansion coupled with rigorous finite element method, to simulate the installation, consolidation, and loading processes of pre-bored pile, will be utilized in the analysis. To achieve the goal, the LSU research team needs to work closely with the geotechnical engineers and staff of DOTD to eventually develop appropriate analytic models for evaluating the pre-boring effect. The models should

- Represent the field conditions of Louisiana, especially reflecting those soil profiles that are generally considered for pile installation with pre-boring technique;
- Incorporate the current practice of using the pre-boring procedures in DOTD, such as the requirements related to the maximum depth of pre-bored hole and the pre-bored hole diameter usually recommended in Louisiana;
- Take into account of the pile size and geometry typically involved in Louisiana; and
- Have the capability of evaluating the skin resistance reduction both at EOID (pile drivability) and in the long run (long-term capacity).

Objective

The objective of this project is to develop a general numerical approach, with use of the ABAQUS finite element program, to evaluate the reduction factor of shaft resistance for pre-bore piles pertaining to the long-term capacity. The effects of the pre-bored hole size and soil conditions constitute the particular emphases of the numerical analysis. Reduction factor curves are generated for various combinations of pre-bore size and soil conditions with the aim of incorporating the reduction factors into the current pile analysis and design software, through directly lowering the α or β coefficient involved to determine the pile capacity in Louisiana soils involving pre-boring. The ultimate desire of this research is to develop practical formulas that could be used for design and construction of pre-bored piles in Louisiana State.

Scope

This research performs a comprehensive numerical study to explore the impacts of the size of pre-drilled hole on the long-term shaft resistance of the pile within the pre-bored zone. Researchers developed a practical numerical model that considers a thin horizontal soil disc sufficiently far from the ground surface and the pile base using the ABAQUS package to investigate the effects pre-boring on the behaviour of the pile at different stages. The numerical model integrates the entire process from pile installation through subsequent consolidation to pile loading and hence is capable of reflecting the shaft resistance reduction mechanism of pre-bored piles. Leveraging on the finite element model, long-term shaft resistance factor curves and shaft resistance reduction factor curves are generated for typical Louisiana soil strata to provide guidelines for design and construction of pre-bored piles in Louisiana. The reduction factor curves after carefully calibration potentially can be implemented into the current pile analysis and design software, through directly lowering the α or β coefficient involved to determine the reduced pile capacity. Based on the numerical results for pre-bored piles in Louisiana soil, a preliminary protocol which includes the site selection, the soil properties investigation, the instrumentation, the testing procedure, and the data collection is proposed for future instrumented pile field tests to verify the numerical results. To facilitate the design of pre-bored piles, practical formulas were developed based on simplified cavity expansion solution to assess the driving force, the setup and long-term shaft resistance within the pre-bored zone. The proposed practical formulas properly take the size of pre-drilled hole, the installation effects, the consolidation of the soil, as well as the shearing mode of the soil adjacent to the pile into consideration, and hence is capable of yielding satisfied predictions when compared with the results generated from the finite element model. Extensive parametric studies are conducted to investigate the impacts of pre-drilled hole size, overconsolidation ratio and earth pressure coefficient at rest on the driving force, the setup and long-term shaft resistance reduction of pre-drilled piles. This study not only reveals the shaft resistance reduction mechanism of pre-bored piles, but also provides a simple and reliable approach to evaluate the shaft resistance of pre-bored piles, which will help geotechnical engineers to appropriately design the size of pre-drilled hole and evaluate the effects of pre-boring on the shaft resistance

Methodology

Numerical Model and Analysis

Various Stages Involved in a Pre-bored Pile

A reasonable evaluation on the behaviour of a pre-bored pile must include all the stages undergone by the soil adjacent to the pile. Figure 2 graphically illustrates the various stages typically encountered in the installation and loading of a driven pile in pre-bored soil, which consists of pre-boring, pile driving, excess pore pressure dissipation, and loading. Hence, for a representative short segment of the long pile at certain depth z of thickness dz, as shown in Figure 2, the ultimate shaft resistance can be expressed as follows:

$$q_s = \sigma'_{hf} \cdot \tan\delta' = (\sigma'_{h0} + \Delta\sigma'_{hi} + \Delta\sigma'_{hc} + \Delta\sigma'_{hl}) \cdot \tan\delta' \qquad (5)$$

where, σ'_{h0} = in-situ horizontal stress; $\Delta\sigma'_{\mathrm{hi}}$ = horizontal stress change induced by pile installation within pre-bored soil; $\Delta\sigma'_{hc}$ = stress change due to subsequent soil consolidation; $\Delta\sigma'_{hl}$ = stress change during the loading process; and δ' has been previously defined as the peak mobilized soil-pile friction angle.

Figure 2. Stages in installation and loading of a driven pile in pre-bored soil

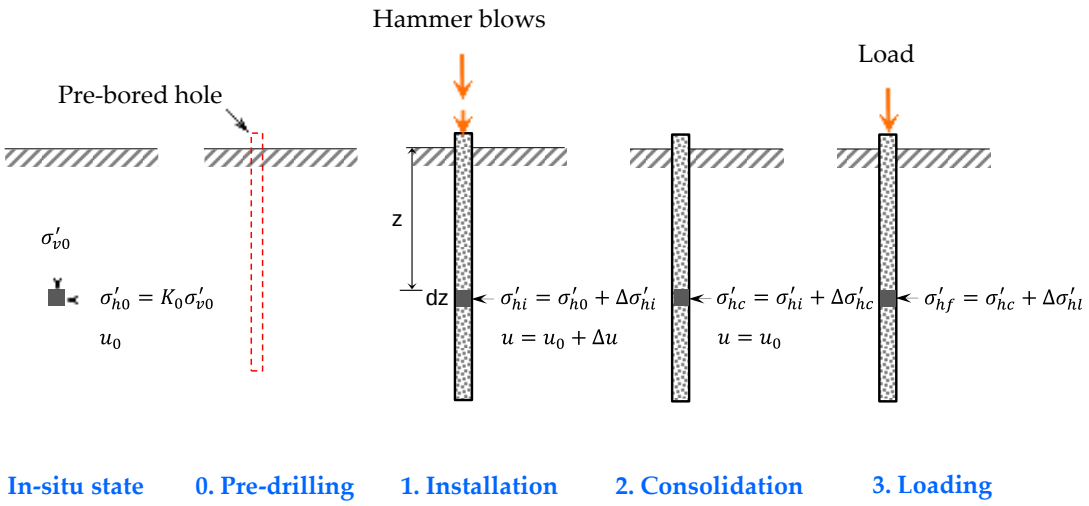

More importantly, such a decomposition scheme makes it possible to evaluate the three different categories of pile capacity. Furthermore, the one-dimensional treatment in nature by considering a thin slice of pile/soil is very useful to find the unit ultimate shaft resistance at various soil depths, and hence allows the reduction factor of side friction to be qualified pertinent to any specific soil conditions/layers. The overall effects of pre-boring on the total shaft resistance Q_s therefore may be readily determined by considering the soil stratigraphy and integrating over the surface of the pile. In the following, the numerical model will be constituted according to the three different stages involved in the pile installation and loading, and the corresponding numerical analyses for the stress changes will be described individually.

Finite Element Model

As shown in Figure 3, the numerical model adopted in this study is constituted using ABAQUS software [76] to simulate a thin horizontal soil disc which is sufficiently far from the ground surface and the pile base. The height of the soil disc is 3 mm and the external radius is 30 times of pile diameter *D*. The pile diameter is assumed to be 20 cm. Compared with the pile diameter, the external radius of the model is large enough to eliminate the potential impact of the boundary effect and to ensure satisfactory predictions. The mesh of the model consists of 300 linear quadrilateral coupled pore

pressure elements (CAX4Ps in ABAQUS package) in the whole domain. To trace the behaviour of the soil adjacent to the pile, the mesh is refined by increasing mesh density in the left domain of the model. A reasonable thickness of 3 mm, suggested by Basu et al. [71], is chosen for the leftmost soil element to represent the shear band formed in the soil adjacent to the pile.

Figure 3. Geometry and boundary condition of finite element model

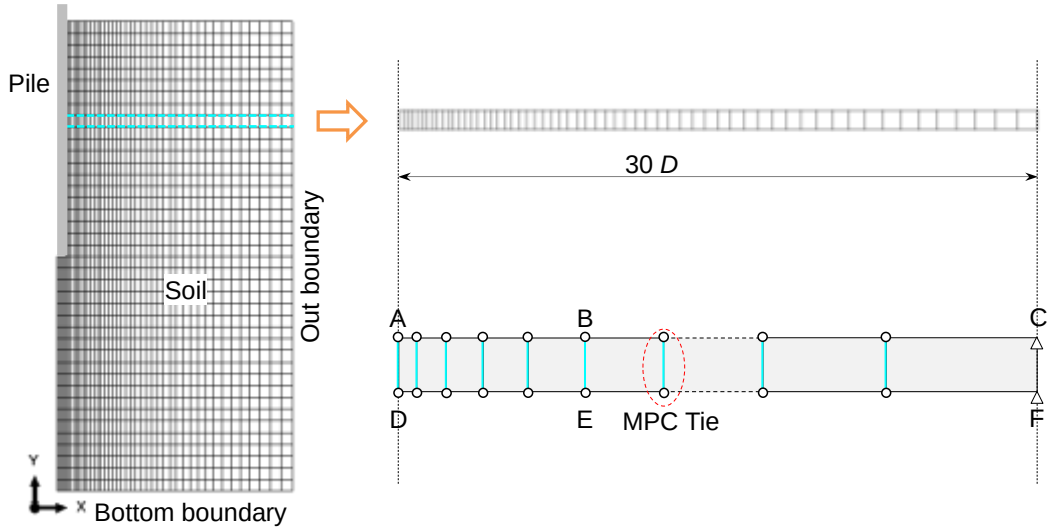

Similar to the numerical model of Potts and Martins [7], the DOFs of nodes on vertical line are tied together through the “multi-point constraints tie (MPC TIE)” function of ABAQUS to prevent the relative displacement between the up boundary AC and low boundary FD, and to enforce no rotation of the elements, which in fact simplifies the problem considered to a one-dimensional situation in each stage but with no loss of the two-dimensional feature of the problem. Theoretically, pile installation is a two-dimensional axisymmetric problem in nature, because pile installation causes both vertical and horizontal displacements of the soil adjacent to the pile. This could be easily accomplished by applying horizontal displacement followed by vertical shearing on the leftmost nodes of the model. In fact, the soil around the shaft during loading also deforms in a manner similar to plane strain in the vertical plane, thus the model could also be applied in the subsequent consolidation and loading analysis because the model restricts the rotation of the element. Therefore, as stated previously, the present FE model is capable of integrating the stages of installation, consolidation, and loading in a consistence way. To fix the vertical movement of the model, zero vertical displacement

condition is imposed over the outer boundary. A constant pressure, equal to the in-situ horizontal stress, is applied on the outer boundary to represent stress boundary condition in the far field.

Steps Involved in Pre-bored Pile Simulation

Installation. Generally, a thorough pile modeling involves five typical stages: generation of initial stresses, pre-boring, installation, subsequent consolidation, and loading. Since this study primarily focuses on the effects of the size of pre-bored pilot hole on the long-term pile capacity, the borehole stability during drilling is beyond the scope of this study. Therefore, it is assumed in this study that the stability of the pre-bored hole itself is not an issue and a pre-bored hole is directly preset at the left of the model. Before installation analysis, initial stresses should be generated to the soil disc by a geostatic step of ABAQUS to reproduce the in-situ stress field. After the generation of the initial stress, the installation of a pile with a pre-bored hole size of $a_{\mathrm{p,pre}}$ is approximately taken as undrained expansion of a cylindrical cavity from its initial cavity radius $a_{\mathrm{p,pre}}$ to the radius of pile radius a_{p}, and followed by vertically shearing the surrounding soil to critical state. As shown in Figure 4, this process is accomplished by first applying horizontal displacement $\delta u_{\mathrm{r}} = a_{\mathrm{p}} - a_{\mathrm{p,pre}}$ and then imposing vertical displacement δu_v on the leftmost nodes of the soil disc until the stresses reach constant values. During this process, undrained boundary conditions are imposed on the boundaries to simulate the undrained installation. It should be noted here that, although the installation-induced vertical displacements of the soil is limited to a thin soil band immediate vicinity of the pile (refer to as the “shear bands”) [71, 77], the shearing effects will further change the stress state of the soil at the pile shaft, which primarily governs the behaviour of the pile. Hence, the present numerical model, incorporates both the horizontally squeezing and vertically shearing effects due to pile installation, is more advance than the ones which only employ the cylindrical cavity expansion to simulate pile installation.

Figure 4. Schematic of different phase simulations

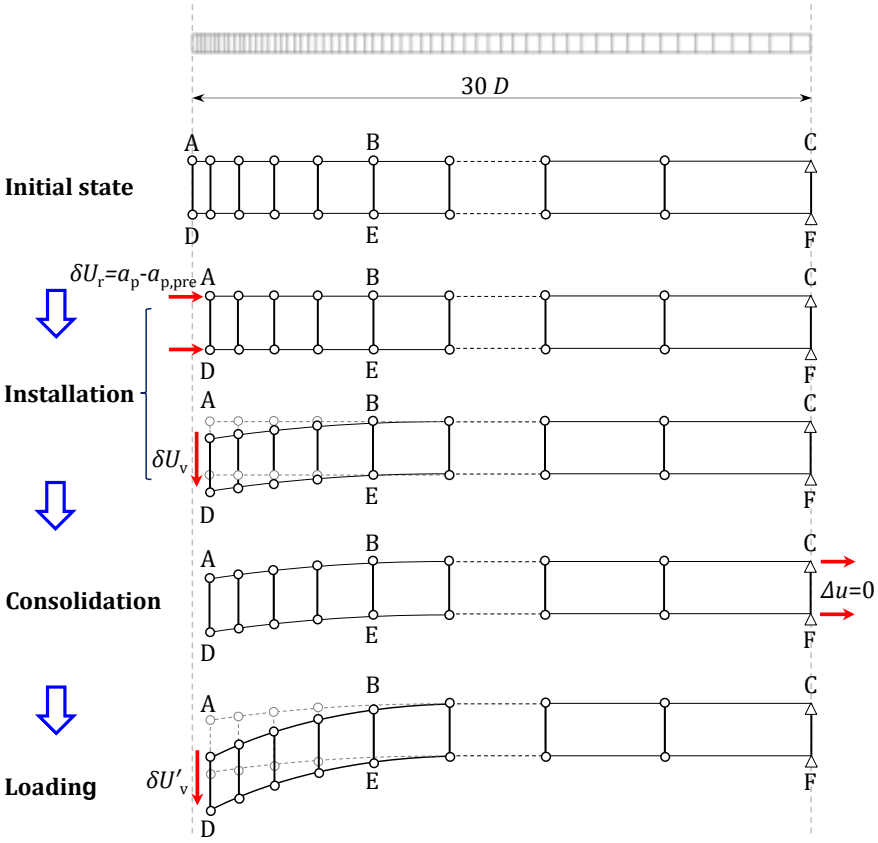

Consolidation. After pile installation, the installation induced excess pore water pressure dissipates predominantly in the radial direction due to radial pore pressure gradients [4, 62]. The field tests conducted by Roy et al. [27] in a soft Champlain clay in west of Quebec also manifested this phenomenon. Hence, consolidation of the surrounding soil is simulated by imposing zero pore pressure condition on the outer boundary in current numerical model (see Figure 4), which allows the excess pore water dissipated in the radial direction. A significant relaxation in total stress during consolidation, caused by the difference in stiffness of the soil at different radial location around the pile after installation [59], can be reflected in the coupled pore pressure elements CAX4Ps of ABAQUS, which is based on Biot's coupled consolidation theory. To consider the time elapsed in the consolidation phase, the "*SOIL, CONSOLIDATION" procedure, which is designated for the coupled pore fluid diffusion analysis in ABAQUS, is adopted in the numerical model to analyze the consolidation of the soils around the pile.

Loading. When the excess pore water pressure fully dissipates, pile loading is performed to investigate the pre-boring effects on the long-term load carrying capacity of the pile. In this study, loading is assumed to be an undrained process and the pile-soil contact is perfectly rough, which means no slippage occurs during loading until the soil reaches the ultimate state and hence the vertical displacement of the soil at the pile-soil interface is equal to the displacement of the pile. As indicated by the pile loading test of London Clay [78], the soils far from the pile base and the ground surface deformed vertically in a form similar to plane strain in vertical plane. Based on this observation, the numerical model employed in this study ties the DOFs of the nodes lying along the vertical line to guarantee shearing takes place only in the vertical direction, which is similar to the model proposed by Potts and Martin [7] but explicitly considers the installation and consolidation stages. To load the pile to failure, vertical displacement increments are imposed on the leftmost nodes of the soil disc until no further changes in stress state after consecutive displacement increments, during which an undrained boundary condition is imposed to simulate the undrained loading.

In all stages, the changes in effective stress and excess pore water pressures, as well as the void ratio of the surrounding soil, are monitored to reveal the mechanism of the different behaviours of pre-bored piles, which will be analyzed and discussed in detail latter in the report.

Soil Model and Parameters

The widely used modified Cam-clay model [79, 80] along with the large deformation theory is used to describe the behaviour of the saturated soil. As shown in Figure 5, the yield function of this model can be expressed as

$$F(p', q, p_c') = q^2 - M^2[p'(p_c' - p')] \tag{6}$$

where, M is the slope of the critical state line in the $p' - q$ plane; p_c' is the isotropic preconsolidation pressure; p' and q, two stress parameters used in the Cam-clay model, are the mean effective stress and deviator stress, respectively, which are defined as:

$$p' = \frac{1}{3}(\sigma_1' + \sigma_2' + \sigma_3') \tag{7}$$

$$q = \sqrt{\frac{1}{2}[(\sigma_1' - \sigma_2')^2 + (\sigma_2' - \sigma_3')^2 + (\sigma_1' - \sigma_3')^2]} \tag{8}$$

Figure 5. Definition of overconsolidation ratio and yield surface of modified Cam-clay model

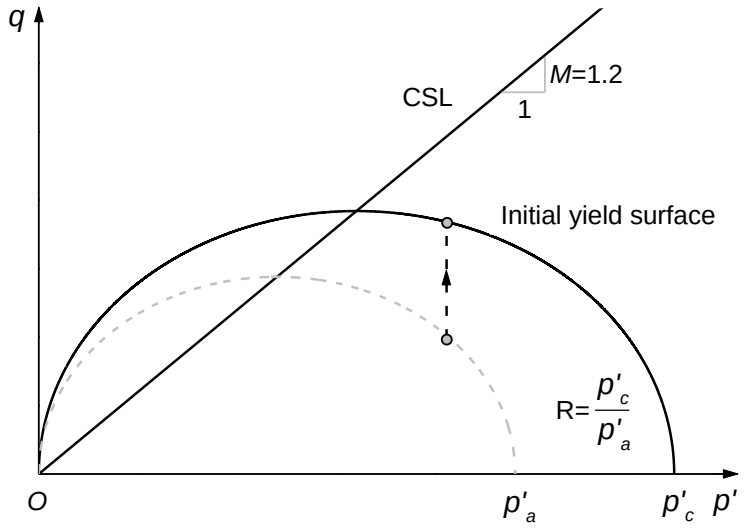

Apart from the parameter *M*, four other parameters (λ, κ, υ_{cs}, and *G*) are needed to define the model, in which λ and κ are the slopes of the virgin consolidation line and swelling line in the $e' - \ln p'$ plane, respectively; υ_{cs} is the specific volume at unit p' on the critical state line in the compression plane and *G* is the shear modulus. The model parameters *M*, λ, κ and υ_{cs}, could be easily determined from isotropic consolidation tests and triaxial tests, while the shear modulus *G,* which depends on the stress state, could be theoretically determined as follows

$$G = \frac{3(1-2v)\upsilon p\prime}{2(1+v)\kappa} \tag{9}$$

where, v is Poisson's ratio; $\upsilon = 1 + e$ is the specific volume.

As show in Figure 5, the overconsolidation ratio *R* in Cam-clay model is defined as the ratio of the isotropic preconsolidation pressure p_c' to the isotropic mean effective stress p_a' (corresponding to current stress state p_0', q_0), which is different from the conventional definition of overconsolidation ratio OCR. The overconsolidation ratio *R* can be related to the conventional overconsolidation ratio OCR through the following relationship

$$R = \frac{1+2K_{0nc}}{1+2K_0}\mathrm{OCR} \tag{10}$$

where, K_{0nc} and K_0 are defined as:

$$K_{0nc} = 1 - \sin\varphi' \tag{11}$$

$$K_0 = K_{0nc}\mathrm{OCR}^{\sin\varphi'} \tag{12}$$

The Cam-clay model used in this analysis can reasonably model the elasto-plastic behaviour of the soil and is capable of predicting the critical state. However, it should be noted that this model is unable to predict the residual state of the soil, and hence it cannot reflect the strain soft behaviour of the soil in the vicinity of the pile. Therefore, the reduction factors presented in this report are only suitable to short rigid piles, though still needing careful calibration before application to designing long flexible piles.

Validation by Rigorous Analytical Solution

Chen and Abousleiman [1] presented a rigorous semi-analytical solution for the undrained expansion of a cylindrical cavity in modified Cam Clay soil. By assuming large strain deformation in the plastic region and adopting Lagrangian description, the formulation of the cavity expansion problem was elegantly reduced to solving a system of first order ordinary differential equations for the radial, tangential, and vertical effective stresses in the plastic zone. The pore pressure subsequently was found to be readily determinable from the radial equilibrium equation in terms of the total stresses. The semi-analytical solution derived in Chen and Abousleiman's work followed the rigorous definitions for the two effective stress invariants without any approximation; thus, it may not only provide an exact and realistic theoretical framework for predicting the soil responses around the cavity, but also serve as a valuable benchmark for verifying various cavity expansion numerical methods involving the critical state plasticity model. Given the fact that pile installation is simulated by undrained expansion of a cylindrical cavity in MCC soil from the initial radius of the pre-bored hole to the radius of the pile followed by vertically shearing, the present numerical model regarding expansion due to pile installation could be well validated by comparing with the rigorous analytical solution of Chen and Abousleiman [1]. To get straightforward comparisons, the soil properties selected here are identical to that of Chen and Abousleiman [1] (summarized in Table 1), in which K_0 denotes the static earth pressure coefficient; σ'_{h} and σ'_{v} represent the horizontal and vertical in situ stresses, respectively. v_0 is the initial value of the specific volume; G_0 is the initial shear modulus; and k_{h} is the horizontal permeability coefficient.

Table 1. Soil properties used to verify numerical model [1]

R	K_0	σ'_h: kPa	σ'_v: kPa	v_0	G_0
1	0.625	100	160	2.09	4348
1.2	0.624	100	160	2.06	4302
3	1	120	120	1.97	4113
10	1.2	144	72	1.80	3756
M=1.2, λ=0.15, κ=0.03, ν=0.278, v_{cs}=2.74; k_h=1E-7 m/s					

Figure 6 compares the cavity pressures calculated from the numerical model with those obtained from the rigorous solution of Chen and Abousleiman [1], in which the instant cavity radius a is normalized with the initial cavity radius $a_{\mathrm{p,pre}}$ and the cavity pressure σ'_a is normalized with the in-situ mean effective stress p'_0. It can be seen that the present numerical model perfectly predicts the cavity pressure during cavity expanding from its initial radius of $a_{\mathrm{p,pre}}$ to the pile radius a_{p}. As seen in the figure, the cavity pressure increases greatly before $a/a_{\mathrm{p,pre}} < 2$. After that, the cavity pressure gradually approaches a constant value, which indicates that the soil at the cavity wall reaches the critical state. This phenomenon indirectly demonstrates that if the radius of the pre-bored hole is larger than 50% of the pile radius, pre-boring will significantly reduce radial total stress of the surrounding soil immediately after installation, the effects of which will further impact the long-term load carrying behaviour of the pile.

Figure 6. Comparisons of cavity pressures during cavity expansion

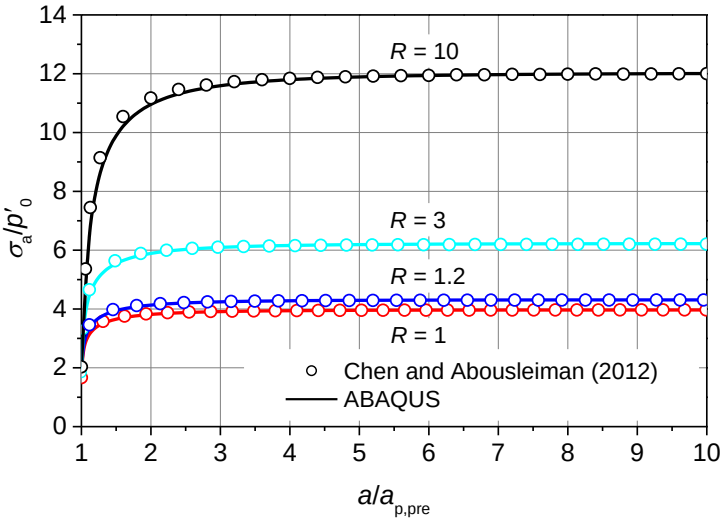

Figure 7 plots the variation of the normalized excess pore pressure $\Delta u/p'_0$ at cavity wall during cavity expansion phase, which shows good agreement between the numerical

model and the rigorous solution. It is interesting to see that both the numerical results and analytical solution predicts the negative excess pore water pressures at the initial stage of cavity expansion in the heavily consolidated soil ($R = 10$), which was also observed from the field tests conducted in heavily consolidated clays [29]. This phenomenon indicates that if the overconsolidation ratio R of the soil and the radius of the pre-bored hole are larger enough, negative excess pore pressure are probably developed immediately after pile installation, which would result in decrease of effective stress and pile load carrying capacity after installation.

Figure 7. Comparisons of excess pore water pressure at cavity wall during cavity expansion

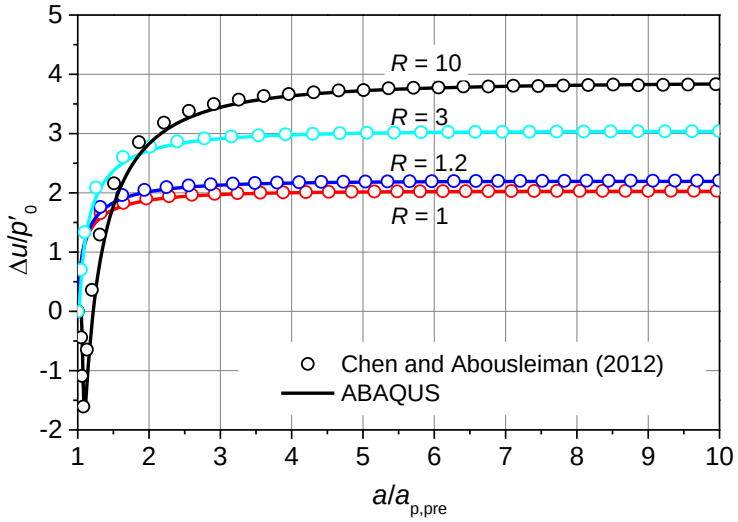

The distribution of stress components and the excess pore water pressures around the pile immediately after cavity expansion in normally consolidated clay ($R = 1$), both from the numerical model and the rigorous solution, are plotted in Figure 8. Given that the stress components in other soils show similar patterns in distribution, only the results in normally consolidated soil ($R = 1$) are shown here. Figure 8 also shows fairly close agreements between the two approaches. From the figure, one can observe that pile installation causes substantial changes in stress state of the surrounding soil. After expansion, the soil in the vicinity of the pile reaches the critical state and the horizontal effective stress increases significantly and becomes the major principal stress. Since the shaft resistance is predominantly governed by the radial effective stress acting on the shaft, it demonstrates that installation has positive effects on the long-term load carrying capacity of the pile.

Figure 8. Comparisons of stress components distributions around cavity immediately after cavity expansion in normally consolidated clay

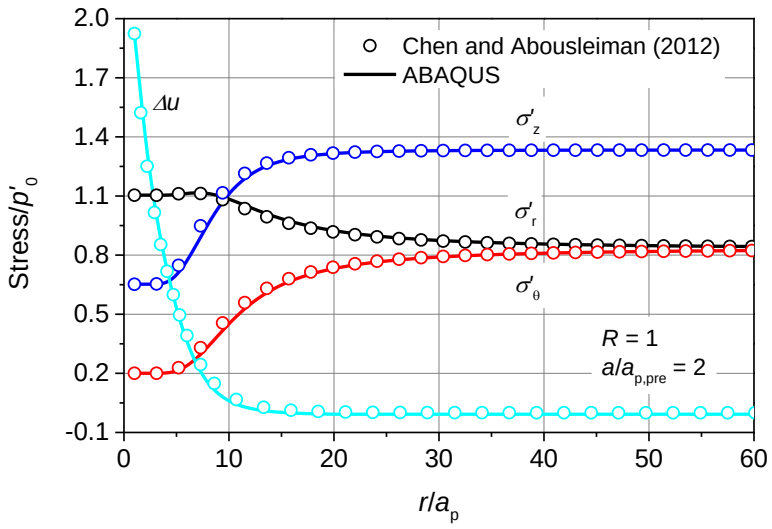

Figure 9 shows the effective stress path of a soil element at the pile shaft during expansion. The comparison again indicates perfectly agreement between the numerical model and the rigorous solution of Chen and Abousleiman [1]. All of the above comparisons sufficiently demonstrate the developed numerical model could yield accurate predictions for the expansion due to pile installation, and hence assures the reliability of the model in the subsequent analysis.

Figure 9. Stress path during cavity expansion (a) $R = 1$; (b) $R = 10$

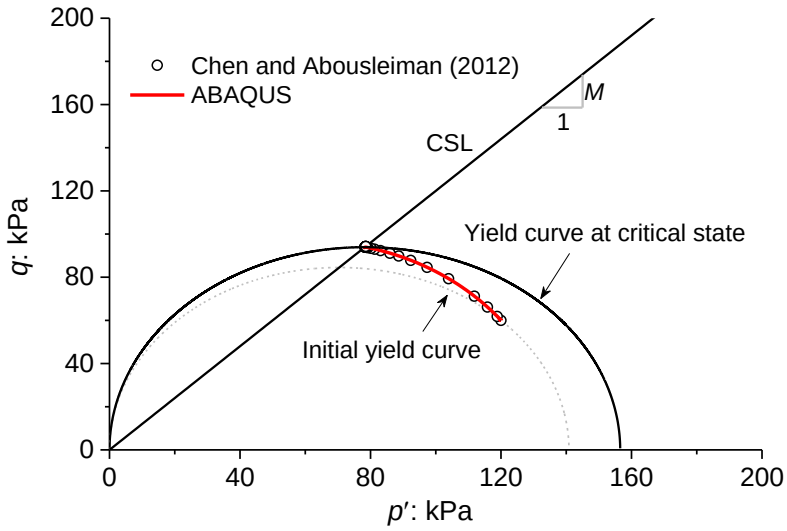

(a)

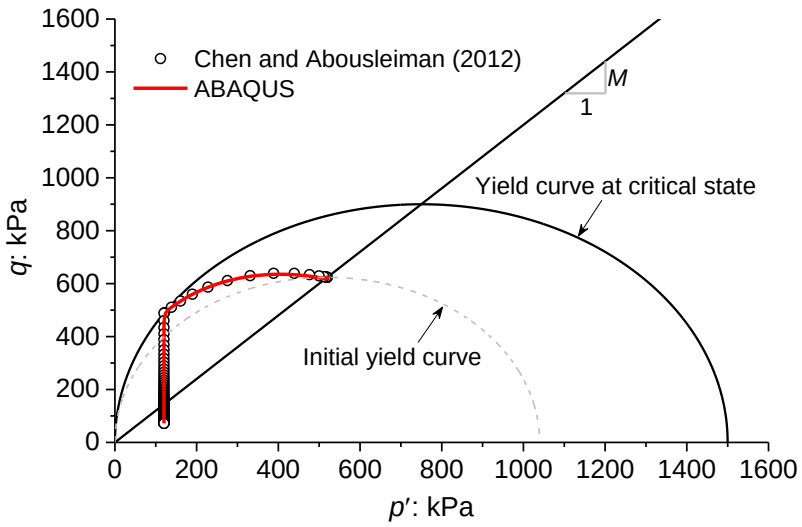

(b)

Reduction Factors for Typical Louisiana Soils

In this part, the numerical model is used to explore the impacts of the pre-bore size on the long-term shaft resistance reduction of pre-bored piles in Louisiana soils. Three representative sites (soil profiles) located at the new Bayou Lacassine Bridge of Highway 14 in Jefferson Davis Parish, Louisiana, are chosen to investigate the reduction factors. Based on the numerical simulations, the reduction factor curves are produced for the three typical Louisiana soil strata, which may provide guidelines for better design and construction of pre-bored piles in Louisiana. These reduction factors potentially can be implemented into the current pile analysis and design software, through directly lowering the α or β coefficient involved to determine the reduced pile capacity. The outcomes of the numerical analysis are also expected to be able to provide guidance for the location of pile instrumentation in the future field validation tests.

Geology and Subsoil Condition of Three Representative Sites in Louisiana

Since the soil conditions vary for different locations of Louisiana, this work is not intended as an exhausting evaluation of the reduction factors for all Louisiana soils with varying parameters. The three representative sites investigated here are located at new

Bayou Lacassine Bridge of Highway 14 in Jefferson Davis Parish, Louisiana (see Figure 10). Site 1 and site 3 are at the two ends of the new Bayou Lacassine Bridge, respectively, while site 2 is in the waterway which is located at the middle of the bridge.

Figure 10. Location of three sites investigated

Haque et al. [81] conducted a thorough investigation on the soil profiles of the three sites to investigate the pile behaviors in these sites. Figure 11 and Figure 12 show the soil profiles explored from boreholes and some basic in-situ soil properties from CPT tests of site 1 and site 3, respectively. It can be seen that the soil stratum of site 1 consisted of dark gray clay in the top 13 m followed by reddish light-brown fat clay down to 16 m. Below the light-brown clay layer, a light-brown lean clay layer with a small amount of silt and sand was extended to a depth of 21 m. The subsurface soils of site 3 mainly consisted of 21 m gray or brown lean clay with occasional traces of silty and sandy clay. The observed long-term groundwater table is approximate at 2.44 m below the ground surface. A series of laboratory consolidation tests, triaxial tests, and dissipation tests were conducted on the high quality Shelby tube samples retrieved from both boreholes at different depths by Abufarsakh et al. [12] to investigate the detailed parameters for MCC model, which are listed in Table 2, Table 3, and Table 4, respectively.

Figure 11. Soil profile and in-situ soil properties of site 1 [81]

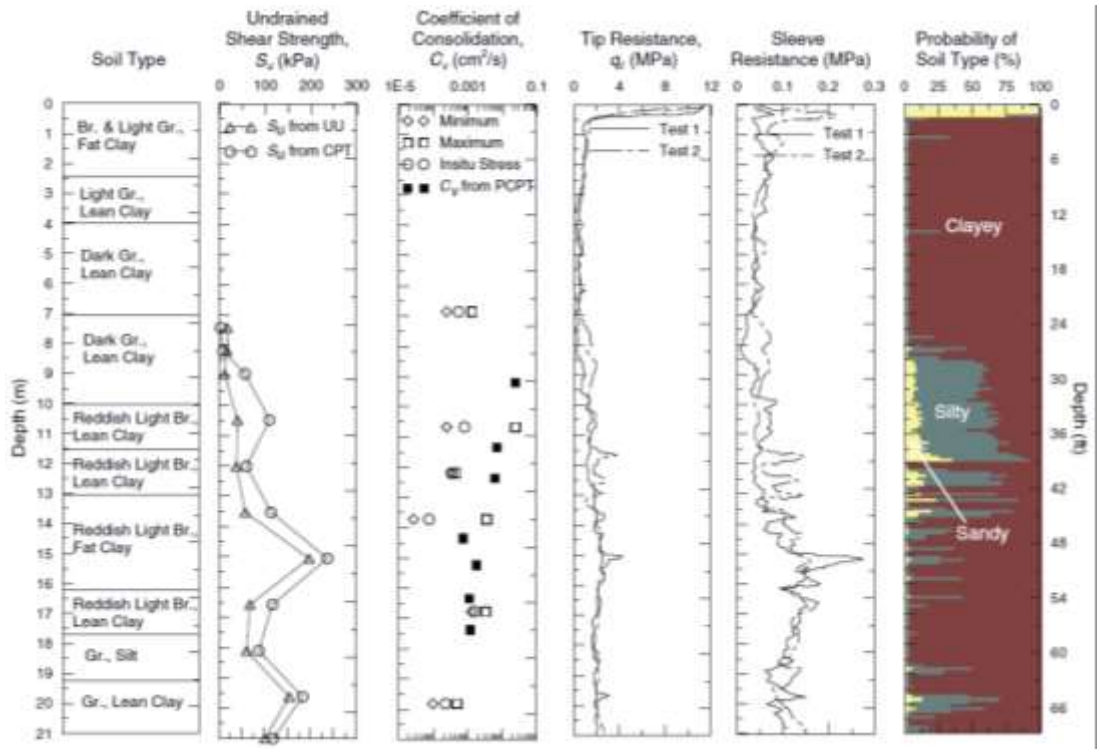

Figure 12. Soil profile and in-situ soil properties of site 3 [81]

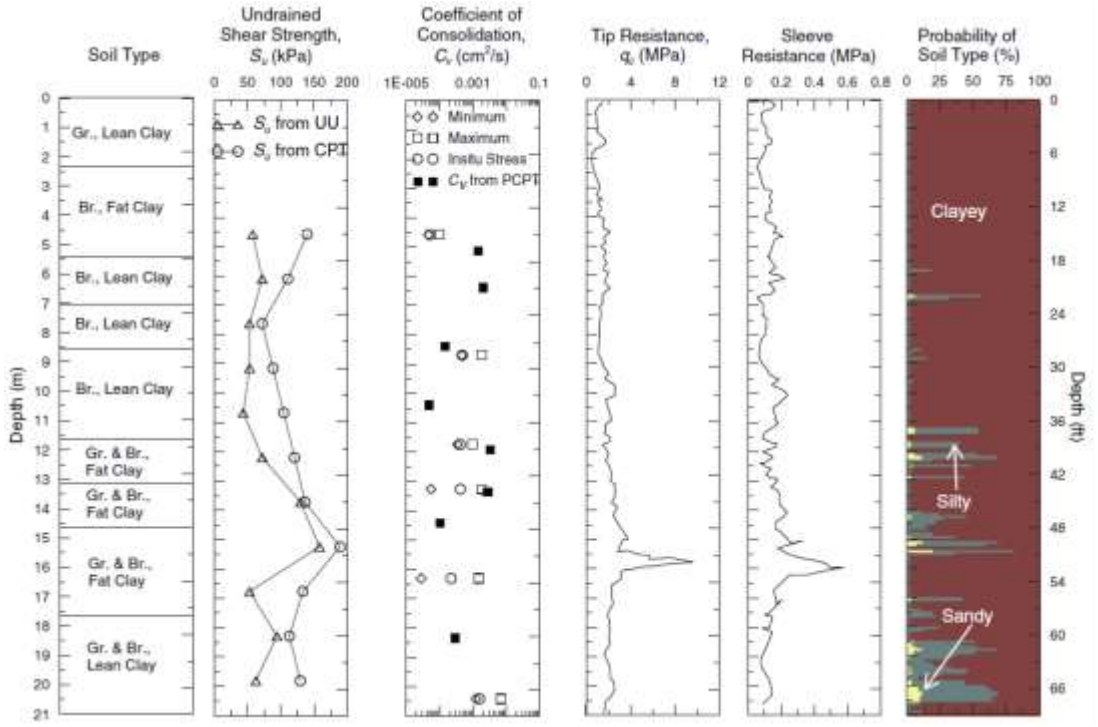

Table 2. Soil parameters of site 1 for MCC model [12]

Layer	Depth (m)	e_0	K_0	OCR	M	λ	κ	K (10^{-9}m/s)	σ'_{v0} (kPa)
1	0-6	0.74	0.6	2.30	0.95	0.078	0.013	8.15	31.41
2	6-9	0.57	0.6	2.00	1.00	0.078	0.013	6.09	34.22
3	9-11	0.65	0.6	1.80	1.10	0.078	0.013	16.5	109.3
4	11-14	0.60	0.7	1.40	0.90	0.056	0.019	5.86	230.1
5	14-21	1.00	0.7	1.00	0.75	0.093	0.014	1.54	589.6

Table 3. Soil parameters of site 2 for MCC model [12]

Layer	Depth (m)	e_0	K_0	OCR	M	λ	κ	k (10^{-9}m/s)	σ'_{v0} (kPa)
1	0-5.5	1.20	1.4	4.00	1.16	0.080	0.03	4.36	95.02
2	5.5-7.6	0.70	0.7	3.00	1.23	0.080	0.03	4.36	109.85
3	7.6-10.4	1.00	0.85	2.50	0.72	0.140	0.05	3.28	255.28
4	10.4-13.4	0.90	0.85	2.00	0.72	0.150	0.05	2.91	351.08
5	13.4-14.9	0.70	0.8	2.00	1.10	0.120	0.04	2.33	229.50
6	14.9-16.0	0.70	0.7	1.80	1.11	0.110	0.04	2.45	276.49
7	16.0-18.0	1.20	0.6	1.20	1.05	0.130	0.04	1.89	328.56
8	18-22.60	0.60	0.6	1.00	0.93	0.120	0.04	1.05	496.54

Table 4. Soil parameters of site 3 for MCC model [12]

Layer	Depth (m)	e_0	K_0	OCR	M	λ	κ	k (10^{-9}m/s)	σ'_{v0} (kPa)
1	0-6.4	0.50	1.2	4.00	0.61	0.104	0.035	3.8	179.96
2	6.4-7.6	0.70	0.8	2.50	1.17	0.100	0.029	4.2	102.16
3	7.6-10	0.70	0.8	2.00	0.90	0.091	0.026	0.62	144.29
4	10-11.6	0.80	0.75	1.70	0.90	0.108	0.035	0.12	249.64
5	11.6-13	0.70	0.8	1.45	0.62	0.108	0.035	7.6	344.95
6	13-16	1.50	0.8	1.40	1.12	0.147	0.061	8.9	321.84
7	16.0-20	0.70	0.67	1.40	0.92	0.100	0.03	0.17	303.39
8	20-23	0.80	0.6	1.00	0.93	0.056	0.013	0.66	348.06

Reduction Factors and Shaft Resistance Factors for Typical Louisiana Soils

Based on these parameters listed in Table 2, Table 3, and Table 4, the reduction factors R_{qs} and the shaft resistance factors α and β are produced by the numerical model for different soil layers of the three sites. These factors, after carefully calibration with the field data, can potentially be applied to the pre-bored piles installed in similar soil stratum of Louisiana, especially these reduction factors, can be directly implemented into the current pile analysis and design software [49] to obtain the reduced pile capacity in similar soil stratum of Louisiana.

Shaft resistance factor and reduction factor of Site 1. Figure 13 plots the reduction factors R_{qs} for different layers of site 1. As seen in Figure 13, the reduction factor R_{qs} decreases with the increase of the size of the pre-bored hole, which demonstrates that the ultimate shaft resistance decreases with the increase of the size of the pre-bored hole according to the definition of R_{qs}. However, the reduction factor decreases insignificantly in the range $0 < a_{\mathrm{p,pre}}/a_{\mathrm{p}} < 50\%$, in which the reduction factor reduces by only 6% and 9% for layer 5 and layer 1, respectively. In the range $a_{\mathrm{p,pre}}/a_{\mathrm{p}} > 50\%$, the reduction factor decreases significantly with the increase of the size of the pre-bored hole. For the hole size proposed by LTRC [21], i.e., $a_{\mathrm{p,pre}}/a_{\mathrm{p}} = 80\%$, the side resistance of layer 1 and layer 5 are about 65% and 77% of the side resistance of a full-displacement pile, respectively. Note that using pre-boring 80% of the side dimension for square piles is roughly equivalent to $a_{\mathrm{p,pre}}/a_{\mathrm{p}} = 70\%$, and for such a value of prebored size the side resistance reduction factor at this site ranges from 0.77 to 0.85. In addition, it can be seen from Figure 13 that the reduction factor decreases with the layer number in site 1, which indicates pre-boring will cause more reduction in the shaft resistance in the upper layer soils of site 1. This is probably because the upper layer

soil is overconsolidated and hence is stiffer than the lower layer soil which is normally consolidated.

Figure 13. Reduction factors in different layers of site 1

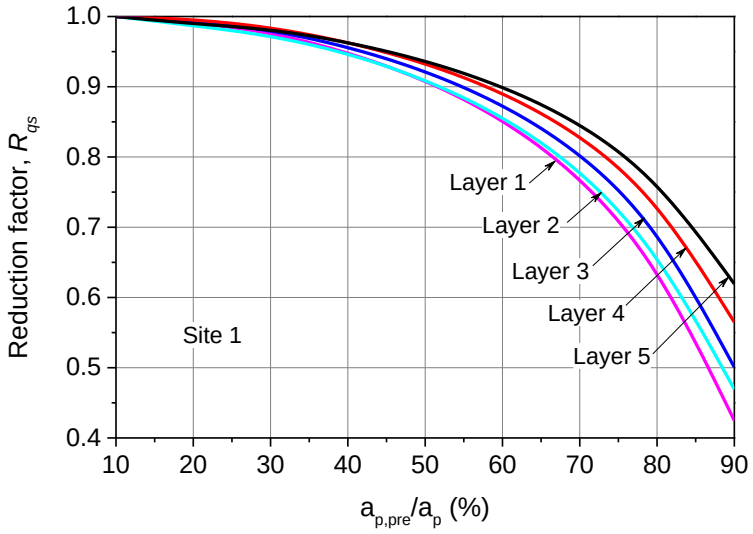

Figures 14 and 15 plot the shaft resistance factors α and β for different layers of site 1, respectively. As seen in Figures 14 and 15, the shaft resistance factors α and β decrease with the increase of the size of the pre-bored hole. Upon inspection of Figures 14 and 15, it can be found that the shaft resistance factors α and β also decrease significantly when $a_{\mathrm{p,pre}}/a_{\mathrm{p}} > 50\%$, while decrease insignificantly in the range of $10\% < a_{\mathrm{p,pre}}/a_{\mathrm{p}} < 50\%$. For the hole size $a_{\mathrm{p,pre}}/a_{\mathrm{p}} = 80\%$, the shaft resistance factor α in site 1 is in the range of 0.5–0.9 and the shaft resistance factor β is the range of 0.21–0.37.

It also can be seen from Figures 14 and 15 that the resistance factor α decreases with the layer number but the shaft resistance factor β does not increase or decrease with layer number in site 1. The shaft resistance factor β of the layer 3 is larger than the factors in other layers. This means that the shaft resistance of a pre-bored pile does not directly relevant to the layer number or the depth.

Figure 14. Shaft resistance factors α in different layers of site 1

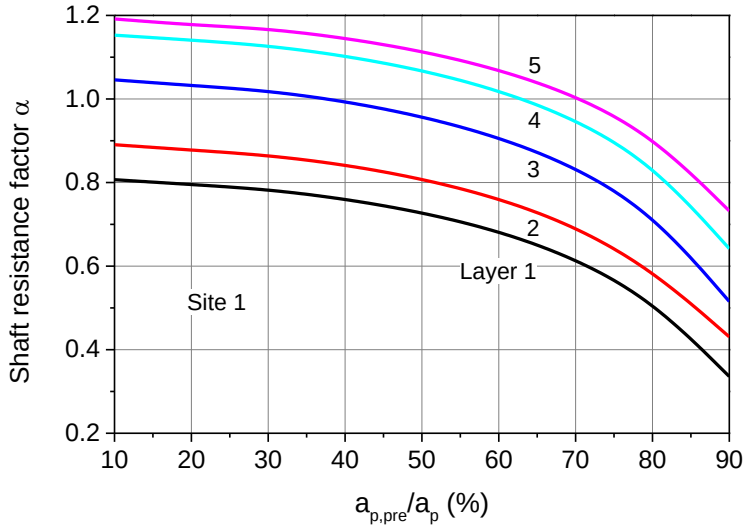

Figure 15. Shaft resistance factors β in different layers of site 1

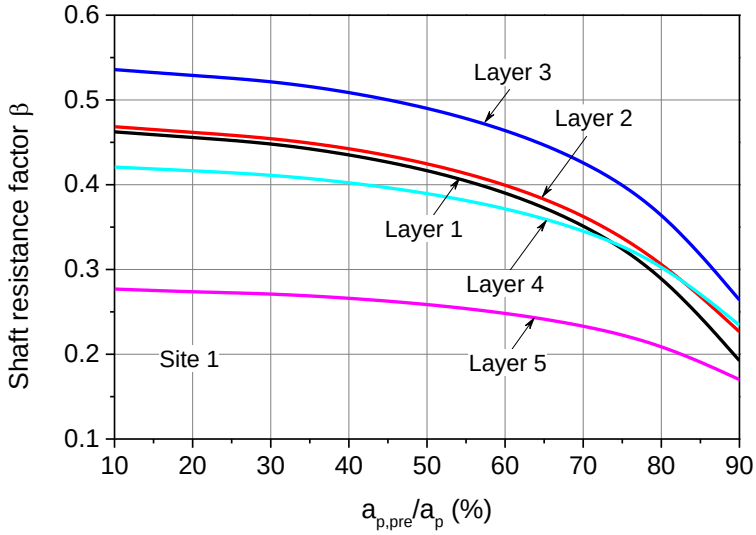

Shaft resistance factor and reduction factor of Site 2. Figure 16 shows the reduction factors R_{qs} for different soil layers of site 2. As seen in Figure 16, the reduction factor does not vary significantly with the layer number in site 2, which indicates that the soil is relative homogeneous at site 2. It also can be seen from Figure 16 that the reduction factor R_{qs} decreases significantly when $a_{\mathrm{p,pre}}/a_{\mathrm{p}} > 50\%$ but decreases insignificantly in the range of $10\% < a_{\mathrm{p,pre}}/a_{\mathrm{p}} < 50\%$ in site 2. When the size of the pre-bored hole increases from 10% to 50% of the pile radius, the reduction factor

decreases by 10%-12%, which means the pre-boring only reduces 10%-12% of the long-term load carrying capacity of the pile. However, the reduction factor decreases by 45%-60% when $a_{\mathrm{p,pre}}/a_{\mathrm{p}}$ increases from 50% to 90%. Hence, if the size of the pre-bored hole is larger than 50% of the pile radius, the long-term load carrying capacity will be greatly reduced. For the hole size proposed by LTRC [21], i.e., $a_{\mathrm{p,pre}}/a_{\mathrm{p}} = 80\%$, the side resistance is about 58%–67% of the side resistance of a full-displacement pile in site 2. The reduction factor for $a_{\mathrm{p,pre}}/a_{\mathrm{p}} = 70\%$ (corresponding to 80% pre-boring size in terms of side dimension for the case of square piles) falls in the range of 0.72–0.79, which indicates the side resistance is around 72%–79% of that of a full-displacement pile in site 2.

Figure 16. Reduction factors in different layers of site 2

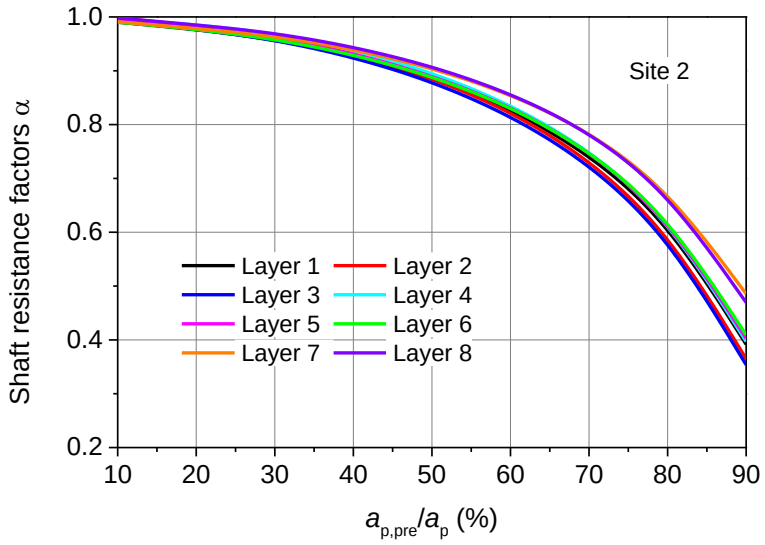

Figures 17 and 18 show the shaft resistance factors α and β for different layers of site 2, respectively. As seen in Figures 17 and 18, the shaft resistance factors α and β decrease with the increase of the size of the pre-bored hole as anticipated. Again, it can be seen that the shaft resistance factors α and β decrease significantly when $a_{\mathrm{p,pre}}/a_{\mathrm{p}} > 50\%$, while decrease insignificantly in the range of $10\% < a_{\mathrm{p,pre}}/a_{\mathrm{p}} < 50\%$. For the hole size $a_{\mathrm{p,pre}}/a_{\mathrm{p}} = 80\%$, the shaft resistance factors α fall in the range of 0.59-0.67 for most soil layers except layer 4 and layer 7. Compared with the shaft resistance factor α, the shaft resistance factors β of different soil layers in site 2 are very scattered. It can be seen that the shaft resistance factors β of layer1 and layer 2 are apparently larger than those of

other soil layers, probably because the upper layer is moderately overconsolidated with larger value of R and K_0.

Figure 17. Shaft resistance factors α in different layers of site 2

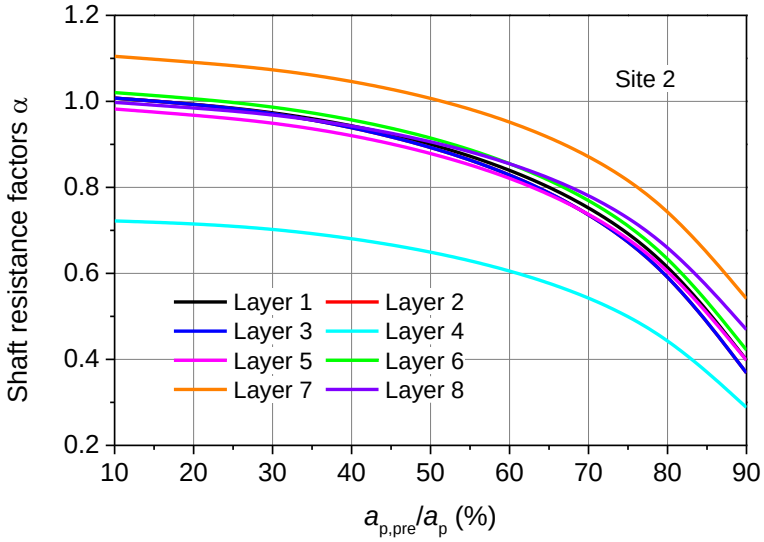

Figure 18. Shaft resistance factors β in different layers of site 2

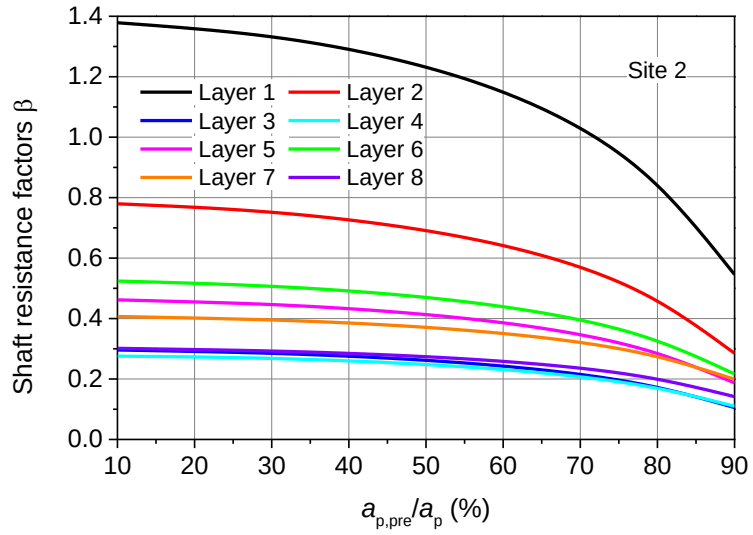

Shaft resistance factor and reduction factor of Site 3. Figure 19 plots the reduction factors R_{qs} for different soil layers of site 3. It can be seen from Figure 19 that the reduction factor curves in site 3 are similar to those in site 1 and site 2. The reduction

factor R_{qs} again decreases significantly when $a_{p,pre}/a_p > 50\%$. For the hole size proposed by LTRC [21], i.e., $a_{p,pre}/a_p = 80\%$, the reduction factor is in the range of 0.45-0.75 for different soil layers, which means the side resistance is about 45%–75% of the side resistance of a full-displacement pile in site 3. When $a_{p,pre}/a_p = 70\%$, the reduction factor falls in the range of 0.63-0.85 at this site. Moreover, it can be observed from Figure 19 that the reduction factor of layer 1 is smaller than that of layer 8, which indicates that more shaft resistance will be reduced by pre-boring in the overconsolidated upper layer of site 3.

Figure 19. Reduction factors in different layers of site 3

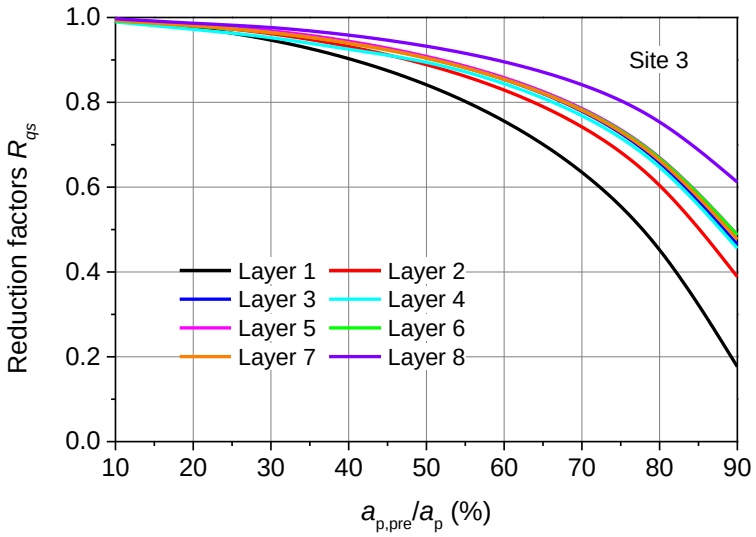

Figure 20 and Figure 21 show the shaft resistance factors α and β for different layers of site 3, respectively. As seen in Figures 20 and 21, the shaft resistance factor curves in site 3 display similar pattern to those in site 1 and in site 2. The resistance factors α and β again decrease significantly when $a_{p,pre}/a_p > 50\%$, while decrease insignificantly in the range of $10\% < a_{p,pre}/a_p < 50\%$. For the hole size $a_{p,pre}/a_p = 80\%$, the shaft resistance factor α in site 3 falls in the range of 0.2-1.0 and the shaft resistance factor β is in the range of 0.13-0.38. Unlike site 1, the shaft resistance factor α does not increase with the layer number, which demonstrates the resistance factors α do not directly depend on the depth of the soil. From these observations, it can be deduced that the shaft resistance of a pre-bored pile primarily depends the size of the pre-bored hole, the overconsolidation ratio, the static earth pressure, the undrained shear strength as well as the friction angle of the soil.

Figure 20. Shaft resistance factors α in different layers of site 3

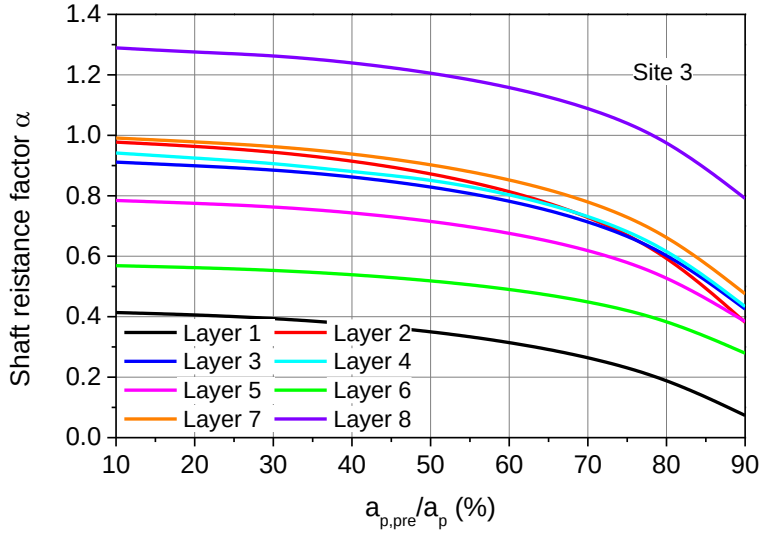

Figure 21. Shaft resistance factors β in different layers of site 3

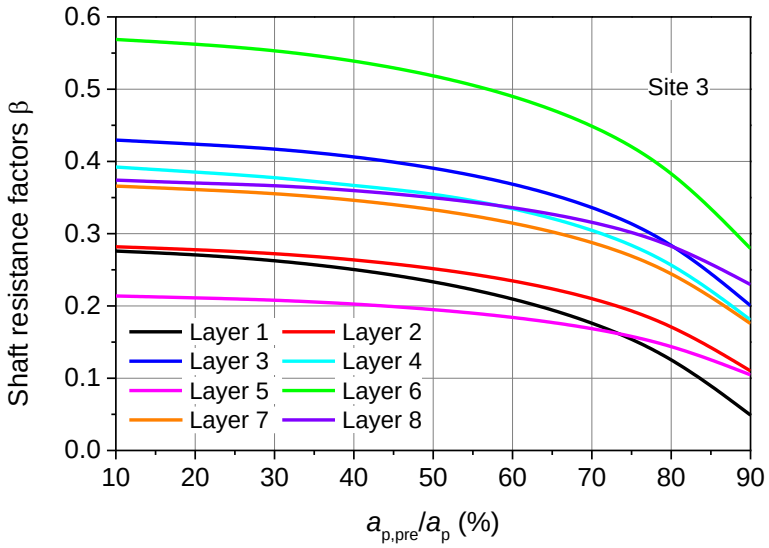

Recommendations for Pile Field Tests in Louisiana

The reduction factors produced by the numerical model should be further calibrated with the field data before they can be applied for use in evaluating the drivability and long-term capacities of real world pre-bored piles. However, after carefully searching the database of Transportation Research Information Services (TRIS), Transportation Research Board (TRB) and American Society of Civil Engineers (ASCE) journal

archives, as well as the publications by Deep Foundation Institute (DFI), Pile Driving Contractors Association (PDCA), and International Association of Drilling Contractors (IADC), it is found that there have been no field tests specifically conducted in Louisiana for quantitatively investigating the impacts of pilot hole size on the load carrying capacity of pre-bored piles.

Recently, Ghose-Hajra and Tavera [2] compiled the state-of-the-art and best practice results nationwide and recommended multiple pile driving sites for future testing of piles in Louisiana as well as the development of an instrumentation testing plan for field data collection with different sizes of pre-bored hole. However, they provided merely a rough guideline for examination of the driven pile capacity within pre-bored soils, yet without any specified recommendations on the size of pre-bored hole to be investigated. Due to the high cost involved, it is impractical to conduct instrumented pile loading tests for each size of pre-bored hole. Hence, based on the numerical analysis conducted in this research, a more detailed preliminary protocol is proposed herein for future pile field tests in Louisiana.

Firstly, the site selection for the intended pile load tests is critical, as the sites must reflect the typical field conditions that require the pre-boring to be used for pile installation. Ghose-Hajra and Tavera [2] investigated the subsurface geologic characteristics of Louisiana and recommended two representative sites for pile field tests. Figure 22 shows the subsurface stratigraphy usually encountered in the two scenarios. As seen in the figure, site 1 is located at north of Louisiana. The soil profile mainly consists of a firm to stiff clay of 20 ft. thickness, and an underlying stiff to very stiff clay layer extending to the elevation of 200 ft. Site 2 is at south of Louisiana. The typical subsurface soils consist of 50 ft. of very soft to soft clay (layer I), 50 ft. of medium to dense sand layer (Layer II) overlaying 100 ft. of stiff clay (Layer III). Since pre-boring technique is usually used in hard/stiff soils to facilitate pile driving, preference should be given to the soil profiles at the north of Louisiana.

Figure 22. Two typical soil profiles of Louisiana

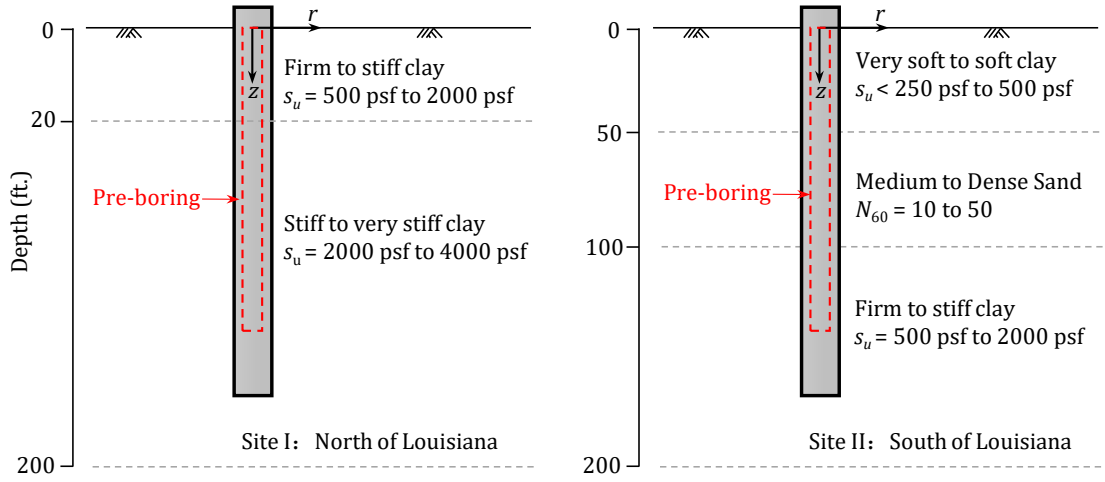

Before conducting the pile tests, soil boring and CPTu sounding are recommended to explore the detailed information and basic properties of the subsurface soils. Apart from the CPTu, the dissipation tests should be conducted at different depths to measure the corresponding coefficients of consolidation. While the soil parameters M, υ_{cs}, λ, and κ for the modified Cam Clay model can be determined through the isotropically consolidated undrained triaxial compression (CIUC) laboratory testing, conducted on the high-quality Shelby tube samples retrieved from the bore-hole. Given the fact that the identified stiff to very stiff clays of site 1 have a thickness of approximately 180 ft, a depth interval of 10 ft. is recommended for data collection to well capture the variation of soil properties with depth.

It is recommended that the pile be instrumented with stress transducer, soil pressure transducers, pore pressure transducers, and the vibrating wire strain gauge to record the driving force, the soil pressure, the pore water pressure and the strain of the pile during the test. The suggested instrumentations are shown in Figure 23. During pile installation, the driving force, the deformation of the pile, the soil pressure and the pore water pressure measurements recorded by these transduces will be used to check the validity of the developed numerical model. Since the piles in saturated clayey soils exhibits setup effects after installation, it is recommended that the static pile loading test should to be conducted when the reading of the pore water pressure transducer approaches the hydrostatic porewater pressure.

The quick test procedure suggested by ASTM standard D1143 [82] is recommended for the static loading tests. According to the quick test procedure, the loads should be applied step-by-step with an increment of 5% of the anticipated failure load. During each load interval, the settlement at the pile head should be recorded after the load has been applied and maintained for a time interval of 5 min. Since the numerical analysis shows that the reduction factor decrease significantly when $a_{\mathrm{p,pre}}/a_{\mathrm{p}} > 50\%$ for different soil layers at different sites, it is recommended that the pile tests should be conducted for the cases of $a_{\mathrm{p,pre}}/a_{\mathrm{p}} = 60\%,\ 70\%,\ 80\%$ and 90%. A full displacement pile test, i.e., $a_{\mathrm{p,pre}}/a_{\mathrm{p}} = 0\%$, is also recommended to be conducted as the reference for comparison.

Figure 23. Recommended instrumentation of model pile

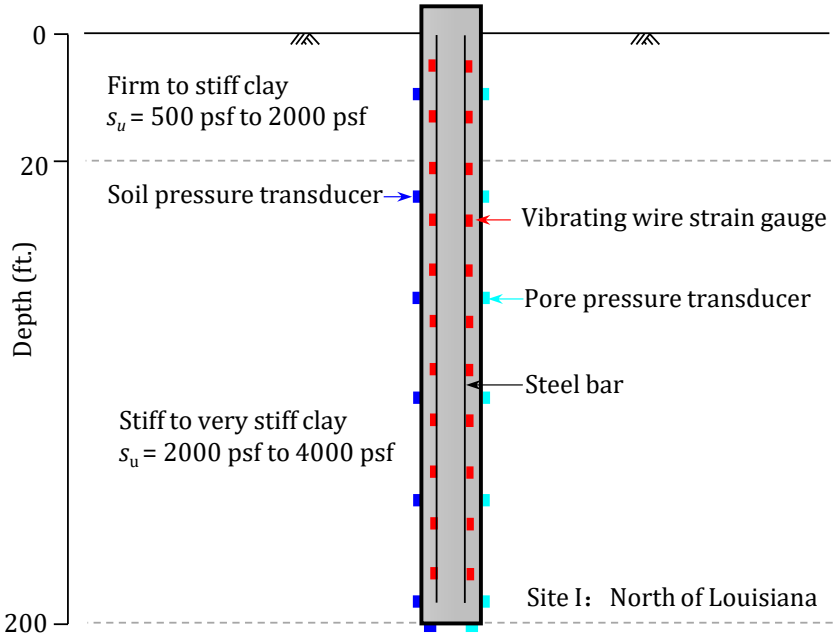

The field data gathered from the pile load tests should compared with the numerical results. Whenever necessary, some correction factors may be introduced to better fit the data collection and to improve the accuracy of the theoretical/numerical method proposed for predicting the side friction of pre-bored piles.

Development of Design Formulas for Pre-bored Piles

This part continues on the topic of driving force and shaft resistance of pre-bored piles but special attention is given to the setup of pre-bored piles besides the long-term shaft

resistance. To evaluate the shaft resistance of the pre-bored piles, the changes of the stress state, excess pore water pressures and the shear strength in every stage involved from installation to loading, should be properly taken into consideration in deriving the analytical approach.

Figure 24. Schematic illustration of stages involved in installation and loading of a pre-bored pile

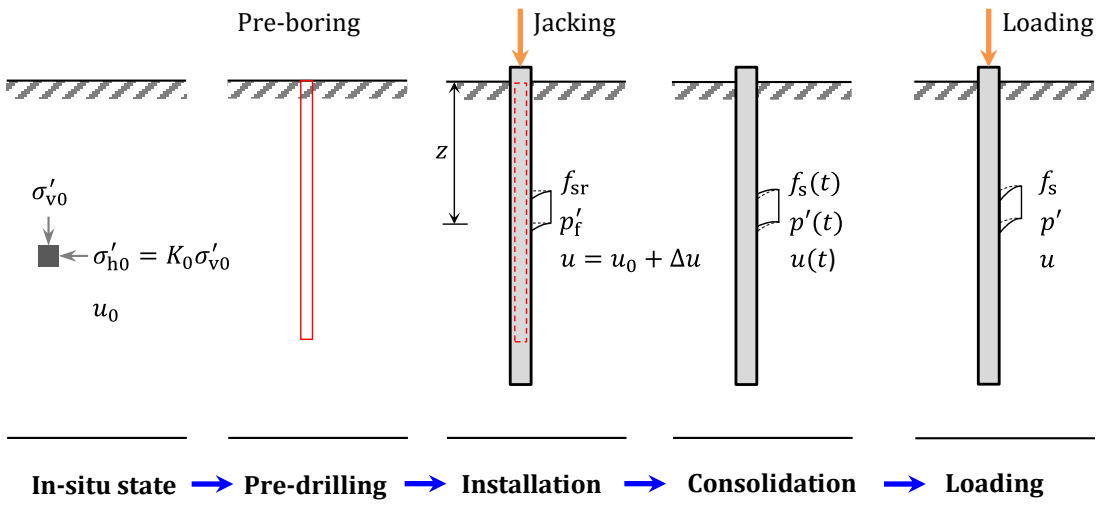

Figure 24 illustrates the various stages typically encountered in the installation and loading of a pre-bored pile, which consists of pre-boring, pile installation, consolidation, and loading. As seen in the figure, the foundation is K_0-consolidated with in-situ static pore water pressure u_0. The in situ horizontal effective stress σ'_{h0} equals to the product of in situ vertical effective σ'_{v0} and coefficient of earth pressure at rest K_0. Before pile installation, a pilot hole, the radius of which is smaller than the radius of the pile, is first drilled to the prescribed depth. As a first approximation, it is assumed that the unloading during pre-drilling is an elastic process and the stress state can be fully recovered when the wall of the hole expands to the initial location during pile installation. Hence, the stability of the pre-bored hole itself is not an issue and the contraction of the pre-drilled hole and the change of the stress state during pre-boring phase are ignored in this study. After pre-boring the hole, the displacement pile is installed in the pre-drilled hole with the radius of the hole expanding from the initial radius $a_{p,pre}$ to the pile radius a_p as the pile tip pushes the wall of the pre-drilled hole away from the path of the pile. During this stage, the soil surrounding the pile is severely squeezed and sheared to the residual state with residual shaft resistance equal to f_{sr}. Due to the squeezing and shearing effects, excess pore water pressure Δu is generated in the soil adjacent to the pile, which results

in the decreases of the mean effective stress p' and the shear strength s_u of the surrounding soil. After pile installation, the excess pore water pressure generated by installation dissipates over time under the hydraulic gradient accompanying the increase of mean effective stress. As a result, the shear strength of the soil recovers from the residual state and the load carrying capacity of the pile increases with time, which is referred to as setup effects. During consolidation, the locked residual shaft resistance f_{sr} at the pile-soil interface experiences a little release with strain of the soil induced by consolidation. Given the fact that the strain during consolidation is relatively small, the release of the residual shaft resistance f_{sr} during consolidation is ignored in this study. After primary or full consolidation, static load test will be conducted to determine the load-carrying capacity of the pile. In this phase, the shaft resistance f_s that relates to the shear strength of the soil adjacent to the pile will be mobilized with the vertical displacement of the pile until reaches the ultimate state. Since the load carrying capacity of the pile mainly depends on the shear strength of the soil adjacent to the pile, the setup, shaft resistance of pre-bored piles as well as the reduction effects of pre-boring can be essentially attributed to the changes of the stress state of the soil around the pile in every stage involved from installation to loading of the pre-bored pile. Hence, determinations of the stress state and shear strength of the soil in every phase constitute the major work of this part.

Mechanical Model for Pre-bored Pile Installation

Figure 25 schematically shows installation of a displacement pile in the pre-drilled hole. As shown in Figure 25a, the soil in the vicinity of the pre-drill hole will be pushed outwards away from the path of the pile and simultaneously be vertically sheared to residual state during pile installation in the pre-drilled hole. The horizontal strain of the soil resembles closely that around an expanding cylindrical cavity [59], while the vertical strain is similar to that developed under plane strain condition in the vertical plane [83]. Based on this deformation mechanism of the soil around the pile, the pile installation process can be approximately split into two separate phases: horizontal undrained expansion of the pre-drilled hole and vertically shearing of the soil in the vicinity of the pile to residual state. Although the horizontal and vertical strains occur simultaneously during pile installation, separating this process allows the analytical solution to be derived so as to evaluate the pile installation effects. Basu et al. [71] and Abufarsakh et al. [12] also treated pile installation as expansion of a cylindrical cavity followed by vertical shearing the soil to failure and investigated pile installation effects through finite element analysis, the results of which showed sufficient accuracy when compared with the field

tests results. Hence, the pile installation is firstly regarded as undrained expansion of a cylindrical cavity and thus the installation effects can be evaluated through the cavity expansion solution.

Figure 25. (a) Pre-bored pile installation; (b) expansion of pre-drilled hole

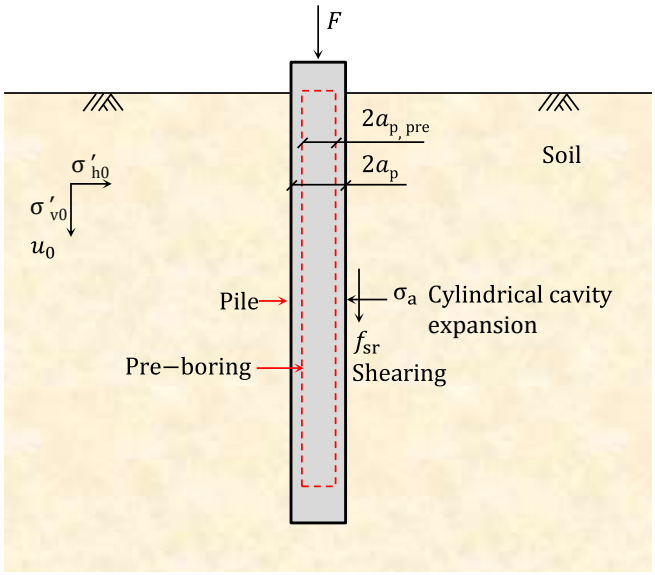

(a)

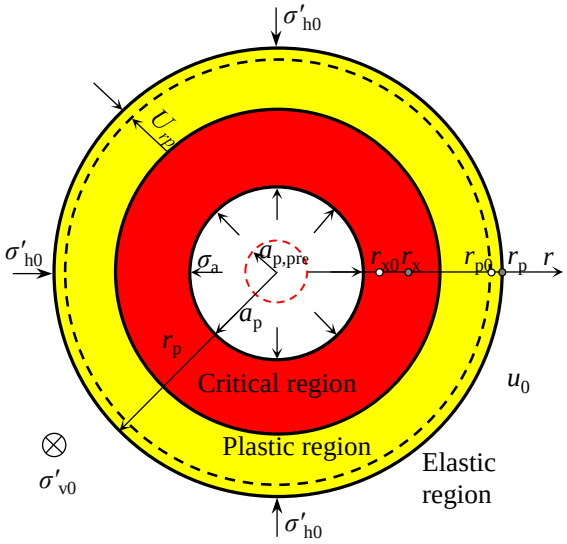

(b)

Figure 25b shows the top view of the pre-drilled hole expanding from its initial radius $a_{\mathrm{p,pre}}$ to the pile radius a_{p}. Three typical zones, the internal critical state zone, the intermediate plastic zone and external elastic zone are formed around the hole after expansion. Chen and Abousleiman [1] presented an exact semi-analytical solution for undrained expansion of a cylindrical cavity in critical state soils, which, however, is not easily implemented in the pile installation and subsequent consolidation analysis as numerical method must be used to solve the complicated governing differential equations. Therefore, a simplified analytical solution is developed using the MCC model based on the following three important observations from Chen and Abousleiman [1] to assess the expansion effects:

- In the critical zone, the vertical effective stress equals to the average of the radial and tangential effective stresses regardless of the in-situ stress state of the soil;
- As shown in Figure 26, the effective stresses instantly reach critical state values once the cavity expands, whereas the total stresses still keep increasing until $a/a_{\mathrm{p,pre}} = 3$, after which the total stresses also gradually reach constant values;
- The soil immediately reaches the critical state after yielding, and thus the distribution of the value of $\sigma'_{\mathrm{r}}-\sigma'_{\theta}$ in the plastic region can be approximately assumed to equal to $\sigma'_{\mathrm{rf}}-\sigma'_{\theta\mathrm{f}}$, as shown in Figure 27, where σ'_{r} and σ'_{θ} are the radial and tangential effective stresses in the plastic zone; σ'_{rf} and $\sigma'_{\theta\mathrm{f}}$ denote the radial and tangential effective stresses in the critical state zone.

Figure 26. Variations of stress components at wall of pre-drilled hole during expansion: (a) $R = 1$; (2) $R = 3$ [1]

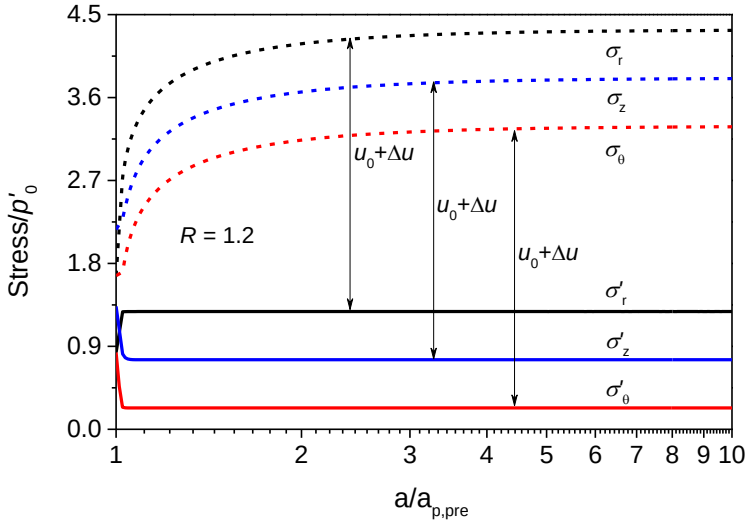

(a)

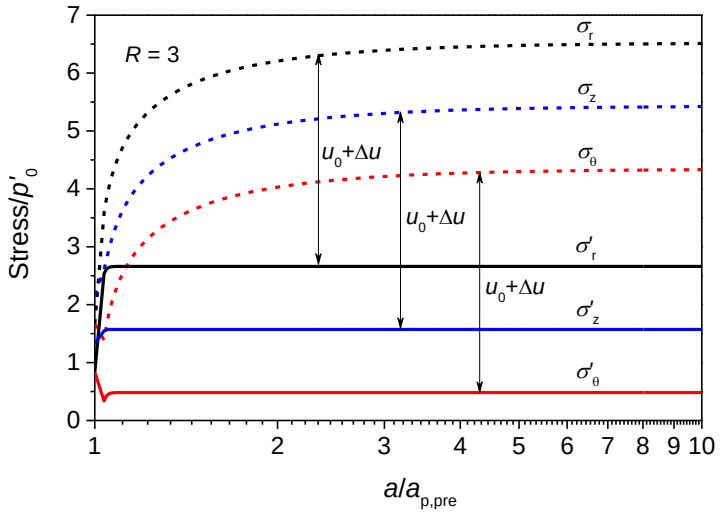

(b)

Figure 27. Actual and assumed distributions of $\sigma'_r - \sigma'_\theta$ around pre-drilled hole

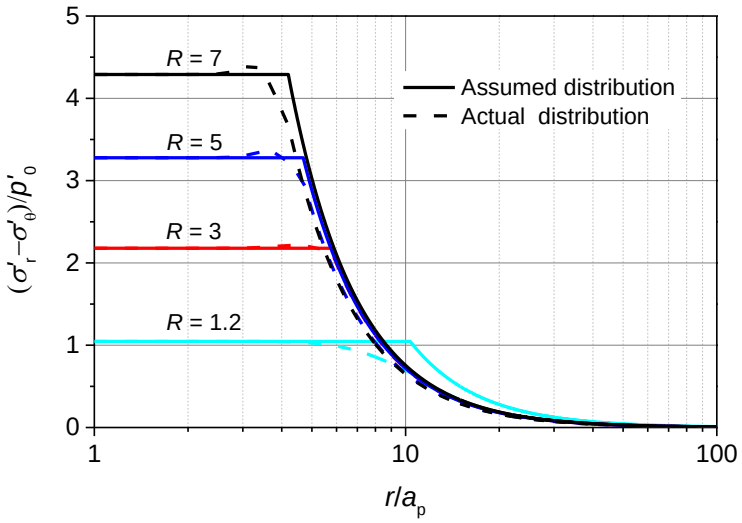

During the expansion phase, the equilibrium equation of a soil element around the hole can be expressed in terms of the effective stress as follows:

$$\frac{\partial \sigma_r}{\partial r} + \frac{\sigma_r - \sigma_\theta}{\partial r} = 0 \qquad (13)$$

Simplified Solution for Pile Installation

Simplified Cavity Expansion Solution. Based on the elasticity theory, the three effective stress components σ'_r, σ'_θ and σ'_z, the radial displacement U_r, and the excess pore water pressure Δu in the elastic zone can be easily determined by combing the equilibrium equation, Hooke's law and the small strain theory as follows [1, 73]:

$$\sigma'_r = \sigma'_{h0} + \left(\sigma'_{rp} - \sigma'_{h0}\right)\left(\frac{r_p}{r}\right)^2 \qquad (14)$$

$$\sigma'_\theta = \sigma'_{h0} - \left(\sigma'_{rp} - \sigma'_{h0}\right)\left(\frac{r_p}{r}\right)^2 \qquad (15)$$

$$\sigma'_z = \sigma'_{v0} \qquad (16)$$

$$U_r = r_x - r_{x0} = \frac{\sigma'_{rp} - \sigma'_{h0}}{2G_0}\frac{r_p^2}{r} \qquad (17)$$

$$\Delta u = 0 \tag{18}$$

where, G_0 is the in situ shear modulus of the soil; r_p represents the radius of the plastic zone around the hole; σ'_rp is the radial effective stress at the elastic-plastic (E-P) boundary. The values of σ'_rp and r_p can be determined from the yield function of the MCC model and the undrained expansion condition. The detailed expressions for σ'_rp and r_p can be given as [1]:

$$\sigma'_\mathrm{rp} = \sigma'_\mathrm{h0} + \frac{1}{\sqrt{3}}\sqrt{q_\mathrm{p}^2 - \left(\sigma'_\mathrm{h0} - \sigma'_\mathrm{v0}\right)^2} \tag{19}$$

$$r_\mathrm{p} = 2G_0\sqrt{\frac{a_\mathrm{p}^2 - a_\mathrm{p,pre}^2}{(\sigma'_\mathrm{rp} - \sigma'_\mathrm{h0})(4G_0 - \sigma'_\mathrm{rp} + \sigma'_\mathrm{h0})}} \tag{20}$$

where, q_p is the deviator stress at the E-P boundary, which is given as

$$q_\mathrm{p} = Mp'_0\sqrt{R\left(1 + \frac{\eta_0^2}{M^2}\right) - 1} \tag{21}$$

where, $p'_0 = (2\sigma'_\mathrm{h0} + \sigma'_\mathrm{v0})/3$ is the initial mean effective stress; $\eta_0 = q_0/p'_0$ is the initial stress ratio; q_0 is the in-situ deviator stress.

For the MCC model, the critical state condition can be given as

$$q_\mathrm{f} = Mp'_\mathrm{f} \tag{22}$$

where, p'_f and q_f denote the mean effective stress and the deviatoric stress at the critical state. For undrained loading, p'_f and q_f of MCC model can be given as (Woods 1990):

$$p'_\mathrm{f} = p'_0\left(\frac{R}{2}\right)^{\Lambda} \tag{23}$$

$$q_\mathrm{f} = Mp'_0\left(\frac{R}{2}\right)^{\Lambda} \tag{24}$$

where, $\Lambda = 1 - \kappa/\lambda$ is the plastic volumetric strain ratio.

Based on the first observation, the vertical effective stress should be the average of the radial and tangential stresses in the critical state zone:

$$\sigma'_{zf} = \frac{1}{2}(\sigma'_{rf} + \sigma'_{\theta f}) \quad (25)$$

where, σ'_{rf} , $\sigma'_{\theta f}$ and σ'_{zf} are the radial, tangential, and vertical effective stresses in the critical region.

Combining equations (25)-(27), the radial and tangential stress components σ'_{rf} and $\sigma'_{\theta f}$ can be obtained as:

$$\sigma'_{rf} = p'_f + \frac{\sqrt{3}}{3} M p'_f \quad (26)$$

$$\sigma'_{\theta f} = p'_f - \frac{\sqrt{3}}{3} M p'_f \quad (27)$$

Integrating the equilibrium equation from the plastic radius to an arbitrary location, the radial total stress in the plastic region can be expressed as

$$\sigma_r = \sigma_{rp} - \int_{r_p}^{r} \frac{(\sigma'_r - \sigma'_\theta)}{r} dr \quad (28)$$

Since σ'_r and σ'_θ are unknown variables and depend on the radial location in the plastic region, equation (30) cannot be integrated to give an analytical solution. However, the third observation shows that the value of $\sigma'_r - \sigma'_\theta$ in the plastic region is close to the $\sigma'_{rf} - \sigma'_{\theta f}$ (see Figure 27). Hence, approximately assuming that $\sigma'_r - \sigma'_\theta$ is equal to $\sigma'_{rf} - \sigma'_{\theta f}$ in the plastic region and substituting equations (28) and (29) into equation (30), the radial total stress in the plastic region can be obtained as:

$$\sigma_r = \sigma_{rp} - \frac{2\sqrt{3}}{3} q_f \int_{r_p}^{r} \frac{1}{r} dr = \sigma_{rp} + \frac{2\sqrt{3}}{3} q_f \ln \frac{r_p}{r} \quad (29)$$

Substituting equation (22) into equation (31), the radial total stress in the plastic region around the pre-drilled hole can be finally written as:

$$\sigma_r = \sigma_{rp} + \frac{\sqrt{3}}{3} q_f \ln \frac{4G_0^2(a_p^2 - a_{p,pre}^2)}{r^2(\sigma'_{rp} - \sigma'_{ho})(4G_0 - \sigma'_{rp} + \sigma'_{ho})} \quad (30)$$

The second observation shows that the effective stresses instantly reach critical state values once the cavity expands. Hence, it can be approximately assumed that the effective stress components in the plastic zone equal to those in critical state zone. Then, the tangential and vertical total stresses σ_θ and σ_z can be derived from equations (26) and (27) as:

$$\sigma_\theta = \sigma_{rp} + \frac{\sqrt{3}}{3} q_f \ln \frac{4G_0^2(a_p^2 - a_{p,pre}^2)}{r^2(\sigma'_{rp} - \sigma'_{h0})(4G_0 - \sigma'_{rp} + \sigma'_{h0})} - \frac{2}{\sqrt{3}} q_f \quad (31)$$

$$\sigma_z = \sigma_{rp} + \frac{\sqrt{3}}{3} q_f \ln \frac{4G_0^2(a_p^2 - a_{p,pre}^2)}{r^2(\sigma'_{rp} - \sigma'_{h0})(4G_0 - \sigma'_{rp} + \sigma'_{h0})} - \frac{1}{\sqrt{3}} q_f \quad (32)$$

Based on the principle of effective stress, the excess pore water pressure in the plastic region generated by pile installation can be approximately given as:

$$\Delta u = \sigma_{rp} + \frac{\sqrt{3}}{3} q_f \ln \frac{4G_0^2(a_p^2 - a_{p,pre}^2)}{r^2(\sigma'_{rp} - \sigma'_{h0})(4G_0 - \sigma'_{rp} + \sigma'_{h0})} - p'_f - \frac{\sqrt{3}}{3} M p'_f \quad (33)$$

Effect of Vertical Shearing. Since the soil in the vicinity of the pre-drilled hole immediately reaches the critical state once the pre-drilled hole expands, the vertical shearing will not further alter the mean effective stress and deviator stress of the soil for the Cam Clay model used in the analysis, but will induce shear stress and adjust the magnitudes of the three stress components in the vicinity of the pile. Figure 28 shows the Mohr's stress circle and the corresponding failure stress state of the soil adjacent to the pile in the vertical shearing plane during shearing. As the vertical shearing primarily occurs in the vertical plane, the radius of the Mohr' circle approximately equals to the undrained shear strength of the soil under plane strain condition, $s_{u,ps}$. From the simple geometry shown in the figure, the shear stress, $f_{s,I}$, at the pile shaft can be expressed by the undrained shear strength under plane strain condition as follows:

$$f_{s,I} = s_{u,ps} \cos\varphi' \quad (34)$$

where, φ' is the effective friction angle of the soil.

Figure 28. Mohr's stress circle and failure stress state of soil adjacent to pile in vertical shearing plane

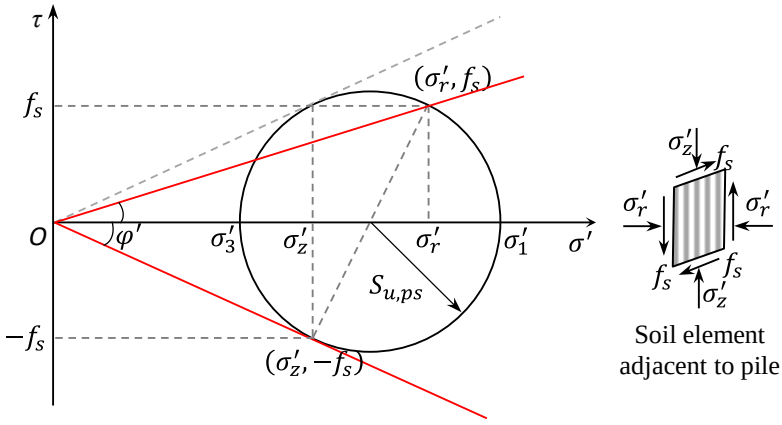

Based on the Mohr-Coulomb strength criterion, the undrained shear strength under plane strain condition $s_{\mathrm{u,ps}}$ can be related to the undrained shear strength under triaxial compression, $s_{\mathrm{u,tc}}$ as follows [83]:

$$s_{\mathrm{u,ps}} = \frac{1}{3}(3 - \sin\varphi')s_{\mathrm{u,tc}} \tag{35}$$

In the critical state soil theory, the undrained shear strength in terms of triaxial compression, $s_{\mathrm{u,tc}}$, can be expressed as:

$$s_{\mathrm{u,tc}} = \frac{1}{2}q_{\mathrm{f}} = \frac{1}{2}Mp'_0\left(\frac{R}{2}\right)^{\Lambda} \tag{36}$$

Combining equations (36)–(38), the shear stress f_{s} at the pile shaft immediately after pile installation can be given as:

$$f_{\mathrm{s,I}} = \frac{1}{6}(3 - \sin\varphi')\cos\varphi' Mp'_0\left(\frac{R}{2}\right)^{\Lambda} \tag{37}$$

It should be noted that in the actual situation, the vertical shearing effect of pile installation shears the soil in the vicinity of the pile to residual state and the shear stress should be related to the residual shear strength of the soil. However, the MCC model used in the analysis is unable to predict the residual state of the soil, although it can reasonably model the elasto-plastic behaviour of the soil and is capable of predicting the critical state. Hence, the shear stress $f_{\mathrm{s,I}}$ presented by equation (39) in fact corresponds to the peak shaft resistance rather than the actual residual shaft resistance f_{sr}. Given the fact that

the actual shaft residual resistance f_{sr} during pile installation is relatively small, the shaft resistance after pile installation primarily stems from the recovered shear strength. Hence, the shear stress $f_{\mathrm{s,I}}$, locked at the pile-soil interface after pile installation, should be subtracted from the ultimate shaft resistance when evaluating the setup and long-term load carrying capacity of the pre-bored piles. Subtraction of the locked shear stress $f_{\mathrm{s,I}}$ will eliminate the errors caused by the soil model and provide conservative but reliable estimation of the setup and long-term shaft resistance, which will be shown later.

Driving Force of Pre-bored Pile

Shaft resistance. As shown in Figure 29, the shaft resistance, f_s, during pile installation is the sliding friction between the soil and the pile shaft, which can be calculated based on Mohr-Coulomb's friction law as:

$$f_s = \sigma'_{rf}\tan\delta' \tag{38}$$

where, δ' is the effective internal friction angle between the pile and the soil. Due to the larger deformation developed at the pile-soil interface during pile driving, the soil adjacent to the pile reaches the residual state and thus the internal friction angle between the pile and the soil during pile installation is much smaller than the effective internal friction angle of the soil and usually equals to the residual friction angle of the soil φ'_r.

Since the effective stress instantly reaches the ultimate value once the cavity expands, the effective stresses acting on the pile shaft will be the same for different sizes of pre-boring during pile installation. Hence, it can be concluded that the shaft resistance is independent of the size of the pre-drilled hole during pile installation. Integrating the shaft resistance along the embedded depth of the pile, the force, $F_{s,pre}$, provided by the pile shaft resistance during installation can be given as:

$$F_{s,pre} = \int_0^h 2\pi a_p f_s dl = \int_0^h 2\pi a_p \left(p'_f + \frac{\sqrt{3}}{3} M p'_f\right)\tan\delta' dl \tag{39}$$

Figure 29. Schematic representation for pre-bored pile installation

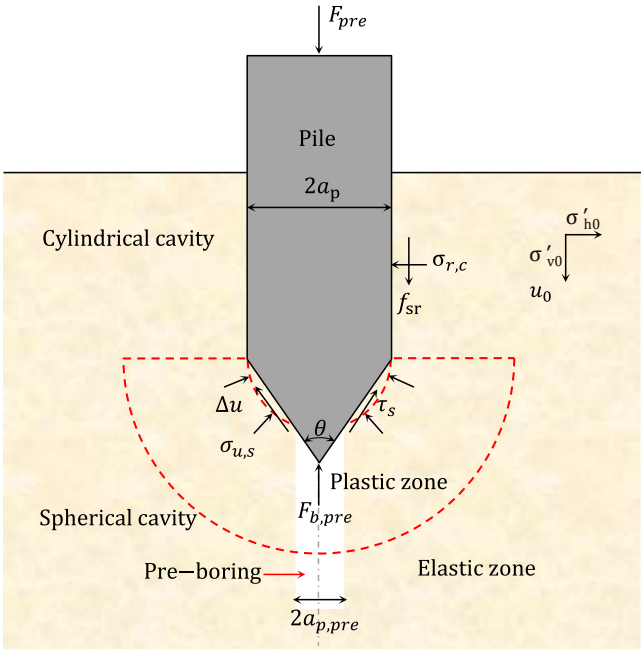

Pile Tip Resistance. As shown in Figure 29, the pile tip resistance during installation consists of the vertical components of the expansion pressure and the sliding friction acting on the pile tip. Hence, based on equilibrium condition in the vertical direction, the force , $F_{b,pre}$, provided by the pile tip resistance during installation can be given as:

$$F_{b,pre} = \pi\left(a_p^2 - a_{p,pre}^2\right)\left(\sigma'_{u,s}\tan\delta\cot\frac{\theta}{2} + \sigma_{u,s}\right) \quad (40)$$

where, θ is the apex angle of the pile tip.

It can be seen from equation (42) that although the sliding friction acting on the pile tip are the same as the effective stress instantly reaches the critical state once the cavity expands, the expansion pressure and the contact area between the pile tip and the soil are different for different sizes of pre-bored hole. This is the primary cause that pre-boring reduces the driving force in hard/stiff soils. It should be noted when the size of pre-bored hole $a_{p,pre}$ approaches the zero, the pile tip force $F_{b,pre}$ calculated from equation (42) becomes the pile tip force of a full displacement pile.

Total Driving Force. Based on equation (41) and (42), the total driving force, F_{pre}, of a pre-bored pile can be obtained by adding up the force $F_{s,pre}$ provided by the pile shaft and the force $F_{b,pre}$ provided by the pile tip:

$$F_{pre} = F_{b,pre} + F_{s,pre} \tag{41}$$

Driving Force Reduction Factor. To evaluate the effects of pre-boring on the drivability of pre-bored piles, a reduction factor, $R_{d,pre}$, is defined as follows:

$$R_{d,pre} = \frac{F_{pre}}{F_d} = \frac{\pi\left(a_p^2 - a_{p,pre}^2\right)\left(\sigma'_{u,s}\tan\delta\cot\frac{\theta}{2} + \sigma_{u,s}\right) + \int_0^h 2\pi a_p\left(p'_f + \frac{\sqrt{3}}{3}Mp'_f\right)\tan\delta' dl}{\pi a_p^2\left(\sigma'_{u,s}\tan\delta\cot\frac{\theta}{2} + \sigma_{u,s}\right) + \int_0^h 2\pi a_p\left(p'_f + \frac{\sqrt{3}}{3}Mp'_f\right)\tan\delta' dl} \tag{42}$$

where, F_d is the driving force of a full-displacement pile.

As seen in equation (44), the reduction factor not only depends on the size of the pre-boring, but also depends on the soil properties as well as the length and diameter of the pile.

Consolidation after Pile Installation

Dissipation of Excess Pore Water Pressure. After pile installation, the effective stress of the surrounding soil increases over time with dissipation of the excess pore water pressure generated by pile installation. As a result, the disturbed soil gradually recovers its strength from the residual state and increases over the in situ shear strength of the soil, which is the primary cause for the setup of the shaft resistance. Theoretically, the consolidation of the surrounding soil can be rigorously modeled by Biot's coupled consolidation theory. However, the specific initial pore water pressures generated by pile installation are not easily implemented in Biot's coupled consolidation theory and it is not easy or nearly impossible to derive a practical analytical solution. Hence, the modified Terzaghi's radial consolidation theory developed by Zheng et al. [63] for consolidation of the surrounding soil after installation is employed here to assess the dissipation of the excess pore water pressure. The governing equations of the modified Terzaghi's consolidation, which introduces a variable coefficient of consolidation $\bar{C}_{\mathrm{h}}$ to considers the change of the permeability with void ratio and the variation of soil modulus with mean effective stress, is given as:

$$\bar{C}_h = \frac{1}{r}\frac{\partial}{\partial r}\left(r\frac{\partial u}{\partial r}\right) = \frac{\partial u}{\partial t} \tag{43}$$

where, $\bar{C}_{\mathrm{h}}$ is the generalized coefficient of consolidation, which is given as follows

$$\bar{C}_{\mathrm{h}} = \frac{k_0}{\gamma_{\mathrm{w}}}\left(\frac{p'}{p_0'}\right)^{\chi}\frac{3p_0'(1+e_0)(1-v')}{\lambda(1+v')} \tag{44}$$

where, $\chi = 1-\lambda/\lambda_{\mathrm{k}}$; λ_{k} is the slope of $e-\ln k$ curve, which is defined as the permeability index; γ_{w} is the unit weight of pore water; e_0 is the void ratio after pile installation, which is equal to the initial void ratio due to the undrained condition during pile installation; k_0 is the initial coefficient of permeability.

The initial conditions for solving equation (45) should be the excess pore water pressures immediately after pile installation, which is given by equation (35). Assuming the pile is impermeable, the boundary conditions used to solve equation (45) can be given as [4]:

$$\left.\frac{\partial u}{\partial t}\right|_{r=a_{\mathrm{p}},t\geq 0} = 0 \tag{45}$$

$$u|_{r=R_{\mathrm{p}},t\geq 0} = 0 \tag{46}$$

where, $R_{\mathrm{p}} = 5\sim 10r_{\mathrm{p}}$ is the radius beyond which the excess pore water pressure remains zero at any time during consolidation.

The generalized coefficient of consolidation $\bar{C}_{\mathrm{h}}$, which depends on the mean effective stress, changes with the radial location and time during consolidation. Hence, to solve the governing equation, the excess pore water pressure distribution zone $a_{\mathrm{p}} \leq a \leq R_{\mathrm{p}}$ and the consolidation time t should be equally divided into l small parts and m short time intervals, respectively, as shown in Figure 30. When l and m are large enough, the generalized coefficient of consolidation for a given radial location r_i and time t_j can be regarded as a constant and thus the governing equation can be solved to give an analytical solution as [63]:

$$u_{i,j} = \sum_{n=1}^{\infty} A_n\left[J_0(\lambda_n r_i) - \frac{J_1(\lambda_n a_{\mathrm{p}})}{Y_1(\lambda_n a_{\mathrm{p}})}Y_0(\lambda_n r_i)\right]\exp\left(-\lambda_n^2 \bar{C}_{\mathrm{h},ij} t_j\right) \tag{47}$$

where, $i = 1, 2, 3 \ldots, l$; $j = 1, 2, 3 \ldots, m$; $u_{i,j}$ is the excess pore water pressure at radial location r_i and time t_j. J_0 and J_1 are the first kind Bessel functions of zero-order and first-order, respectively. Y_0 and Y_1 are the second kind Bessel functions of zero-order and first-order, respectively. λ_n represents the eigenvalues of the Bessel function; A_n denotes the

corresponding integration constants. The values of λ_n and A_n can be determined by making use of the initial condition, boundary condition as well as the orthogonal property of Bessel functions, which are given as follows:

$$J_0(\lambda_n R_\mathrm{p})Y_1(\lambda_n a_\mathrm{p}) - Y_0(\lambda_n R_\mathrm{p})J_1(\lambda_n a_\mathrm{p}) = 0 \tag{48}$$

$$A_n = \frac{\int_{a_\mathrm{p}}^{R_\mathrm{p}} \Delta u\left[J_0(\lambda_n r) - \frac{J_1(\lambda_n a_\mathrm{p})}{Y_1(\lambda_n a_\mathrm{p})} Y_0(\lambda_n r)\right] r dr}{\int_{a_\mathrm{p}}^{R_\mathrm{p}} \left[J_0(\lambda_n r) - \frac{J_1(\lambda_n a_\mathrm{p})}{Y_1(\lambda_n a_\mathrm{p})} Y_0(\lambda_n r)\right]^2 r dr} \tag{49}$$

Figure 30. Discretization of excess pore water pressure distribution zone

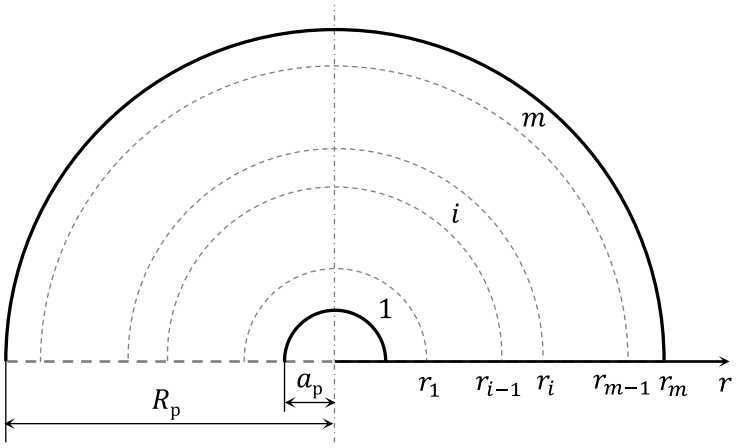

Due to the oscillating property of Bessel functions, numerous λ_n and A_n can be obtained from equations (50) and (51). In practical calculation, the first 40-60 items could yield sufficient accuracy. After determining λ_n and A_n, the excess pore water pressure can be calculated by a simple iterative program that updates the generalized coefficient of consolidation $\bar{C}_{\mathrm{h},ij}$ at different locations after each time interval thorough the following equations:

$$\bar{C}_{\mathrm{h},ij} = \frac{k_0}{\gamma_\mathrm{w}} \left(\frac{p'_{i,j-1} + dp'_{i,j-1}}{p'_{i0}}\right)^{\chi} \frac{3p'_{i,0}(1+e_0)(1-\nu')}{\lambda(1+\nu')} \tag{50}$$

where, p'_{i0} is the initial mean effective stress at location r_i; $p'_{i,j-1}$ and $dp'_{i,j-1}$ are the mean effective stress and increment of the mean effective stress at location r_i and time t_{j-1}, respectively. As the soil around the pile approximately consolidates under the plane strain condition, the increment of the mean effective stress $dp'_{i,j-1}$ can be related to the

decrement of the excess pore water pressure $-du_{i,j}$ at location r_i and time t_{j-1} as follows [4]:

$$dp'_{i,j-1} = -du_{i,j}\frac{1+v'}{3(1-v')} \tag{51}$$

Based on equation (53), the mean effective stress of the soil around the pile during consolidation can be expressed as:

$$p'(t) = p'_{\mathrm{f}} + \frac{1+v'}{3(1-v')}[\Delta u - u(t)] \tag{52}$$

where, $u(t)$ is the excess pore pressure at time t during consolidation, which can be determined by equation (49).

Increase of Shear Strength During Consolidation. After pile installation, the fabric of the surrounding soil is collapsed and the stress history is erased due to the server expansion and shearing effects of pile installation. As a result, the mechanical behaviour of the soil after installation is like that of normally consolidated soils [83]. Hence, based on the critical state soil theory, the undrained shear strength of the soil after pile installation, $s_{\mathrm{u,tc}}(t)$, can be expressed as:

$$s_{\mathrm{u,tc}}(t) = \frac{1}{2}Mp'(t)\left(\frac{1}{2}\right)^{\Lambda} \tag{53}$$

The shear modulus that depends on the current stress state and the specific volume of the soil will also change with time after pile installation. Based on the definition of shear modulus in the critical state soil mechanics, the shear modulus during consolidation can be given as:

$$G'(t) = \frac{3(1-2v')\left(v_0 - \lambda\ln\frac{p'(t)}{p'_0}\right)p'(t)}{2(1+v')\kappa} \tag{54}$$

where, v_0 is the in situ specific volume; κ is the slope of swelling line in the $p'-q$ plane.

Pile Loading

Shaft Resistance. The pile loading test is generally conducted after primary or full consolidation of the surrounding soil to check if the pile reaches the designed load carrying capacity. As indicated by Randolph and Wroth [83], the soil around an axially

loaded pile deforms in a manner similar to plane strain in the vertical plane, the shearing mode of which resembles that of the soil sample in a simple shear test and the corresponding failure stress state can still be represented by Figure 28. Hence, from the Mohr's stress circle and the corresponding failure stress state of the soil shown in Figure 28, the ultimate shaft resistance of after pile installation, $f_{\mathrm{s,L}}(t)$, can be related to the undrained shear strength of the soil $s_{\mathrm{u,tc}}(t)$ as:

$$f_{\mathrm{s,L}}(t) = \frac{1}{3}(3 - \sin\varphi')\cos\varphi' s_{\mathrm{u,tc}}(t) \tag{55}$$

The shaft resistance $f_{\mathrm{s,L}}(t)$ calculated from equation (57) in fact contains the shear stress $f_{\mathrm{s,I}}$ locked at the pile–soil interface, as the mean effective stress represented by equation (54) that used to calculate the shear strength increases from the mean effective stress at critical state. As stated previously, since the shear stress $f_{\mathrm{s,I}}$ calculated from the MCC model overestimates the actual locked residual shear stress f_{sr}, the shear stress $f_{\mathrm{s,I}}$ should be subtracted from the shaft resistance $f_{\mathrm{s,L}}(t)$ to eliminate the errors introduced by the soil model. Hence, the shaft resistance of pre-bored piles after installation, $f_{\mathrm{s,pre}}(t)$, can be conservatively given as:

$$f_{\mathrm{s,pre}}(t) = f_{\mathrm{s,L}}(t) - f_{\mathrm{s,I}} \tag{56}$$

Shaft Resistance Factor. In pile design, the total stress method (α method) remains the most popular approach used in design practice to estimate the shaft resistance, which directly relates the shaft resistance f_{s} to the in situ undrained shear strength $s_{\mathrm{u,tc}}$ through the shaft resistance factor α. Base on the α method, the shaft resistance factor of the pre-bored pile after pile installation, $\alpha(t)$, can be written as:

$$\alpha(t) = \frac{f_{\mathrm{s,pre}}(t)}{s_{\mathrm{u,tc}}} = \frac{1}{3}(3 - \sin\varphi')\cos\varphi' \left[\frac{p'(t)}{p_0'(R)^{\Lambda}} - 1\right] \tag{57}$$

The shaft resistance represented by equation (59) considers the size of pre-drilled hole and the changes of the stress state that occurs during installation, subsequent consolidation and loading, and thus would provide a rational prediction of the shaft resistance for pre-bored pile. It should be noted that when the time approaches infinitely, the shaft resistance calculated from equation (59) should be the long-term shaft resistance factor of pre-bored piles.

Long-Term Shaft Resistance Reduction Factor. The pre-boring reduces the squeezing effects of pile installation, and thus impacts the setup and long-term load shaft

resistance of the pile, which can be represented by a reduction factor that defined as follows:

$$R_{\mathrm{qs}} = \frac{f_{\mathrm{s,pre}}(t)}{f_{\mathrm{s}}(t)} \tag{58}$$

where, $f_{\mathrm{s}}(t)$ is the shaft resistance of the full displacement pile without pre-boring, which can be easily determined following the procedures developed above for pre-boded piles by setting $a_{\mathrm{p,pre}} = 0$.

Validation by Finite Element Model

In this section, the proposed analytical approach will be verified by the finite element model. Since the steps involved in the simulation are consistent with the current analytical framework, the comparisons with the results regenerated from the numerical model could validate the rationality of the assumptions made in the derivation and show the overall validity of the present analytical approach. The soil parameters used in the comparison and analysis are summarized in Table 5, which covers a wide range of soils with different overconsolidation ratios and strengths. Figures 31–34 compare the results from the current analytical approach with those regenerated from the finite element model for different phases involved from pile installation to loading.

Table 5. Soil parameters used in analysis

R	K_0	p_0' kPa	p_c': kPa	v_0	G_0: kPa	S_{u0}: kPa
1.2	0.625	120	169.0	2.06	4302	62.8
3	0.625	120	422.5	1.95	4073	130.7
5	0.625	120	704.2	1.89	3945	196.7
7	0.625	120	985.8	1.85	3861	257.4
M=1.2, λ=0.15, κ=0.03, ν=0.3, v_{cs}=2.74; k_h=1E-7 m/s						

Figure 31. Comparisons of expansion responses at wall of pre-drilled hole: (a) expansion pressures; (b) excess pore water pressure

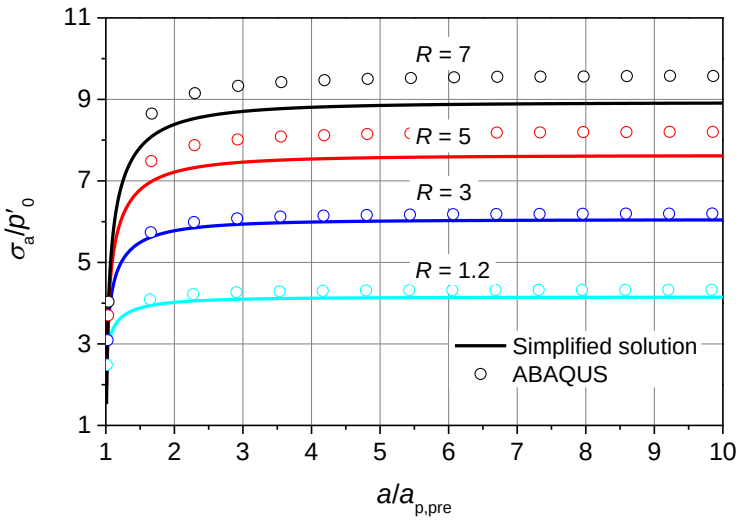

(a)

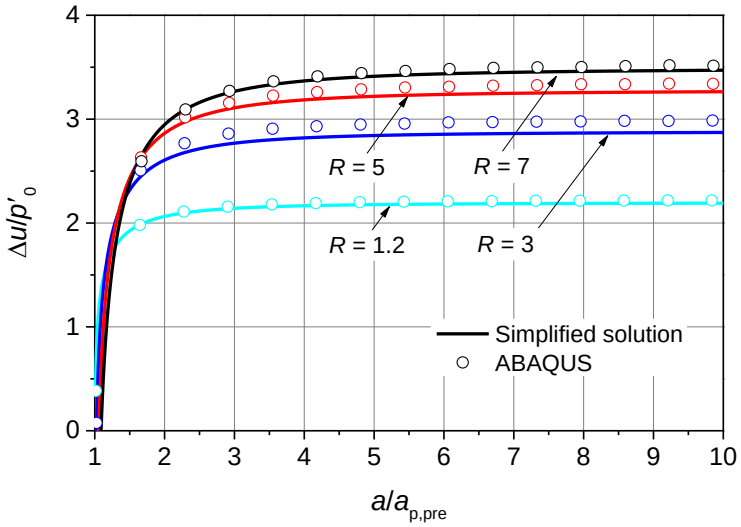

(b)

Figures 31a and 31b show the comparisons of the expansion pressures and excess pore water pressures, respectively, at the wall of the pre-drilled hole during expansion phase. In the figure, the instant radius of the hole a is normalized with the initial radius of the pre-drilled hole $a_{\mathrm{p,pre}}$, and the expansion pressure σ_a and excess pore water pressure Δu are normalized with the in-situ mean effective stress p_0'. It can be seen that both the expansion pressures and excess pore water pressures calculated from the proposed

analytical approach match well with those generated from the numerical model, although the proposed approach slightly underestimates expansion pressures for highly overconsolidated soils with $R = 5$ and 7. This underestimation is acceptable as it results in conservative setup and long-term shaft resistance of the pre-bored piles. It also can be seen that the expansion pressure and excess pore water pressure increases significantly when $a/a_{\mathrm{p,pre}} < 2$, after which the expansion pressure and excess pore water pressure gradually approaches constant values. Since the pre-drilled hole expands in a self-similar manner, it can be deduced that when the size of the pre-drilled hole is larger than 50% of the pile radius, the expansion effects of pile installation will be greatly reduced and hence the subsequent setup and long-term shaft resistance will be significantly impacted. It is also interesting to see that an increase in the value of R results in substantial increase of the expansion pressure and excess pore water pressure at the wall of the pre-drilled hole, which demonstrates than the overconsolidation ratio has a significant effect on the pile installation effects. Hence, the effects of R on the setup, long-term shaft resistance as well as on the shaft resistance reduction factor will be explored in detail later.

Figures 32a and 32b show the comparisons of the dissipation of the excess pore water pressures at the pile shaft for the cases $R = 1.2$ and 3, respectively. Different values of χ are considered in the figure. Note that excess pore water pressure is normalized with the in-situ mean effective stress p_0' and abscissa is the normalized time factor T_{v} $(= 2k_0G_0(1-v)t/\gamma_{\mathrm{w}}(1-2v)a_{\mathrm{p}}^2)$ rather than the real time to facilitate its use for different values of k_0 and a_{p}. As seen in the figure, the dissipation curve with $\chi = 0$ matches well with that generated from the numerical model at the beginning of consolidation, while the curve with $\chi = -0.5$ is more close to the dissipation curve from the numerical model at the end of consolidation. Overall, the curve with $\chi = 0$ shows a good agreement with the curve from the numerical model, which indicates that the proposed approach is capable of yielding satisfied prediction for the dissipation of the excess pore water pressure. It is also interesting to note that the time required to full dissipation of the excess pore water pressure in overconsolidated soil $(R = 3)$ is shorter than that in normally consolidated soil $(R = 1.2)$, which means that the excess pore water pressure dissipates more rapidly in the overconsolidated soil due to the larger coefficient of consolidation of the overconsolidated soil and the higher gradient of the excess pore-water pressure generated in the overconsolidated soil during pile installation.

Figure 32. Comparisons of dissipation of excess pore water pressure at wall of pre-drilled hole during consolidation: (a) $R = 1.2$; (b) $R = 3$

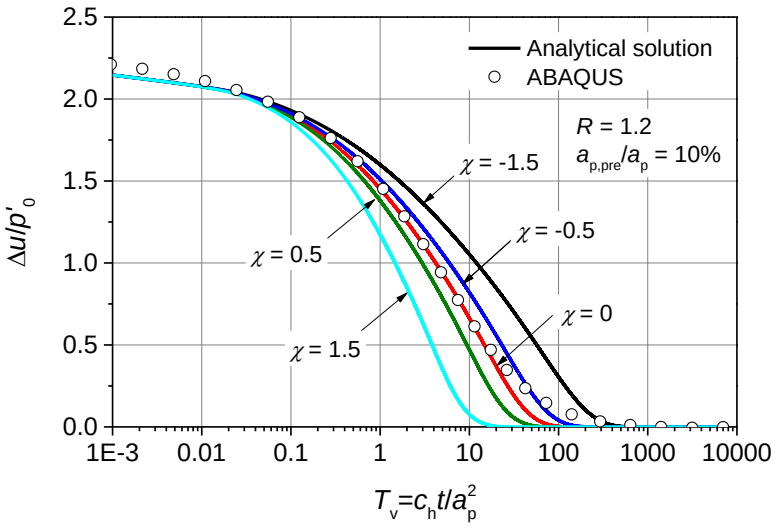

(a)

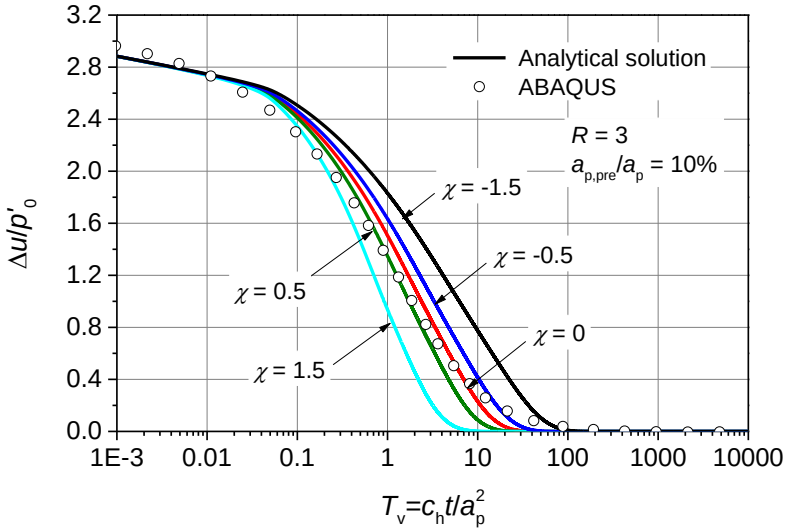

(b)

Figure 33 compares the long-term shaft resistance factor from the proposed analytical approach with that generated from the numerical model for the cases $R = 1.2, 3, 5$, and 7. As seen in the figure, the proposed analytical approach yields satisfied prediction for the long-term shaft resistance factor when compared with the numerical results, as the proposed analytical method only underestimates the shaft resistance factor by 3%-16%.

The underestimation of the shaft resistance will result in a slight conservative design of the pre-bored pile, which is definitely acceptable from the safety standpoint. Since the expansion effects of pile installation is greatly reduced when $a_{\mathrm{p,pre}}/a_{\mathrm{p}} > 50\%$, the shaft resistance factor shows a substantial decrease when $a_{\mathrm{p,pre}}/a_{\mathrm{p}} > 50\%$, while the shaft resistance factor decreases insignificantly in the range $a_{\mathrm{p,pre}}/a_{\mathrm{p}} \leq 50\%$. As the size of pre-drilled hole increases from zero to fifty percent of the pile radius, the reduction factor merely reduces by 4%-7%. This demonstrates that if the size of the pre-drilled hole is smaller than 50% of the pile radius, pre-boring has an almost negligible effect on the setup and long-term shaft resistance of the pile. It is also interesting to see that an increase of the overconsolidation ratio results in significant decrease of the shaft resistance factor, which is consistent with the observations of McClelland [84] and Randolph [59]. However, it should be emphasized that the shaft resistance in fact increases with the overconsolidation ratio according to the definition of the shaft resistance factor, as the in situ strength increases with the overconsolidation ratio.

Figure 33. Comparisons of long-term shaft resistance factor for different overconsolidation ratios

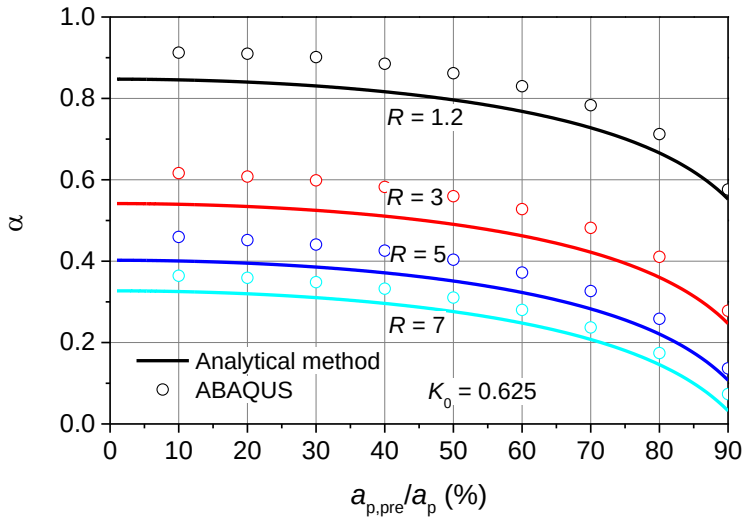

The comparisons of the reduction factor between the proposed analytical approach and the numerical model are plotted in Figure 34. As seen in the figure, the proposed analytical approach yields perfect prediction for the shaft resistance reduction factor, which agree well with the reduction factor generated from the numerical model. As seen in the figure, the reduction factor changes insignificantly in the range $a_{\mathrm{p,pre}}/a_{\mathrm{p}} < 50\%$,

but decreases significantly when $a_{\mathrm{p,pre}}/a_{\mathrm{p}} > 50\%$. This again indicates that pre-boring has an almost insignificant effect on the long-term shaft resistance of the pile if the size of the pre-drilled hole is smaller than 50% of the pile radius, but will greatly reduce the long-term shaft resistance when $a_{\mathrm{p,pre}}/a_{\mathrm{p}} > 50\%$. Moreover, it can be found that the reduction factor decreases with the increase of the overconsolidation ratio, which means the reduction effects of pre-boring on the long-term shaft resistance is more pronounced in the soil with high overconsolidation ratio.

Figure 34. Comparisons of shaft resistance reduction factor for different overconsolidation ratios

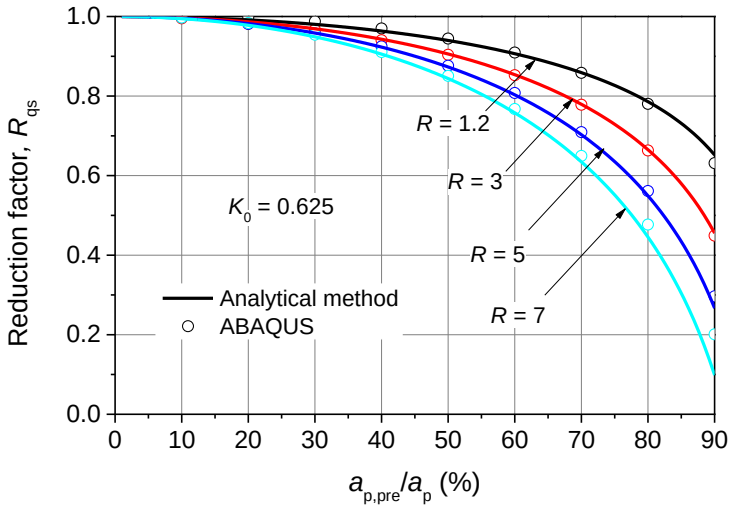

The above comparisons show that the proposed analytical approach is capable of making reasonable predictions for pre-bored pile installation, consolidation and loading, which manifests the validity of the assumptions made in the derivation and the proposed analytical approach. It is also found from the analysis that the size of pre-drilled hole, the overconsolidation ratio and the coefficient of earth pressure at rest have pronounced effects on the installation effects, and hence will further impact the setup and long-term load carrying capacity of the pre-bored piles after installation.

Discussion of Results

Numerical Results and Discussions

Based on the numerical model, the installation effects, subsequent consolidation, and long-term load carrying capacity of pre-bored piles will be investigated in this section. Given the fact that the soil in Louisiana is commonly in normally and lightly overconsolidated state with R in the range of 1–3, it is therefore the soil parameters corresponding to the normally consolidated soil ($R = 1$) and the moderately overconsolidated soil ($R = 3$) listed in Table 1, are chosen for analysis. To reveal the impacts of the size of the pre-bored hole, the results and analysis primarily focus on comparing the behaviours of the piles with different diameters of pre-bored hole in different phases. It should be noted that the ABAQUS finite element model developed in the current work for the finite cavity expansion, which uses the CAX4Ps symmetric elements and requires a preset hole in the meshing/modelling, is incapable of simulating the cavity creation process pertinent to the full displacement piles. However, it is found from the parametric study that the influences of the pre-bored hole size $a_{\mathrm{p,pre}}/a_{\mathrm{p}}$ on the calculated distributions of the stress components around the pile becomes negligible, provided that the hole is smaller than 10% of the pile diameter. Hence, a pre-bore size of $a_{\mathrm{p,pre}}/a_{\mathrm{p}} = 10\%$ can be roughly approximated as the full displacement pile case for the comparison purpose.

Installation

During pile installation, the pile continuously pushes the surrounding soil away and vertically shears the surrounding soils until it reaches the designed depth, which will result in substantial changes in stress state of the surrounding soil. To display the general responses of the soil at the pile shaft during expansion, Figure 35 plots the variations of the normalized stress components of the soil at pile shaft when the pre-bored hole expands from its initial radius $a_{\mathrm{p,pre}}$ to the pile radius a_{p} in normally consolidated soil and moderately overconsolidated soil. Note that the pile investigated here has a pre-bored hole equal to 10% of pile radius and the logarithmic abscissa is used in the figure to clearly show the changes in the early stage of cavity expansion.

Comparing Figure 35(a) and Figure 35(b), it can be found that the changes of the stresses during expansion show a similar manner in both normally consolidated soil and

moderately overconsolidated soil although there are some discrepancies in the magnitude. As seen in the figure, the effective stresses immediately reach constant values at the early stage of cavity expansion, whereas the total stresses still keep increasing until $a/a_{\mathrm{p,pre}} = 3$, after which the total stresses also reach constant values. This indicates that the excess pore water pressure keeps increasing after the soil reaches critical state because the critical state region still develops and expands outwards. Since the cavity expands in a self-similar manner, the ratio of the radius of the critical state region to the radius of cavity will tend to a constant value [85] and hence the excess pore water pressure finally keeps unchanged. Due to the geometric self-similarity nature of the cavity expansion problem [1], cavities with other sizes of initial radius will expand in a similar way and the effective stress will also reach the same constant values immediately after expansion. Therefore, it can be generally concluded that the size of the pilot hole has little effects on the effective stress at the pile shaft during installation, while significantly impacts the excess pore water pressure, the effects of which will propagate to the subsequent consolidation phase and hence influences the long-term load carrying behaviours of piles.

Figure 35. Variations of normalized stresses at cavity wall when pre-boring hole expands from its initial radius $a_{\mathrm{p,pre}}$ to pile radius a_{p} in soils with (a) $R = 1$ and (b) $R = 3$

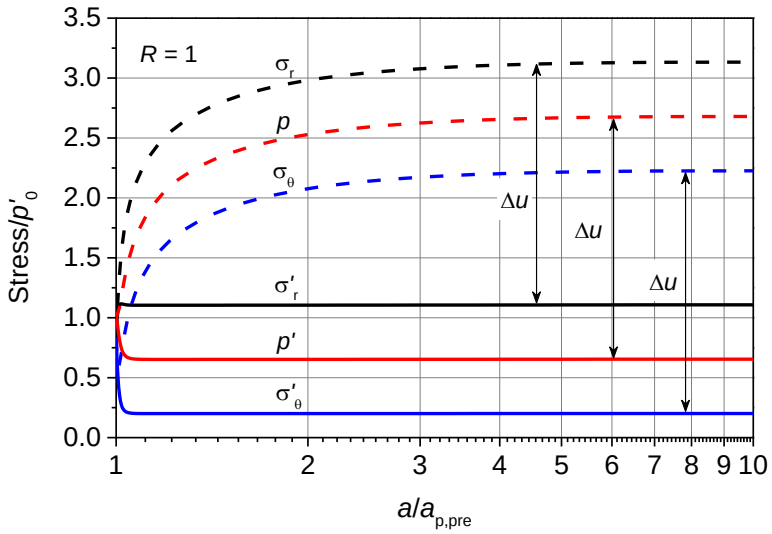

(a)

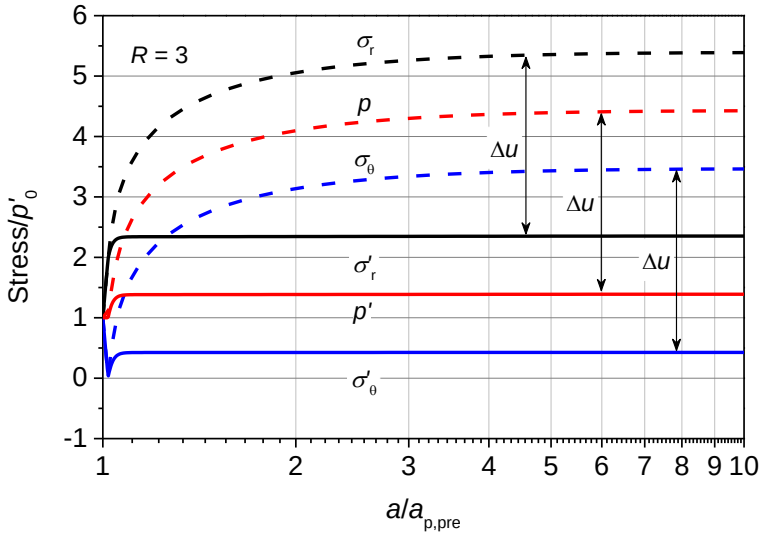

(b)

Figure 36. Distribution of excess pore water pressures around piles with different sizes of pre-bored hole immediately after expansion: (a) $R = 1$; (b) $R = 3$

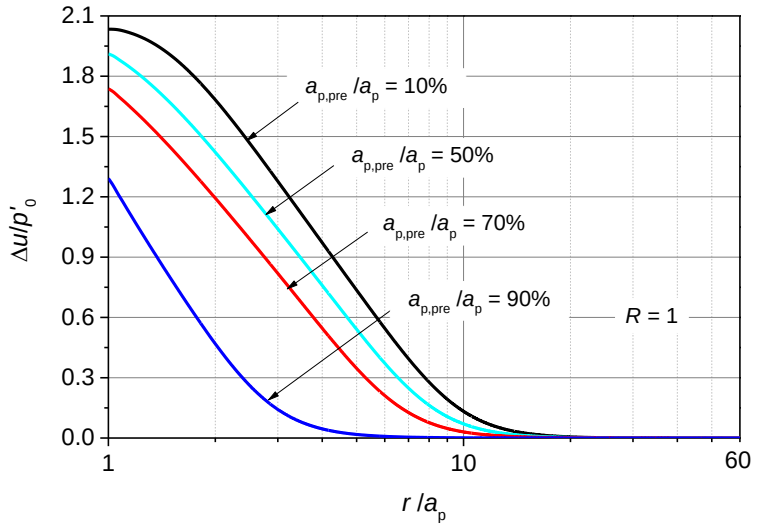

(a)

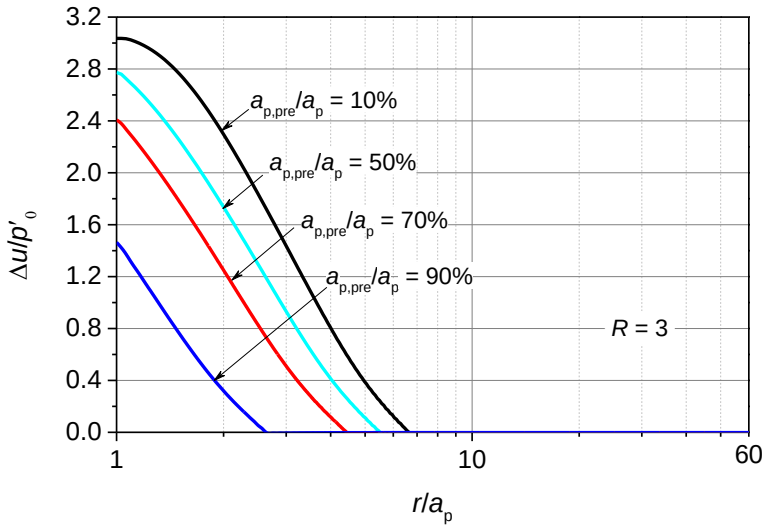

(b)

Figure 36–Figure 39 show the distributions of the normalized excess pore water pressures $\Delta u/p_0'$, radial effective stresses σ_r'/p_0', mean effective stresses p'/p_0' and radial displacements u_r/a_p around piles with different sizes of pre-bored hole immediately after expansion, respectively. The radial location r is normalized with respect to the pile radius a_p and logarithmic abscissa is employed in these figures for the purpose of showing the detailed variations of the variables in the vicinity of the pile.

From Figure 36, one can observe that both the magnitude and the distribution range of the excess pore water pressures decreases significantly with the increase of the size of the pre-bored hole. It indicates that the size of the pre-bored hole not only influences the magnitude of the excess pore water pressure during installation, but also has pronounced effects on the distribution of the excess pore water pressures around the pile. Comparing Figure 36(a) and Figure 36(b), it can be found that pile expansion induces higher excess pore water pressures at the pile shaft in the moderately overconsolidated soils. It also can be seen that the excess pore water pressure generated by expansion is primarily localized in the range of $r/a_\mathrm{p} < 10$, beyond which no significant excess pore water pressure can be observed.

Figure 37. Distribution of radial effective stresses around piles with different sizes of pre-bored hole immediately after expansion: (a) $R = 1$; (b) $R = 3$

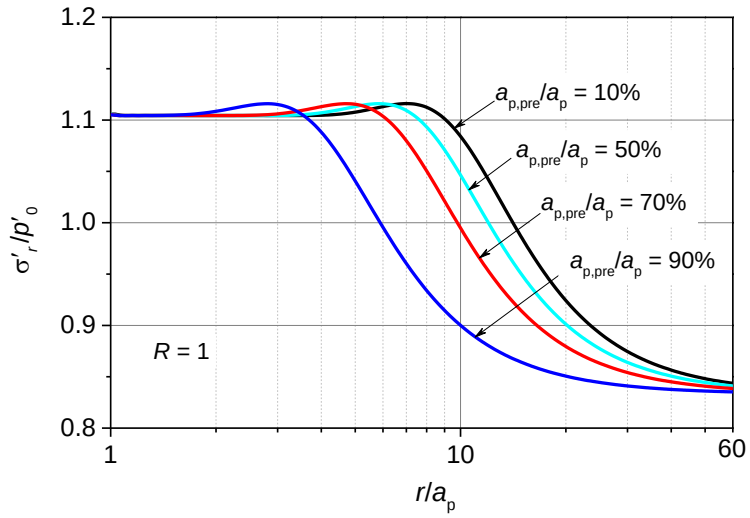

(a)

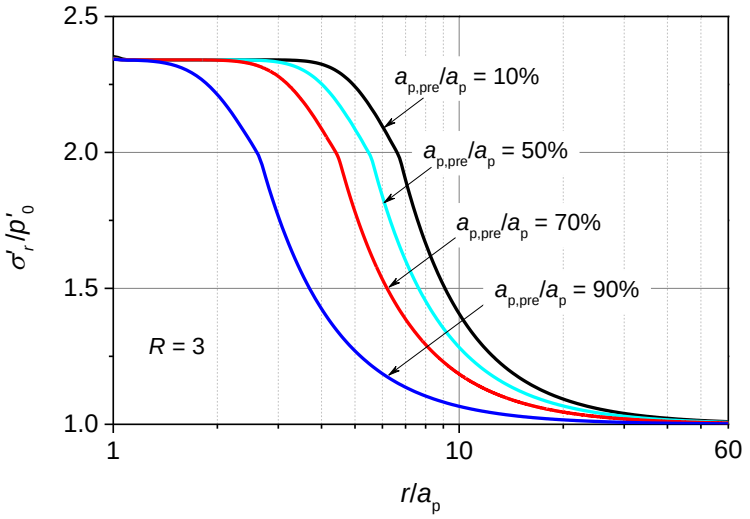

(b)

Figure 38. Distribution of mean effective stresses around piles with different sizes of pre-bored hole immediately after expansion: (a) $R = 1$; (b) $R = 3$

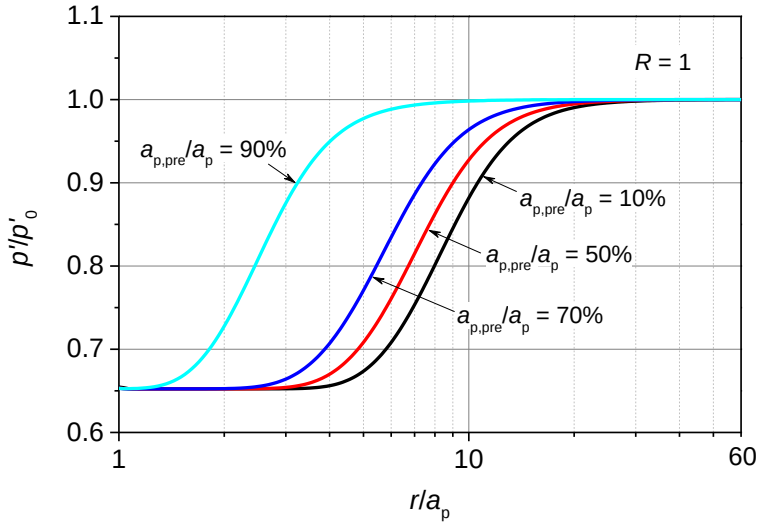

(a)

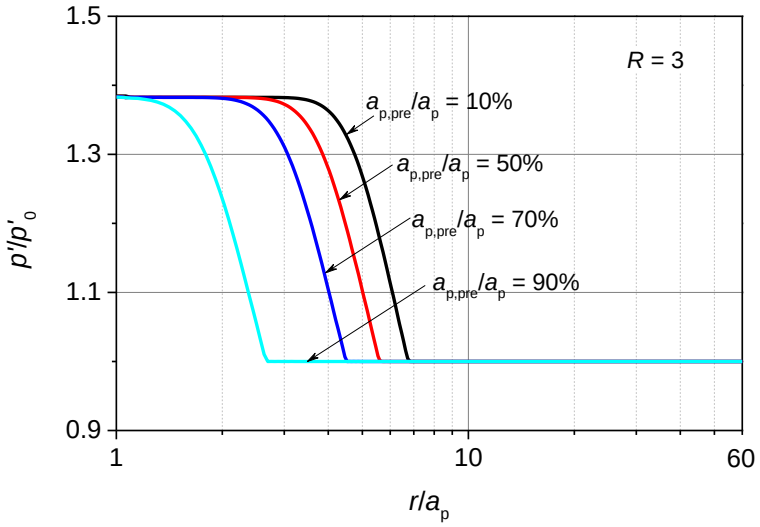

(b)

Figure 39. Distribution of radial displacements around piles with different sizes of pre-bored hole immediately after expansion: (a) $R = 1$; (b) $R = 3$

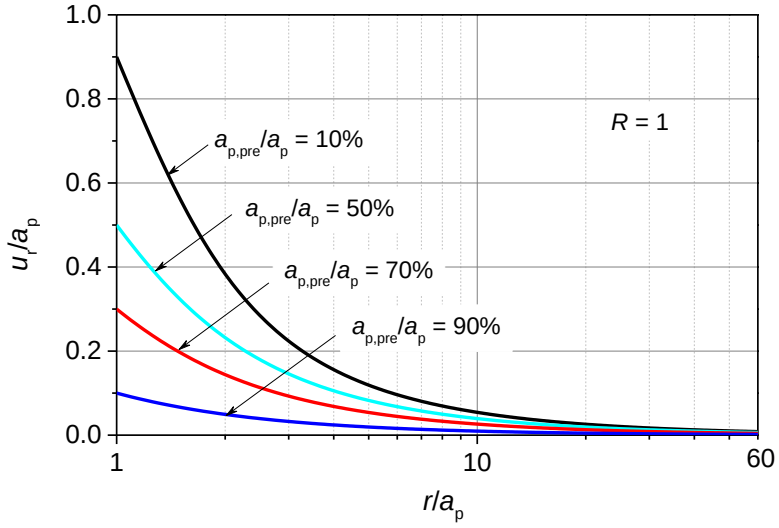

(a)

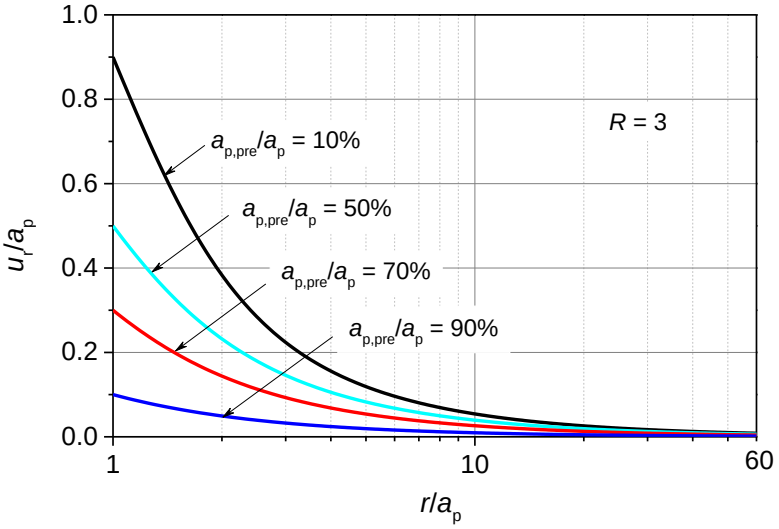

(b)

Figure 37 shows that since the soil immediately reaches the critical state once the cavity expands, all of the radial effective stresses near the cavity wall are the same after installation, although the sizes of the pre-bored hole are different. However, installation a pile with a smaller pre-bored hole causes a wider range within which effective stress changes. It is well known that the ultimate shaft resistance of the pile is primarily governed by the radial effective stress acting on the pile shaft, while the load-settlement behaviour of the pile depends on the stress state of the soil around the pile. Therefore, pre-boring not only alters the long-term ultimate capacity of the pile, but also impacts their load carrying behaviours. Moreover, it can be also observed from Figure 37 that the disturbed range caused by pile installation is primarily located in the range of $r/a_{\mathrm{p}} < 10$. This manifests that the outer boundary of the numerical model is large enough to eliminate the boundary effects and hence ensures the validity of the numerical results.

Figure 38 shows that the region, within which the effective stress changes, decreases with the increase of the size of pre-bored hole. This again demonstrates disturbed range due to pile installation primarily depends on the size of the pre-bored hole. Further inspection of Figure 38, it can be found that the mean effective stresses decrease greatly in the vicinity of the pile in normally consolidated soils while increases substantially in moderately overconsolidated soils after expansion. This is because the stress path of normally consolidated soil reaches the critical line from the wet side, while the moderately overconsolidated soil reaches the critical line from the dry side, which will be further discussed later in the report.

Figure 39 shows that the radial displacement caused by installation increases with the decrease of the pre-bored hole size, which further demonstrates that installation of a pile with smaller size of pre-bored hole generates more significant installation effects, both in magnitude and in range. It can be also observed from Figure 39 that the disturbed range caused by pile installation is primarily located in the range of $r/a_p < 10$. This manifests that the outer boundary of the numerical model is large enough to eliminate the boundary effects and hence ensures the validity of the results. Comparing Figure 39(a) and Figure 39(b), it can be found that the radial displacement is independent of the overconsolidation ratio R. In fact, the radial displacement u_r around the pile shaft is independent of the soil parameters due to the undrained condition, which can be directly determined from the volume conservation condition as follows [1]:

$$u_r = \sqrt{a_p^2 + a_{\mathrm{p,pre}}^2 - r_0^2} - r_{x0} \tag{61}$$

where, r_{x0} and r_0 represent the initial and current radial position of an arbitrary point around the pile.

Figure 40 shows the changes of the stress components of a soil element at the pile shaft during shearing. The vertical shearing displacement δu_v is normalized with the pile radius a_p and all the stress components are normalized with respect to the initial mean effective stress p_0' in the figure. As seen in the figure, the shearing effects further alter the stress state of a soil element in the vicinity of the pile: shearing leads to the reduction of the radial effective stress but the increase of the tangential effective stress as a result of rotation of the principle stresses; the excess pore water pressures increase slightly and approach a constant state again. These phenomena sufficiently demonstrate the significance of the shearing effects on the evaluation of the pile behaviour. Ignoring the shearing effects would possibly overestimate the shaft resistance as the shearing significantly reduces the radial effective stress acting on the pile shaft. Further inspection of Figure 40 reveals that the shearing produces similar effects on the change of the stress state in both normally consolidated soil and moderately overconsolidated soil, although the soil element reaches the constant state at a larger shearing displacement in moderately overconsolidated soil.

Figure 40. Changes of stress components at pile shaft during shearing: (a) $R = 1$; (b) $R = 3$

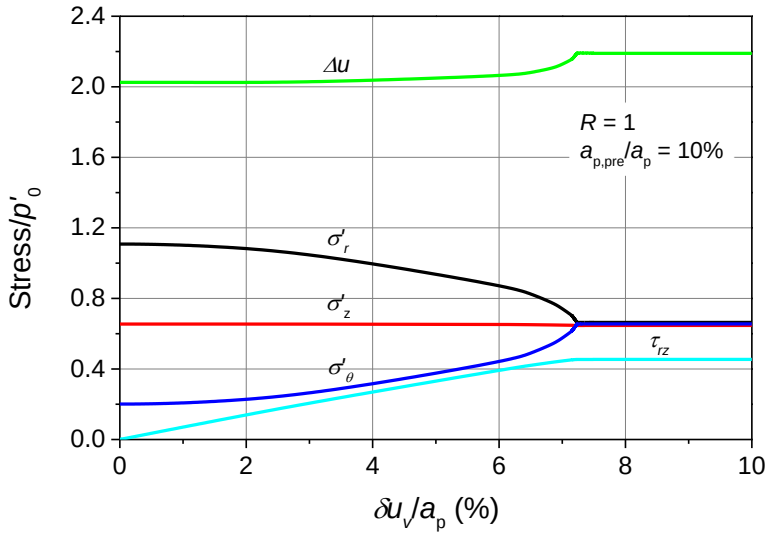

(a)

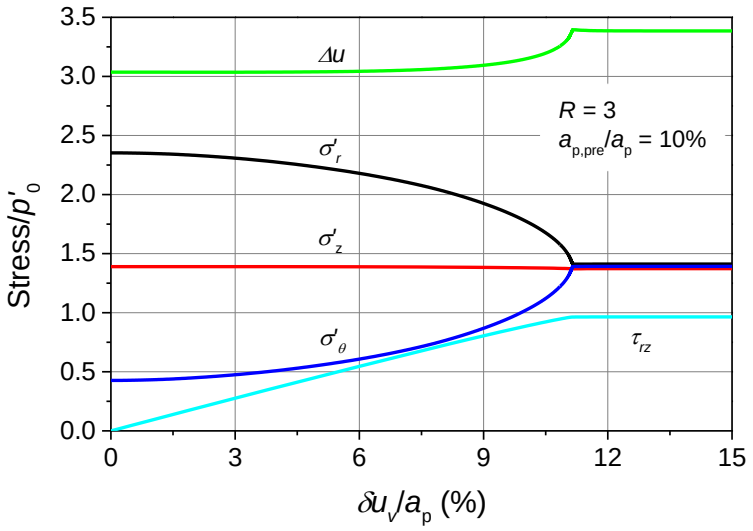

(b)

Figure 41. Distribution of excess pore water pressure around piles with different sizes of pre-bored hole immediately after expansion and after shearing: (a) $R = 1$; (b) $R = 3$

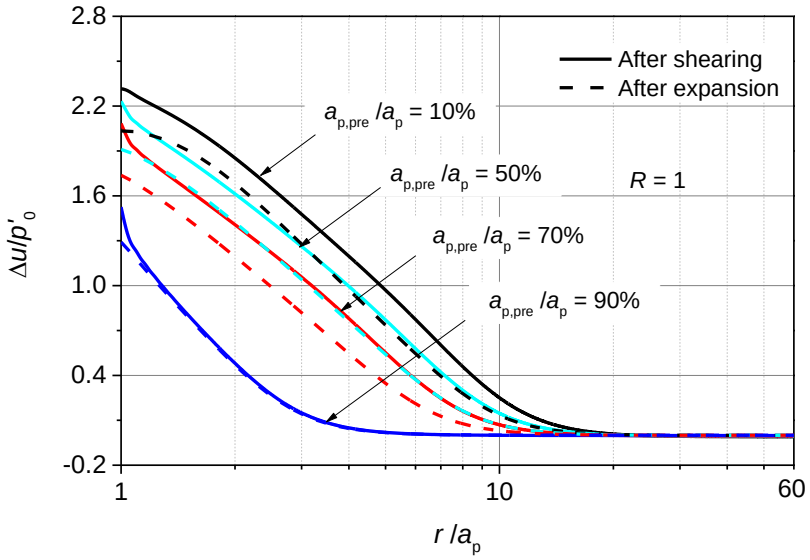

(a)

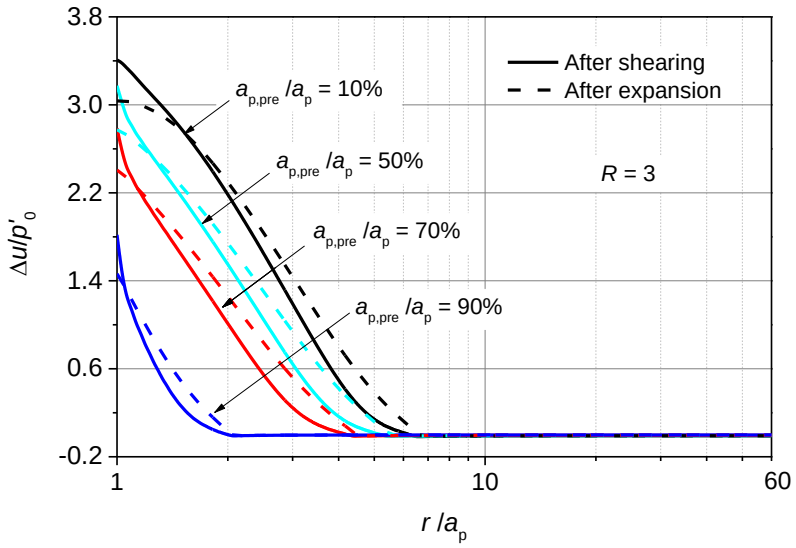

(b)

The distribution of the normalized excess pore water pressure $\Delta u/p'_0$ around piles with different sizes of pre-bored hole after installation are plotted in Figure 41. It can be seen that the shearing effects after expansion further increases the excess pore water pressures in the vicinity to the pile shaft in both the normally consolidated and moderately overconsolidated soils. Further inspection of Figure 41 reveals that the shearing induced excess pore water pressures are just confined in a narrow range around the pile, beyond which there is no significant change in excess pore water pressures. This confirms that the present numerical model is capable of simulating the shearing band formed during shearing.

Figure 42 plots the distributions of the radial effective stress σ'_r around piles with different sizes of pre-bored hole after installation. As shown in the figure, the radial effective stresses in the vicinity of the pile decreases significantly from the value immediately after expansion due to the shearing effects in both normally consolidated and moderately consolidated soils. This again indicates that the simulation of pile installation with cavity expansion theory alone probably overestimates the radial stress acting on the pile shaft, and hence would result in overestimation of the shaft resistance after installation. It also can be seen from the figure that the range of change in radial stress decreases with the increase of the size of the pre-bored hole, which indicates that the shearing effects decrease with the increase of the size of the pre-bored hole.

Figure 42. Distribution of radial effective stress around piles with different sizes of pre-bored hole immediately after expansion and after shearing: (a) $R = 1$; (b) $R = 3$

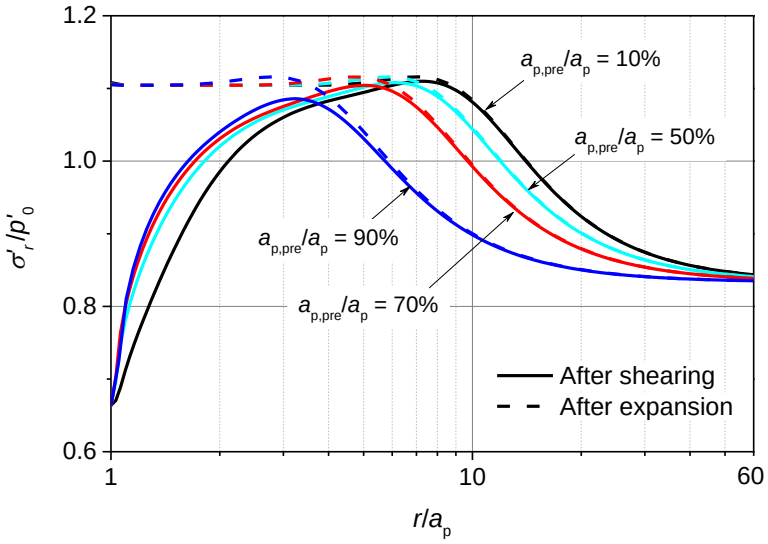

(a)

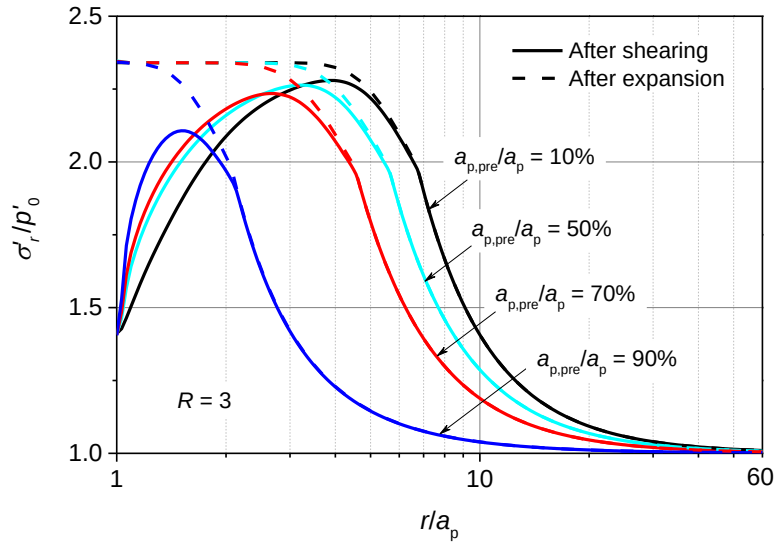

(b)

Consolidation

After installation, the effective stress increases with dissipation of the excess pore water pressure, which is the primary cause for the setup of a displacement pile in clayey soils. For a pile with a pre-bored hole equal to 10% of pile radius, the changes of the total stresses, the effective stresses as well as the void ratio of a soil element at the pile wall during consolidation are plotted in Figure 43. Since the time required for dissipation of the excess pore water pressure depends both on the permeability coefficient and the drainage path, the normalized time factor $T_{\mathrm{v}} = 2k_{\mathrm{h}}G_0(1-v')t/\gamma_{\mathrm{w}}(1-2v)a_{\mathrm{p}}^2$, suggested by Guo [62], is adopted instead of the real time in the figure to facilitate its usage for any values of k_{h} and a_{p}.

Figure 43. Stresses and void ratio of a soil element at pile shaft during consolidation: (a) $R = 1$; (b) $R = 3$

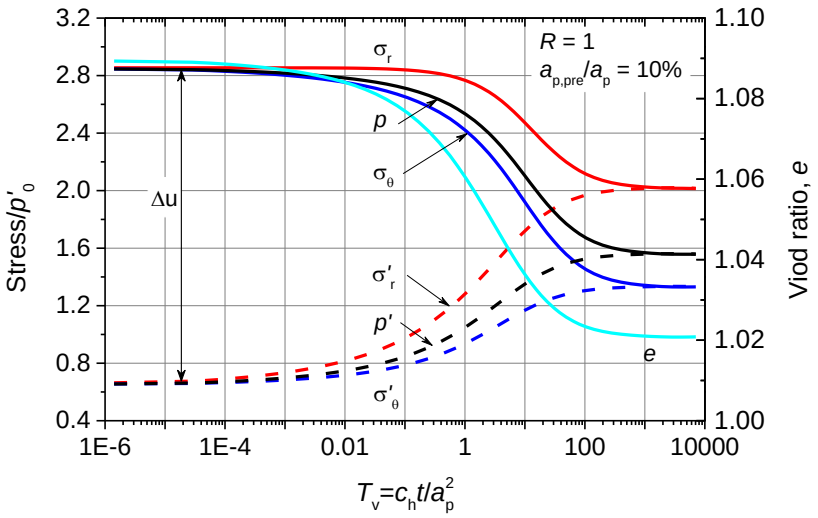

(a)

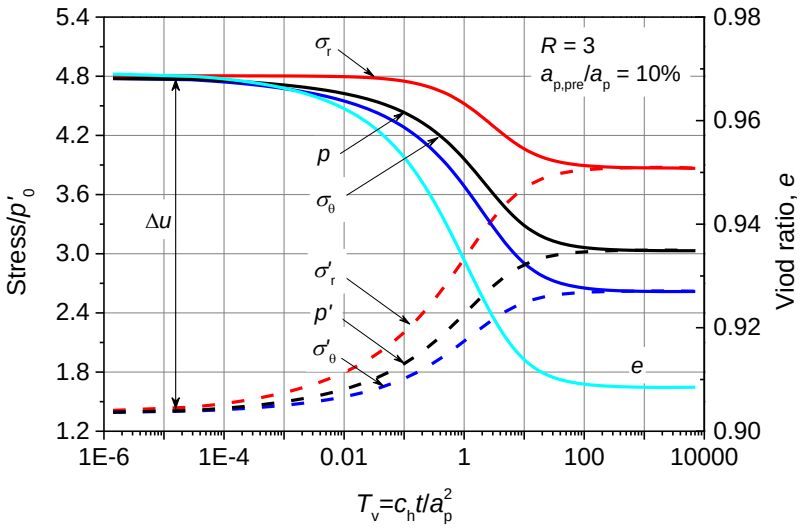

(b)

As seen in Figure 43, all of the effective stresses increase with dissipation of excess pore water pressures during the consolidation phase. An important phenomenon, total stress relaxation that cannot be reflected by the Terzaghi' consolidation theory based analytical solution [4], could be clearly seen in both the normally consolidated and moderately overconsolidated soils. After full dissipation of the excess pore water pressure, the effective stress increases by about 80 percent from its value immediately after pile installation, which would result in apparent setup effects of the pile. Moreover, the void ratio, which closely relates to both the shear strength and the shear modulus, decreases as the effective stress increases. All of these phenomena demonstrate that the load carrying capacity of the pile increases significantly as a result of reconsolidation of the disturbed soil.

Figure 44 plots the radial distribution of excess pore water pressure around a pile with a pre-bored hole equal to 10% of pile diameter at different time during consolidation. It can be seen that the distribution range of the excess pore pressure increases with the decrease of its magnitude as a result of outward flow of pore water. With the decrease of pore pressure gradient, the time required for dissipation of the same amount of excess pore water pressure increases significantly. It also can be seen that the time required for full dissipation of the excess pore water in normally consolidated soil is much longer than that in moderately overconsolidated soil, which means that the dissipation rate in moderately overconsolidated soil is faster than that in normally consolidated soil.

Figure 44. Radial distribution of excess pore water pressures around a pile with a pre-bored hole equal to 10% pile diameter at different times after installation: (a) $R = 1$; (b) $R = 3$

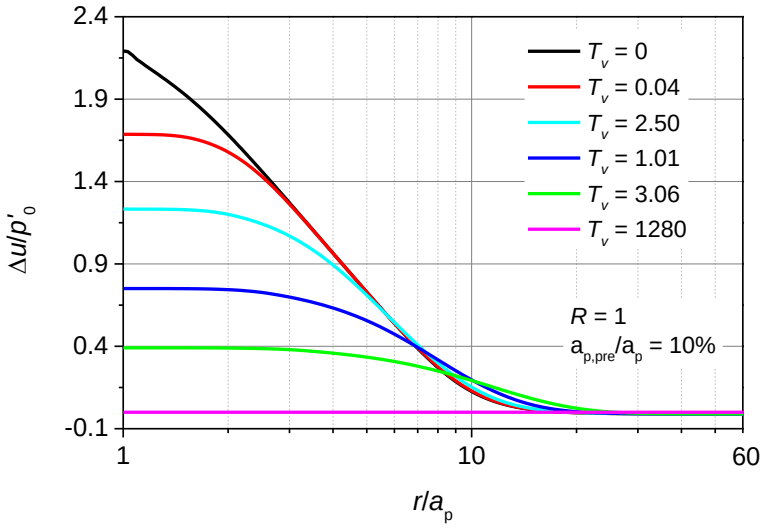

(a)

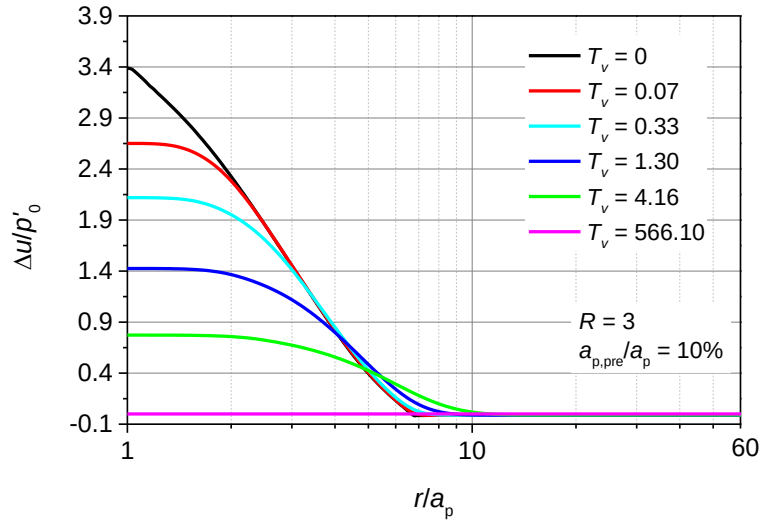

(b)

Figures 45-47 plot the variations of the radial stress, the mean stress and the excess pore water pressures of a soil element at the pile shaft during consolidation for piles with different sizes of pre-bored hole. As seen in these figures, the effective stresses p' and σ'_r

increase as a results of consolidation, while the total stresses p and σ_r decrease with dissipation of excess pore pressure due to the difference in stiffness of the surrounding soil caused by installation [59]. This means that only partial excess pore pressure transforms into the effective stress during consolidation, which addresses the significance of the coupled consolidation theory in analyzing the consolidation of the soil around a pile. It is also interesting to see that the amount of the increase in effective stresses, p' and σ_r', increases with the decrease of the size of the pre-bored hole. This means a pile with smaller size of pre-bored hole yields larger effective stress after full consolidation of the disturbed soils, from which one can conclude that the long-term load carrying capacity decreases with the increase of the size of pre-bored pile. Moreover, the variations of the radial stress, the mean stress and the excess pore water pressures show the same pattern in both normally consolidated and moderately overconsolidated soils, although there are some discrepancies in the magnitude.

Figure 45. Variations of radial total stress and effective stress at pile shaft during consolidation phase for piles with different sizes of pre-bored hole: (a) $R = 1$; (b) $R = 3$

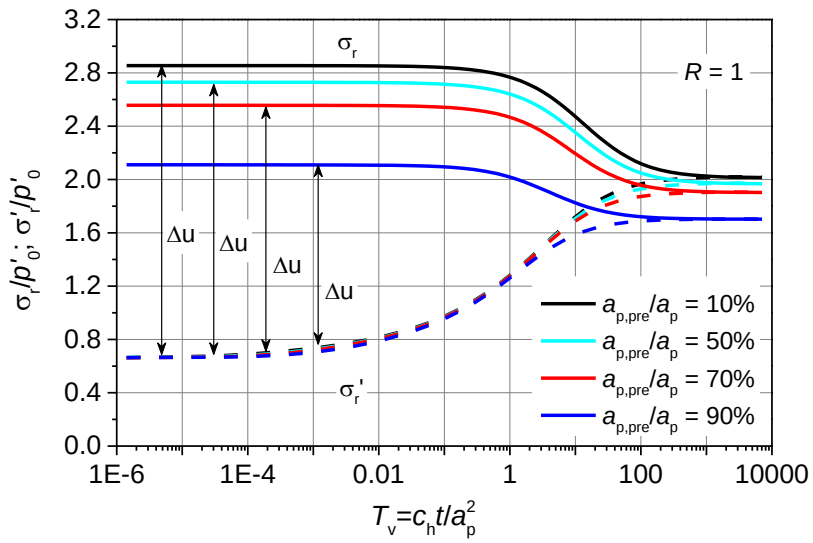

(a)

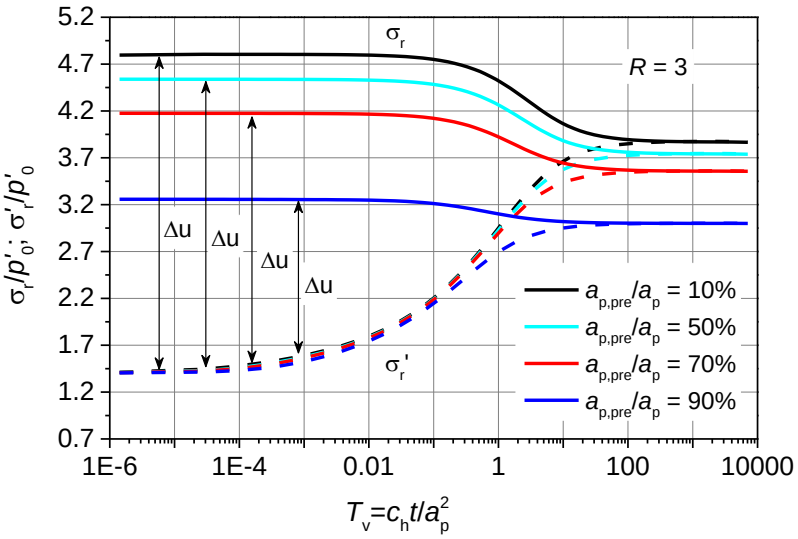

(b)

Figure 46. Variations of total mean stress and effective mean stress at pile shaft during consolidation phase for piles with different sizes of pre-bored hole: (a) $R = 1$; (b) $R = 3$

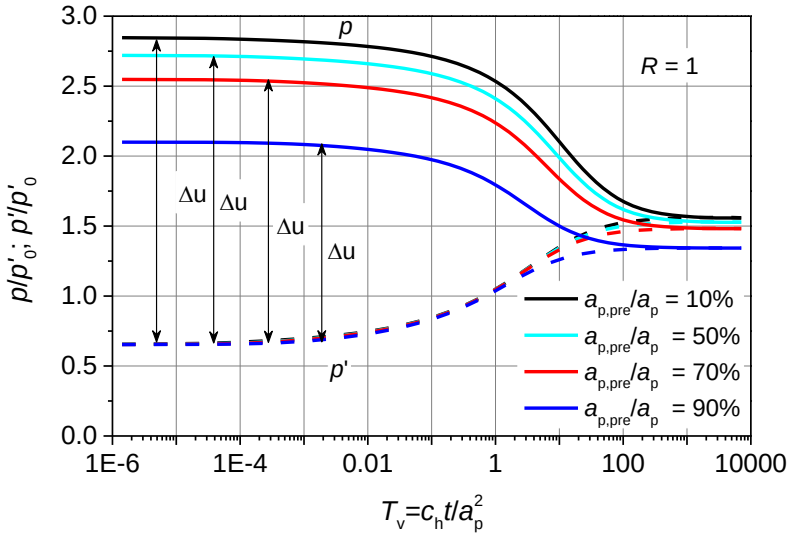

(a)

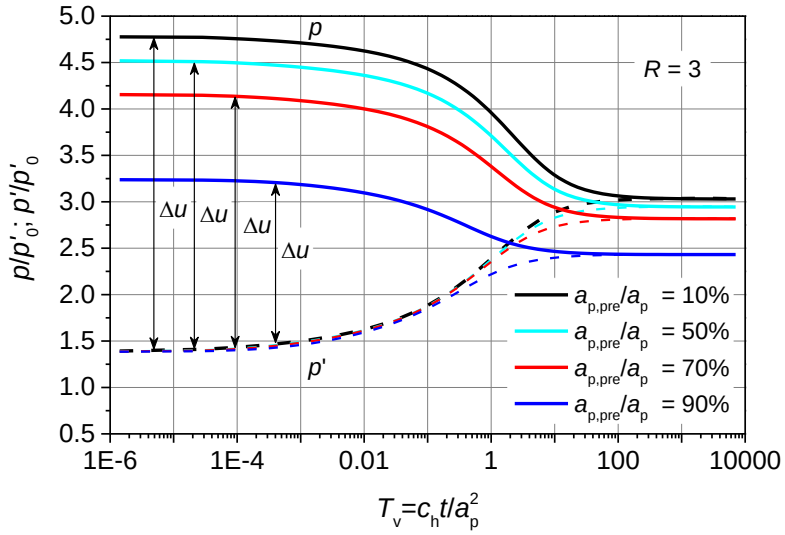

(b)

Figure 47. Variations of excess pore water pressure at pile shaft during consolidation phase for piles with different sizes of pre-bored hole: (a) $R = 1$; (b) $R = 3$

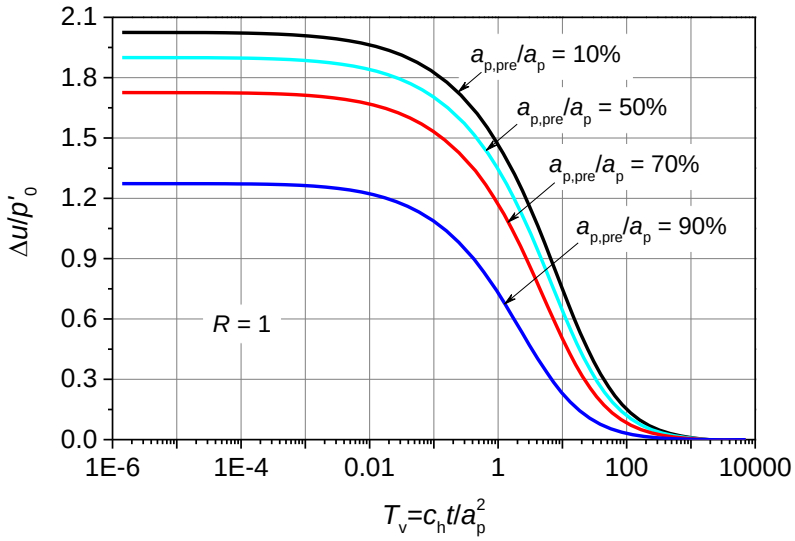

(a)

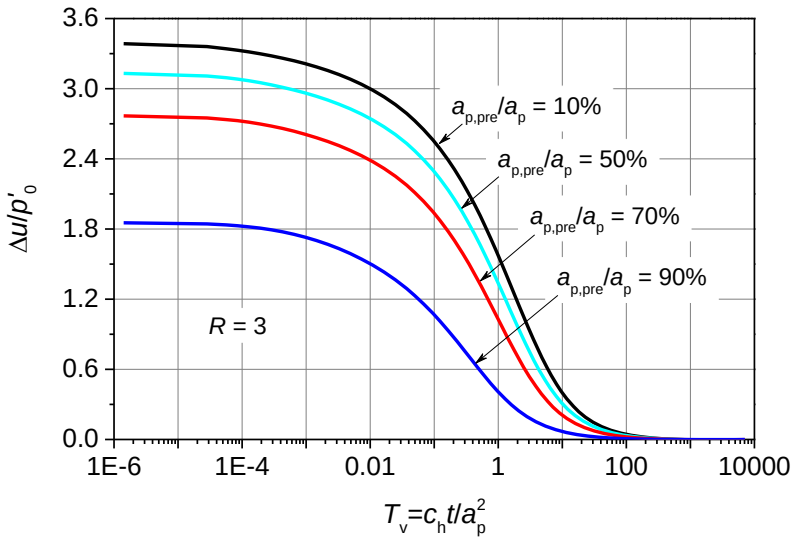

(b)

The distributions of the mean effective stress p' and the radial effective stress σ_r' around piles with different sizes of pre-bored hole after full dissipation of excess pore water pressure are plotted in figures 48 and 49, respectively. The logarithmic abscissa is employed in the figures to clearly display the variable distribution in the vicinity of the pile shaft. It can be seen that, although the stress around the pile with larger size of pre-bored hole is smaller than that around the pile with smaller size of pre-bored hole, both the mean effective stresses and the radial effective stresses are significantly higher than their in-situ values after full consolidation of the surrounding soils. Figure 48 and Figure 49 also show that the range, in which the effective stresses change, increases with the decrease of the size of the pre-bored hole, but the change in effective stresses is mainly localized within the range $r/a_p < 10$. This indicates that pile installation and subsequent consolidation primarily impact the soil in the vicinity of the pile, and their effects diminish as the distance from the pile wall increases. For the region $r/a_p > 10$, the stresses after consolidation are fairly close to the in-situ value and hence the installation effects can be nearly ignored. It is also interesting to note that there is an obvious region in which the mean effective stress is smaller than the in-situ value, which indicates the soil in this region undergoes unloading during consolidation. In fact, since the soil rigidity decreases with radial distance away from the pile after installation, the inner soil consolidates with swelling of the outer soil [59], which results in the relaxation effects in both effective stress and total stress.

Figure 48. Distributions of mean effective stresses around piles after full dissipation of excess pore water pressure: (a) $R = 1$; (b) $R = 3$

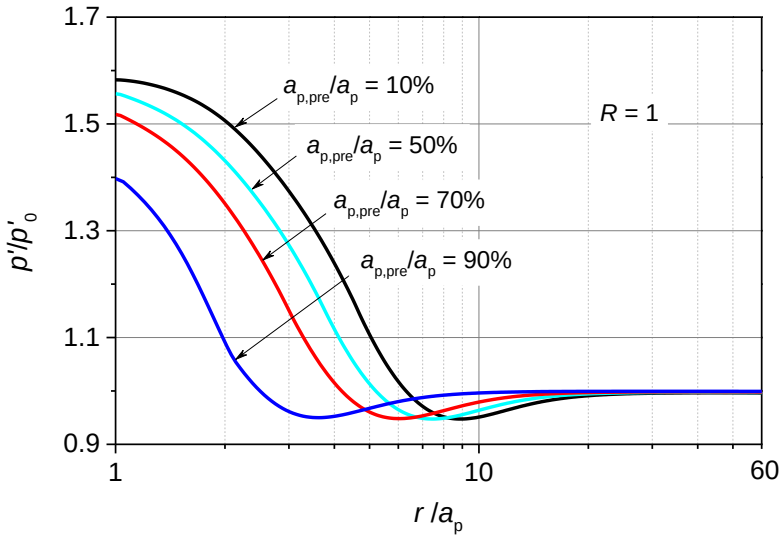

(a)

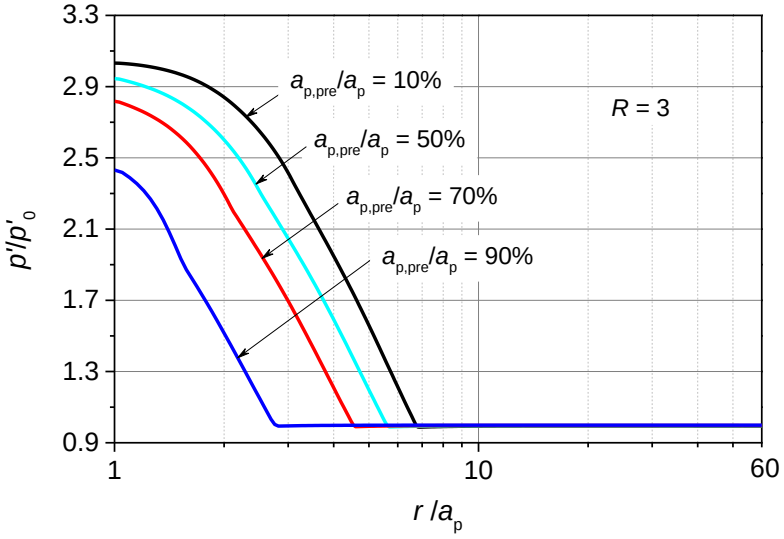

(b)

Figure 49. Distributions of radial effective stresses around piles with different sizes of pre-bored hole after full dissipation of excess pore water pressure: (a) $R = 1$; (b) $R = 3$

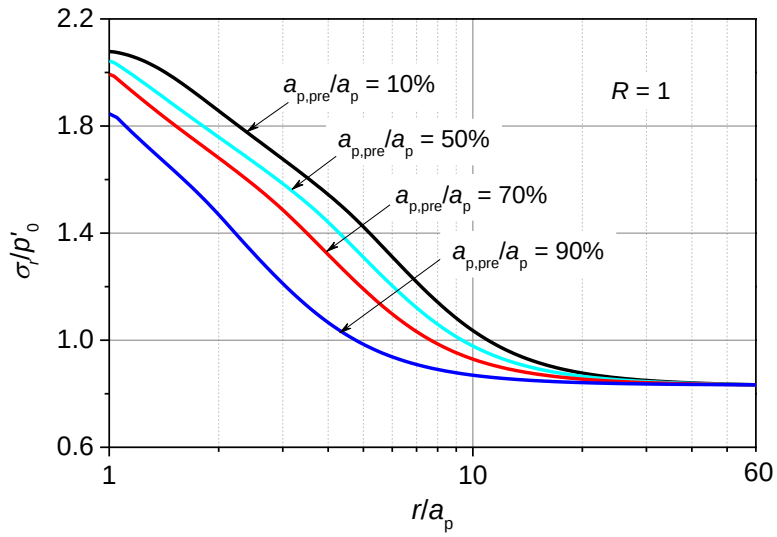

(a)

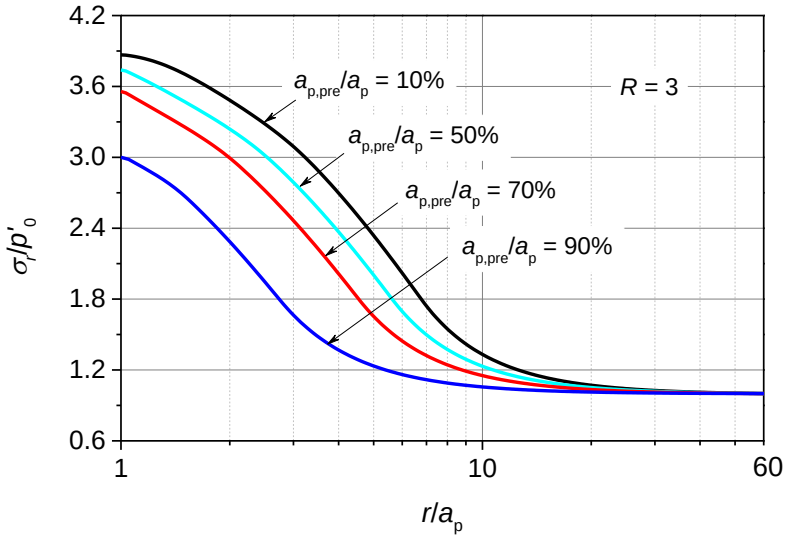

(b)

Loading

The ultimate side resistance of a pile primarily depends on the horizontal effective stress acting on the pile shaft. However, loading would further alter the horizontal effective stress, which in turn will impact the mobilized side resistance. Hence, it is still needed to explore the change in the horizontal stress during loading to determine the mobilized side friction.

Figure 50. Variations of stresses at pile shaft during undrained loading: (a) $R = 1$; (b) $R = 3$

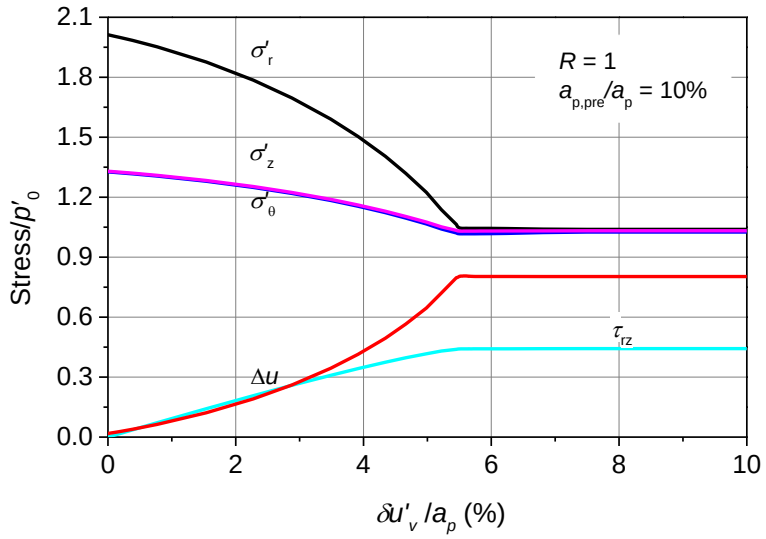

(a)

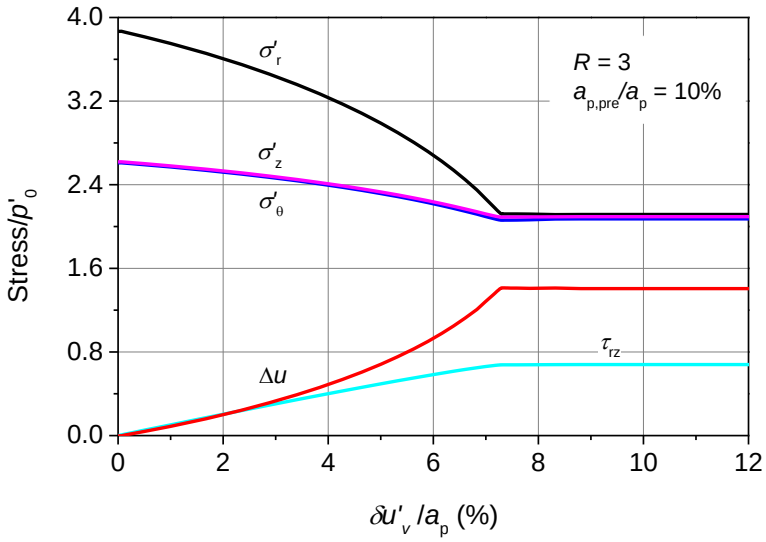

(b)

Figure 50 shows the variations with vertical displacement of the effective radial stress, mean effective stress, as well as the excess pore water pressures during pile loading. The pile displacement is normalized with the pile radius in the figure. As seen in the figure, the radial effective stress, the tangential effective stress and the mean effective stress decrease with the displacement of the pile, because of the undrained loading condition imposed. It also can be found from comparing Figures 50(a) and 50(b) that all the stress components in the moderately overconsolidated soil are apparently higher than those in normally consolidated soil, and hence the side resistance in the moderately overconsolidated soil is larger than that in the normally consolidated soil. It also can be found that the side friction increases with the increase of displacement and reached the ultimate state when $\delta u_v/a_p > 7\%$, after which there is no further mobilization of side resistance with the pile displacement. This demonstrates that the ultimate side resistance would be overestimated with the radial stress after full consolidation of the soil, because the radial stress decreases with the displacement during loading. The present numerical model could properly account for the variation of radial stress during loading, and hence is capable of yielding reasonable ultimate shaft resistance.

Figure 51. Mobilization of side resistance during loading for piles with different sizes of pre-bored hole: (a) $R = 1$; (b) $R = 3$

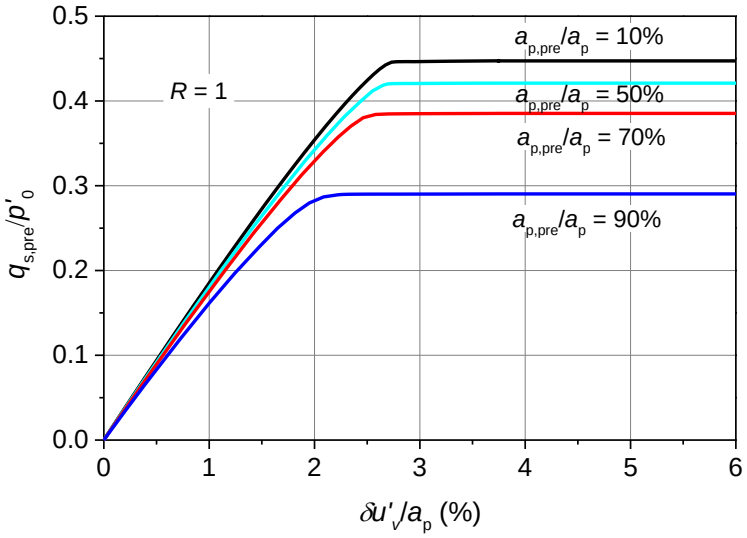

(a)

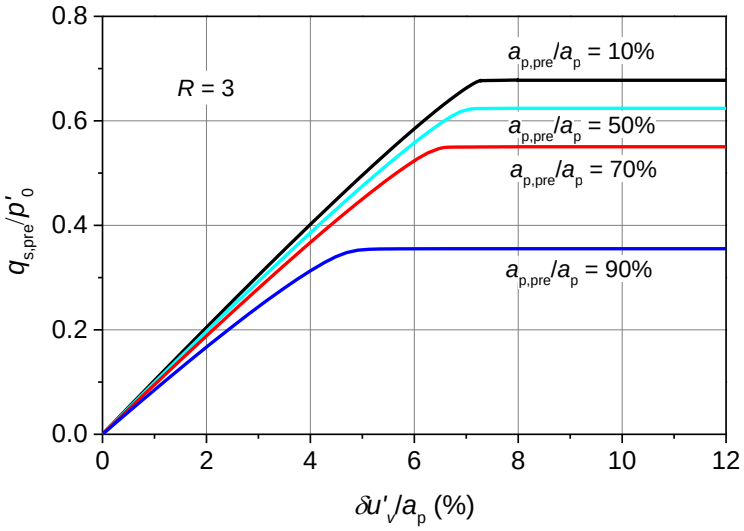

(b)

The mobilizations of the side resistance of piles with different sizes of pre-bored hole during loading are plotted in Figure 51 to investigate the effects of the pre-boring on the long-term load carrying behaviour of the pile. As seen in the figure, because the pile with a smaller pre-bored hole induces stronger enhancement effect on the surrounding soil after consolidation, the pile with smaller pre-bored hole not only exhibits stiffer response during loading, but also yields larger ultimate side resistance. Comparing Figures 51(a) and 51(b), it can be found that the pile in moderately overconsolidated soil exhibits stiffer load carrying response than the pile in normally consolidated soil during loading, which can be well explained by the stress state of the soil around the pile. It should be noted that the ultimate stress presented in this study only corresponds to the peak value, because the MCC model employed here can not reflect the residual behaviour of the soil after peak state. It is therefore the results presented in this report are only suitable to the short and rigid piles. For long and flexible piles, the results are still needed further calibration or more realistic soil model should be adopted to predict the residual stress.

Effective Stress Path

To clarify the mechanism and the effect of pre-boring on the behaviours of the pile, Figure 52 plots the effective stress path of a soil element at the pile shaft for different sizes of pre-bored hole (10%, 70%, and 90% of pile radius) from installation to loading in normally consolidated and moderately consolidated soils.

As seen in Figure 52, the effective stress paths overlap each other in the installation stage, because the soil immediately reaches the critical state once cavity expands. After installation, the stress path moves to the right side of the CSL line as mean effective increases with dissipation of the excess pore water pressures. As indicated by Randolph and Wroth [83], the soil adjacent to a displacement pile will end up in a normally consolidated state after dissipation of the excess pore water pressures. Hence, the increase of the mean effective stress after installation is equivalent to the increase of the preconsolidation pressure of the soil, which leads to the enhancement effects on the surrounding soil. Comparing the stress paths during consolidation, it can be found that the effective stress of the soil element immediately adjacent to the pile with smaller pre-bore hole ends up to a larger mean effective stress point than the others. This clearly demonstrates that installation of a pile with smaller pre-bored hole has stronger enhancement effects on the surrounding soils. When loading the pile, the effective strength path follows the same pattern as the undrained loading assumption is made to the pile installation process. As anticipated, the effective stress path of the soil element immediately adjacent to the pile with smaller pre-bored hole reaches the critical state line at a higher stress point, which corresponding a larger ultimate resistance of the pile.

Figure 52. Effective stress path of a soil element at pile shaft for different sizes of pre-bored hole in $p' - q$ plane: (a) $R = 1$; (b) $R = 3$

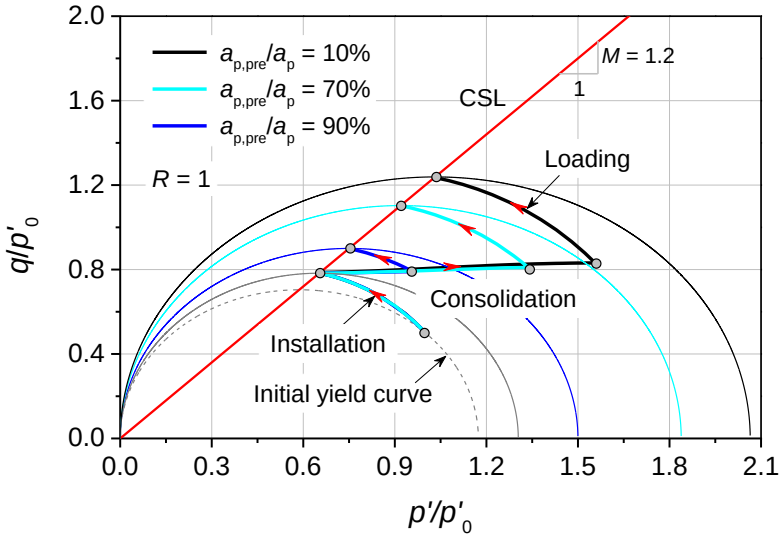

(a)

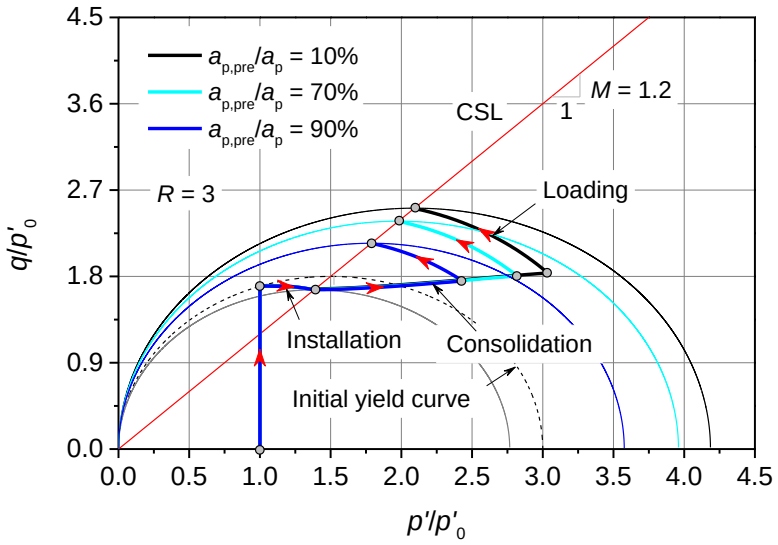

(b)

Figure 53 plots the variation of void ratio of a soil element at the pile shaft for different sizes of pre-bored hole (10%, 70%, and 90% of pile radius) from installation to loading. It can be seen that during pile installation the void ratio keeps constant but the mean effective stress decreases in normally consolidated soils and increases in moderately consolidates soils until it reaches the critical state line because of the undrained assumption made to installation. Since the soil at the pile shaft immediately reaches the critical state at the early stage of cavity expansion, the void ratio reaches the same point after installation. After pile installation, the changes of the void ratio show the same pattern in both normally consolidated and moderately consolidated soils: the void ratio decreases with the increase of mean effective stress as a result of dissipation of the excess pore water pressure. After full consolidation, the void ratio moves to the right side of the critical state line. Because of the stronger squeezing effect generated by installation of a pile with a smaller pre-bored hole, the void ratio around the pile with smaller pre-bored hole is smaller than the other cases. As indicated previously, void ratio relates to the strength and modulus of the soil, thus the denser soil around the pile with a smaller pre-bored hole will yield higher load carrying capacity of the pile. During undrained pile loading, the void ratio keeps constant, and the mean effective stress decreases until the soil reaches the critical state, after which the mean effective stress keeps constant with further shear displacement. As anticipated, the figure shows that the soil element around the pile with a smaller pre-bored hole finally failures at a larger mean effective stress and

smaller void ratio during loading, which corresponds to a higher load carrying capacity of the pile.

Figure 53. $p' - v$ curve of a soil element at pile shaft for different sizes of pre-bored hole: (a) $R = 1$; (b) $R = 3$

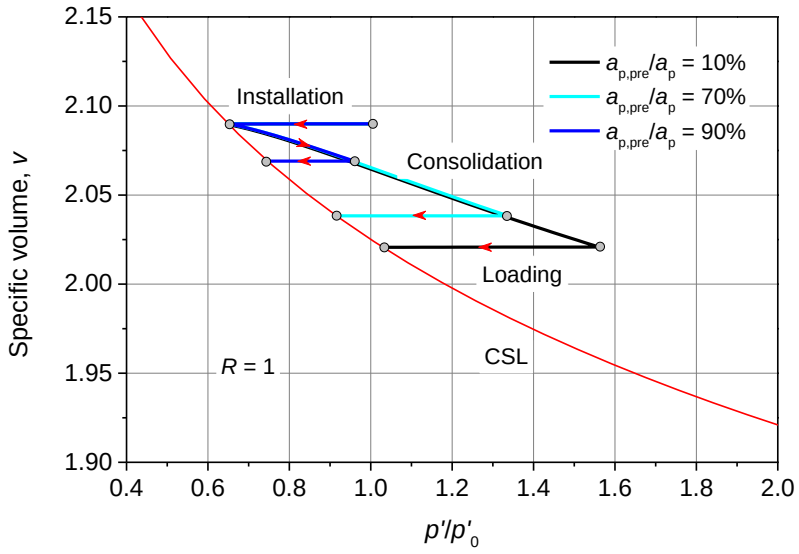

(a)

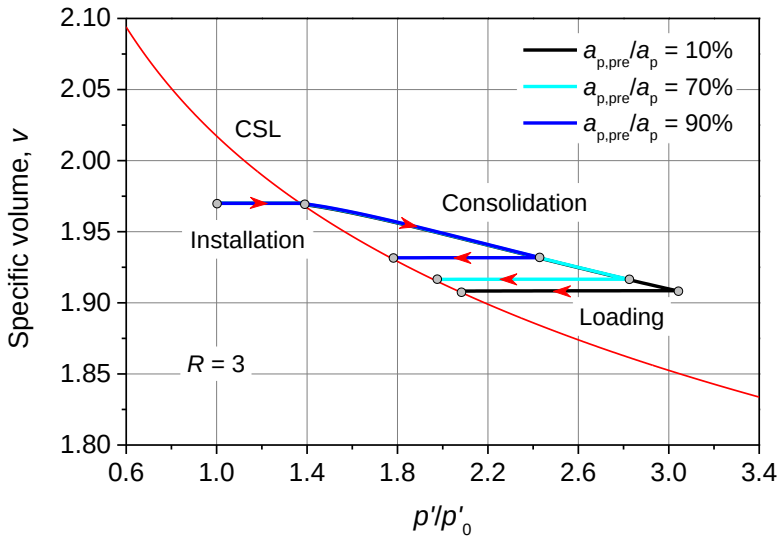

(b)

Reduction Factors for Different Soil Parameters

To investigate the pre-boring effects in different soils, two sets of significant soil parameters, overconsolidation ratio R, and static earth pressure coefficient K_0 are chosen for parametric study. The parameters employed to explore the impacts of R are summarized in Table 6, in which the mean effective stress p_0' and K_0 are the same, while the values of R are different. Table 7 summarizes the parameters used to investigate the impacts of K_0. Based on these parameters, the shaft resistance factors α and β for different values of R and K_0 are plotted in Figures 54 and 55, respectively. The reduction factors R_{qs}, defined as the ratio of the side friction of the pre-bored pile $q_{\mathrm{s,pre}}$ to that of a full displacement pile q_{s}, are plotted in Figure 56 for different values of R and K_0 to facilitate the evaluation of the side friction of a pre-bored pile from that of a full displacement pile.

Table 6. Soil properties used to investigate effects of *R*

R	K_0	p_0' kPa	p_c': kPa	v_0	G_0
1	0.6	120	140.8	2.09	4348
3	0.6	120	422.5	1.95	4307
5	0.6	120	704.2	1.89	3945
7	0.6	120	985.8	1.85	3861
M=1.2, λ=0.15, κ=0.03, v=0.278, v_{cs}=2.74; $k_{h:}$=1E-7 m/s					

Table 7. Soil properties used to investigate effects of K_0

R	K_0	p_0': kPa	p_c': kPa	v_0	G_0
1	0.6	120	144.79	2.08	4341
1	0.8	120	124.44	2.10	4378
1	1.0	120	120.00	2.11	4388
1	1.2	120	122.60	2.10	4383
M=1.2, λ=0.15, κ=0.03, v=0.278, v_{cs}=2.74; $k_{h:}$=1E-7 m/s					

It can be seen from Figure 54 that the shaft resistance factor α decreases with the increase of the size of the pre-bored hole, especially in the range $a_{\mathrm{p,pre}}/a_{\mathrm{p}} > 50\%$, which means the side resistance will be significantly reduced if the size of pre-bored hole is larger 50% of the pile diameter. Upon inspection of Figure 54, it can be found that the shaft resistance factor α decreases with the increase of overconsolidation ratio because the larger value of R corresponds to larger in-situ undrained shear strength. Comparing

Figures 54(a) and 54(b), it can be seen that K_0 has insignificant effects on the shaft resistance factor α, although the resistance factor α increases with the increase of K_0.

Figure 54. Variation of shaft resistance factors α with size of pre-bored hole for different values of (a) *R*; (b) K_0

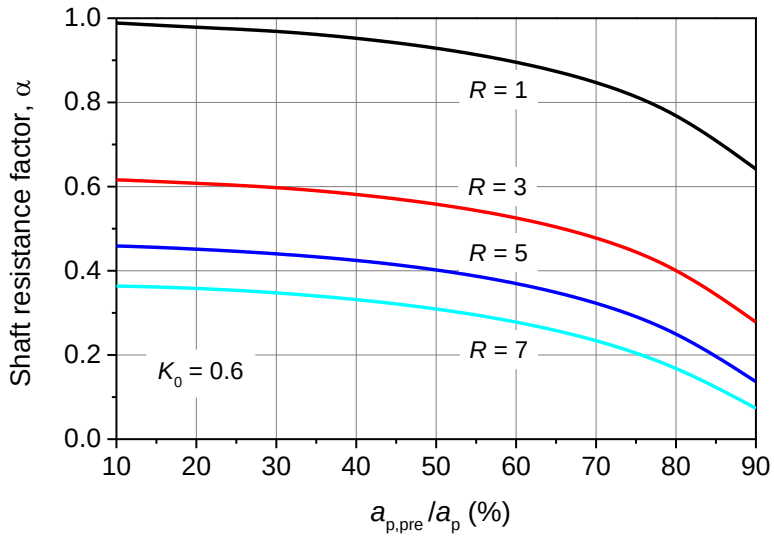

(a)

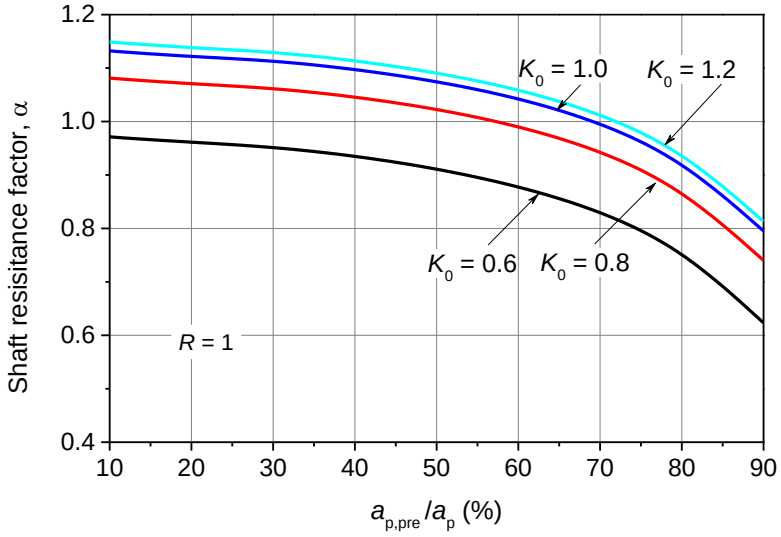

(b)

Figure 55. Variation of shaft resistance factors β with size of pre-bored hole for different values of (a) *R*; (b) K_0

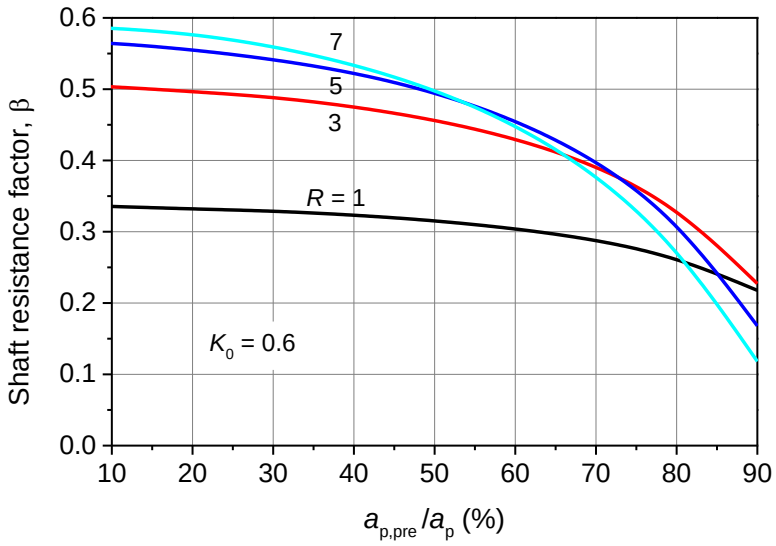

(a)

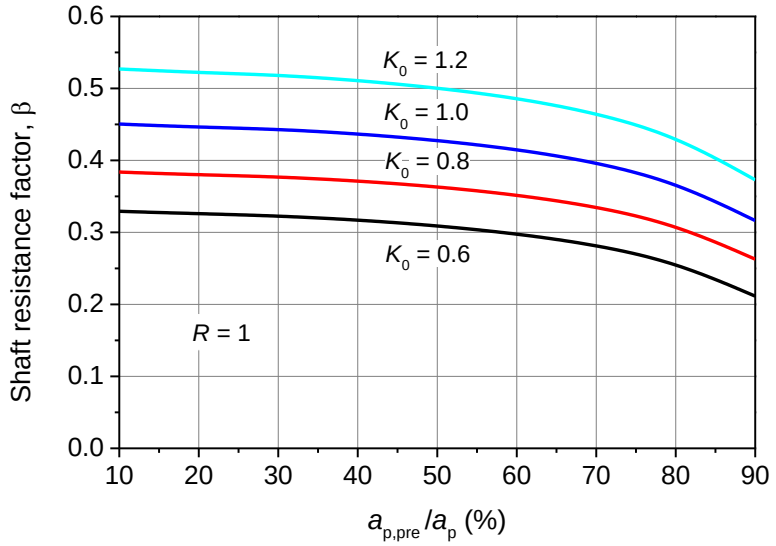

(b)

From Figure 55, it can be seen that the shaft resistance factor β decreases significantly in the range $a_{\mathrm{p,pre}}/a_{\mathrm{p}} > 50\%$. However, the shaft resistance factor β increases with the increases of the overconsolidation ratio, because β is normalized by the in-situ horizontal

effective stress rather than the undrained shear strength. Compared with overconsolidation ratio R, K_0 also has significant effects on the shaft resistance factor β, because the shaft resistance factor β depends on the horizontal effective stress. From Figures 54 and 55, it can be concluded that the shaft resistance factor depends on the overconsolidation ratio, the static earth pressure coefficient and the size of pre-bored hole. Hence, a reasonable assessment of the long-term load carrying capacity should take these significant parameters into account.

Figure 56. Variation of reduction factors R_{qs} with size of pre-bored hole for different (a) R; (b) K_0

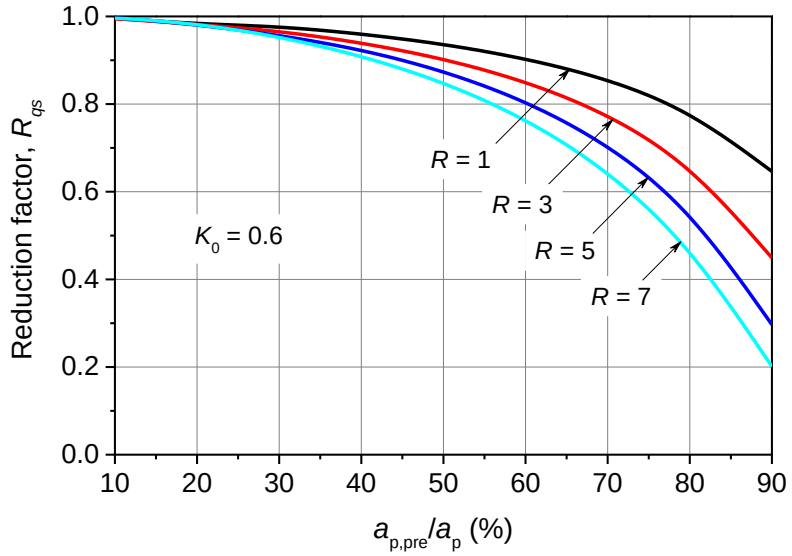

(a)

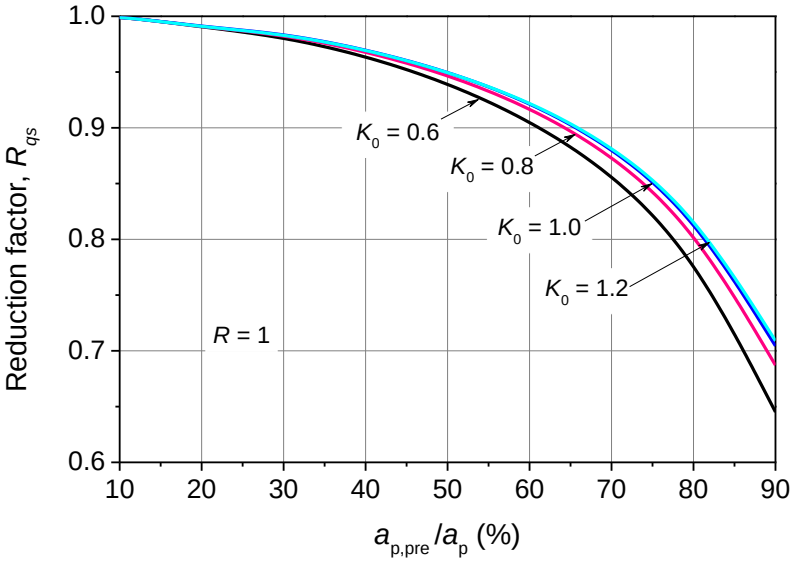

(b)

It can be seen from Figure 56 that, the reduction factor R_{qs} decreases with the increase of the size of the pre-bored hole, which demonstrates that the ultimate side resistance decreases with the increase of the size of the pre-bored hole according to the definition of R_{qs}. However, as shown in Figure 56, the reduction factor decreases insignificantly in the range $0 < a_{p,pre}/a_p < 50\%$, in which the reduction factor reduces by 7% and 14% for $R = 1$ and $R = 7$, respectively. In the range $a_{p,pre}/a_p > 50\%$, the reduction factor decrease significantly with the increase of the size of the pre-bored hole. The shaft resistance increases by an amount of approximately 10%–18% when $a_{\mathrm{p,pre}}/a_{\mathrm{p}}$ decreases from 80% to 70%. For the size of the hole usually adopted in practical engineering (80 % of pile radius), the side resistance of the pre-bored pile is in the order 78% and 50% of the side resistance of a full-displacement pile for $R = 1$ and $R = 7$, respectively. This means that pre-boring will reduce more amount of shaft resistance of piles in stiff/hard soils, although pre-boring could effectively facilitate pile driving in stiff/hard soils. It also can be observed from Figure 56(a) that the reduction factor decreases with the increase of R. Comparing with the effects of R, Figure 56(b) shows that the static earth pressure coefficient K_0 has insignificant effects on side friction. This is because the radial effective stress σ_r' becomes the major principle stress and reaches the critical state with the same stress state during pile installation regardless of the value of K_0.

Parametric Study

In this section, extensive parametric studies are conducted by taking advantage of the proposed practical formulas to further explore the impacts of the size of pre-drilled hole, the overconsolidation ratio and the coefficient of static earth pressure on the driving force, the setup of shaft resistance and long-term shaft resistance of pre-bored piles. The parameters employed in parametric study are the same as those listed in table. 5.

Driving Force Reduction

Figures 57a-57e plot the variations of the driving force reduction factor with the size of the pre-drilled hole for different overconsolidation ratios R, residual friction angles φ_r', ratios of length to diameter l/d, initial shear moduli G_0/p_0', and coefficients of static earth pressure K_0.

Figure 57. Variation of reduction factor with size of pre-bored hole for different values of (a) R; (b) φ_r'; (c) l/d; (d) G_0/p_0' (e) K_0

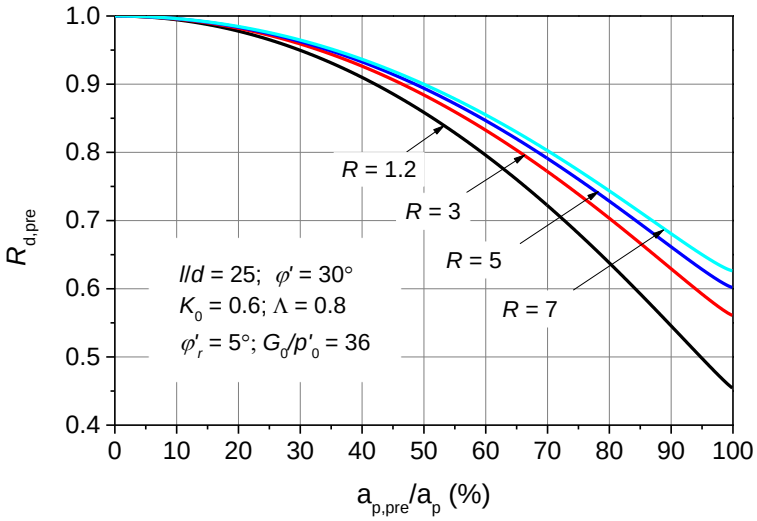

(a)

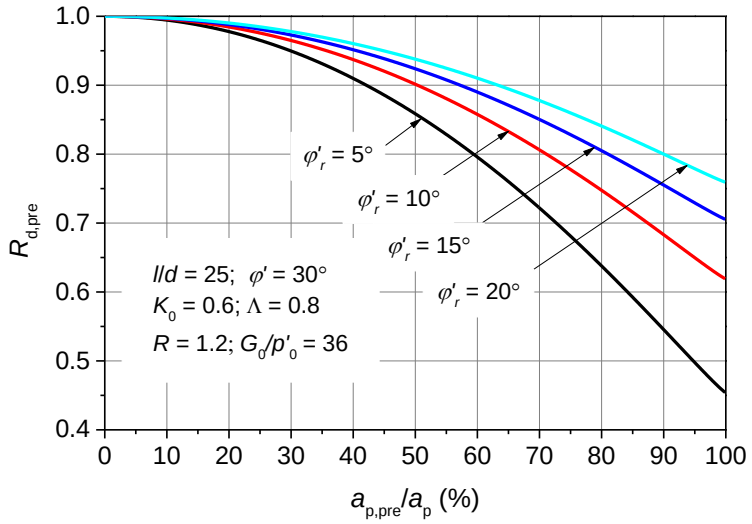

(b)

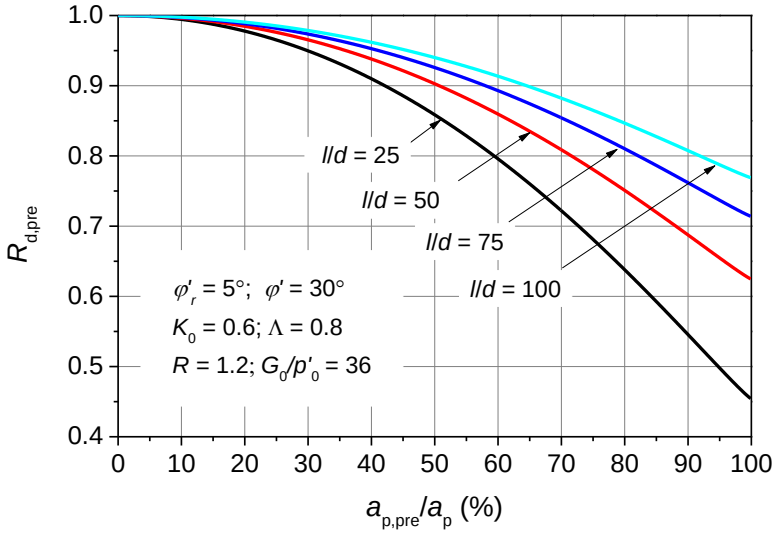
1.0
0.9
0.8
0.7
0.6
0.5
0.4
$R_{d,pre}$
0
10
20
30
40
50
60
70
80
90
100
$a_{p,pre}/a_p$ (%)
l/d = 25
l/d = 50
l/d = 75
l/d = 100
φ'_r = 5°; φ' = 30°
K_0 = 0.6; Λ = 0.8
R = 1.2; G_0/p'_0 = 36

(c)

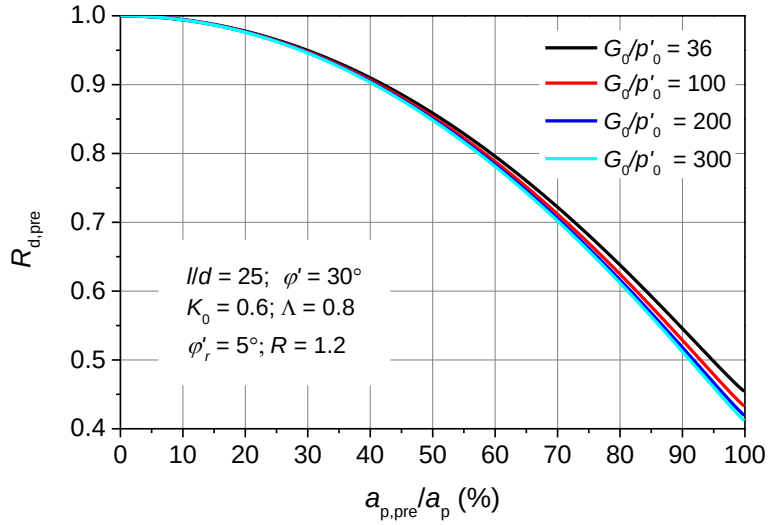
1.0
0.9
0.8
0.7
0.6
0.5
0.4
$R_{d,pre}$
0
10
20
30
40
50
60
70
80
90
100
$a_{p,pre}/a_p$ (%)
G_0/p'_0 = 36
G_0/p'_0 = 100
G_0/p'_0 = 200
G_0/p'_0 = 300
l/d = 25; φ' = 30°
K_0 = 0.6; Λ = 0.8
φ'_r = 5°; R = 1.2

(d)

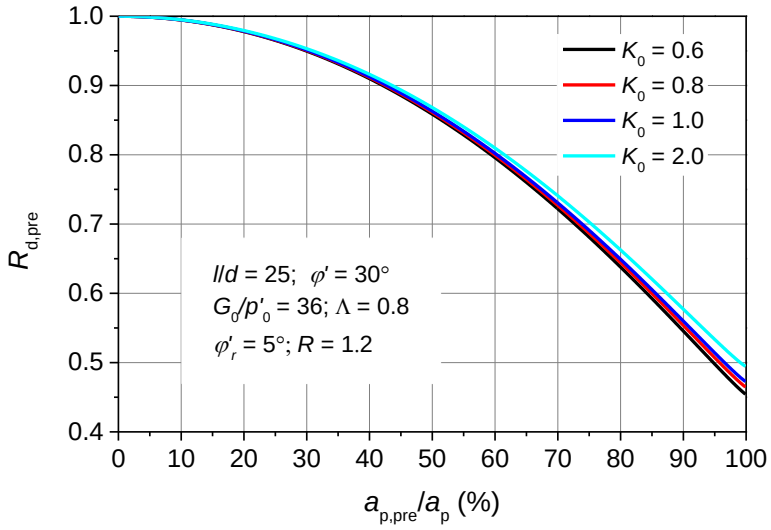

(e)

As seen in these figures, the reduction factor $R_{d,pre}$ increases with the decrease of the size of the pre-bored hole for all the cases investigated. The driving force increases about 4%–6% when $a_{\mathrm{p,pre}}/a_{\mathrm{p}}$ decreases from 80% to 70%. In comparison with Fig. 56, it can be found that the shaft resistance decreases more significantly than the driving force when the size of the pre-drilled hole increases. The shaft resistance increases about 10%–18% at the expense of increase of 4%–6% driving force for a wide range of soils when $a_{\mathrm{p,pre}}/a_{\mathrm{p}}$ decreases from 80% to 70%. The driving force of a pile with pre-bored hole of 80% of the pile diameter is on the order of 65%-85% of driving force of a full displacement pile. Further inspection the above figures reveals that the reduction factor $R_{d,pre}$ primarily depends on the overconsolidation ratio R, residual friction angles φ'_r, ratios of length to diameter l/d, while the initial shear modulus G_0/p'_0 and the coefficient of static earth pressure K_0 has negligible effects on the reduction factor. It can be seen that increases of the overconsolidation ratio R, residual friction angle φ'_r, ratio of length to diameter l/d lead to increase of the reduction factor $R_{d,pre}$, which indicates that the reduction effect of pre-boring on the driving force weakens in the soil with larger values of OCR and φ'_r and l/d.

Effects of Size of Pre-drilled Hole. Figures 58-61 plot the dissipation of the normalized excess pore water pressure $\Delta u/p_0'$, the variations of the normalized undrained shear strength $s_{\mathrm{u,tc}}(t)/s_{\mathrm{u0}}$, the normalized shear modulus $G(t)/G_0$, and the shaft resistance $\alpha(t)$ with the normalized time factor after pile installation for different sizes of pre-drilled hole. The overconsolidation ratio $R = 3$ and $\chi = 0$ are used in the analysis.

Figure 58. Dissipation of excess pore water pressure after pile installation for different sizes of pre-drilled hole

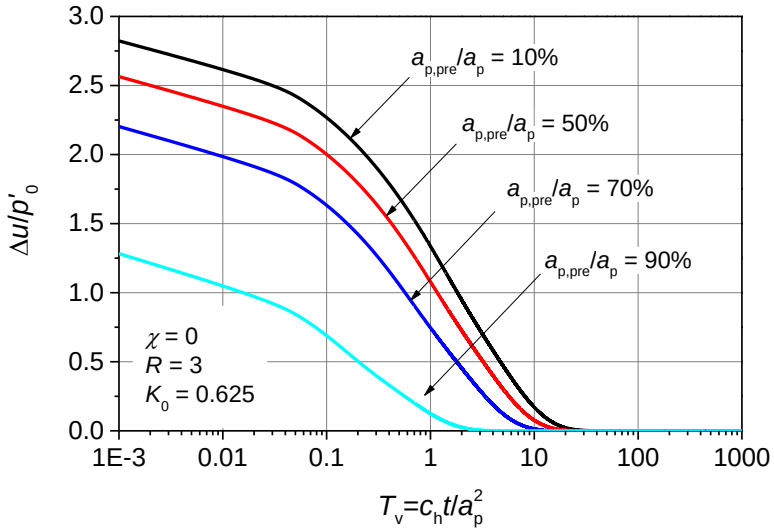

Figure 59. Variation of undrained shear strength ratio with time factor after pile installation for different sizes of pre-drilled hole

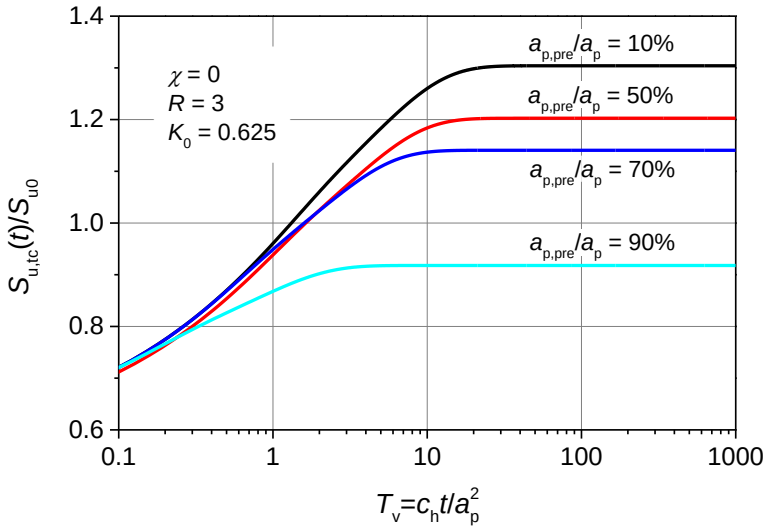

Figure 60. Variation of shear modulus ratio with time factor after pile installation for different sizes of pre-drilled hole

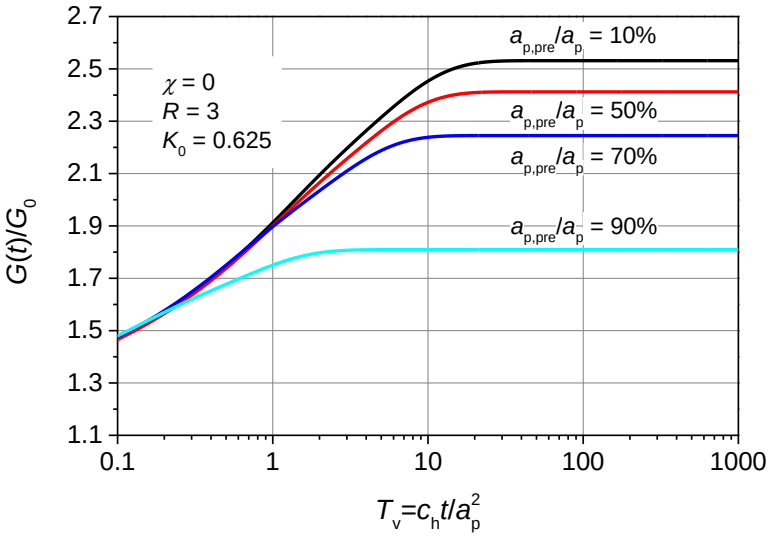

Figure 61. Variation of shaft resistance factor with time factor after pile installation for different sizes of pre-drilled hole

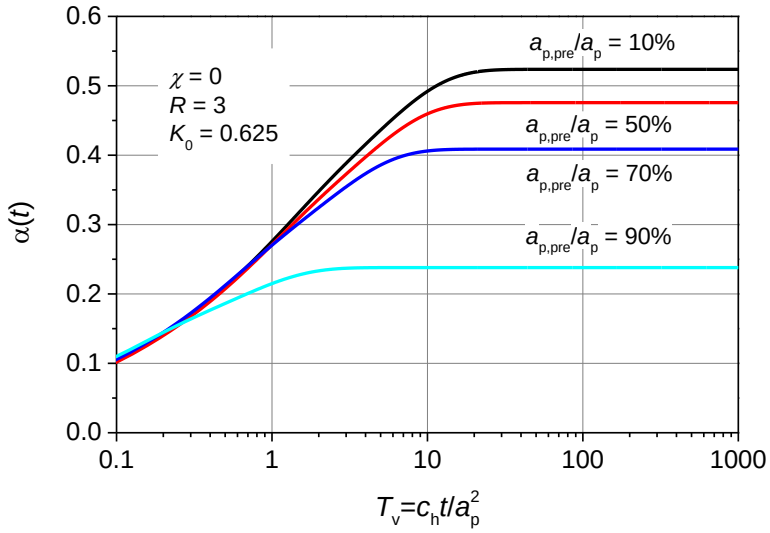

As seen in Figure 58, the magnitude of the excess pore water pressure immediately after pile installation is smaller in the soil adjacent to the pile with larger size of pre-drilled hole, which again indicates that the squeezing effect of pile installation decreases with the increase of the size of pre-drilled hole. It also can be seen that the time required to full dissipate the excess pore water pressure is shorter for the pile with larger size of pre-drilled hole. Corresponding to the dissipation of the excess pore water pressure, Figures 59-61 show that the undrained shear strength, the shear modulus and the shaft resistance increase with dissipation of the excess pore water pressures but the increment decreases with the increase of the size of the pre-drilled hole. Due to the remolding effects of pile installation, the undrained shear strength of the soil adjacent to the pile immediately after pile installation is smaller than the in situ shear strength of the soil. With passage of time, the soil recovers its strength and exceeds the in situ shear strength for the cases $a_{\mathrm{p,pre}}/a_{\mathrm{p}} = 10\%, 50\%$, and 70%. For the case $a_{\mathrm{p,pre}}/a_{\mathrm{p}} = 90\%$, the shear strength after full dissipation of the excess pore water pressure is still smaller than the in situ shear strength, although the soil experience substantial recovery of the strength. All of the above observations manifest that pre-boring will result in a loss of setup and a reduction in long-term shaft resistance and the reduction effect increases with the size of the pre-drilled hole.

Effects of Overconsolidation Ratio. The variations of the excess pore water pressure, the normalized excess pore water pressure $\Delta u/p_0'$, the variations of the

normalized undrained shear strength $s_{\mathrm{u,tc}}(t)/s_{\mathrm{u0}}$, the normalized shear modulus $G(t)/G_0$ and the shaft resistance $\alpha(t)$ with the normalized time factor after pile installation for different overconsolidation ratios are plotted in Figures 62-65. The size of the pre-drilled hole used in the analysis is equal to 50% of the pile radius.

Figure 62. Dissipation of excess pore water pressure after pile installation for different overconsolidation ratios

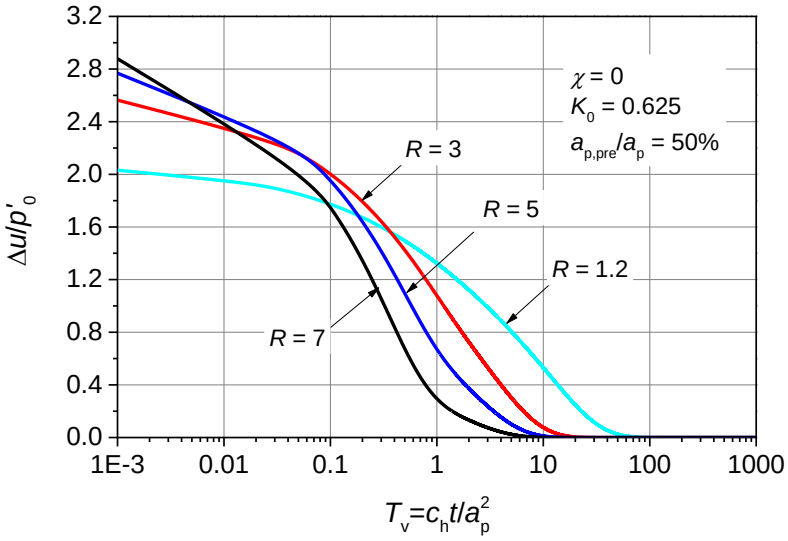

Figure 63. Variation of undrained shear strength ratio with time factor after pile installation for different sizes of pre-drilled hole

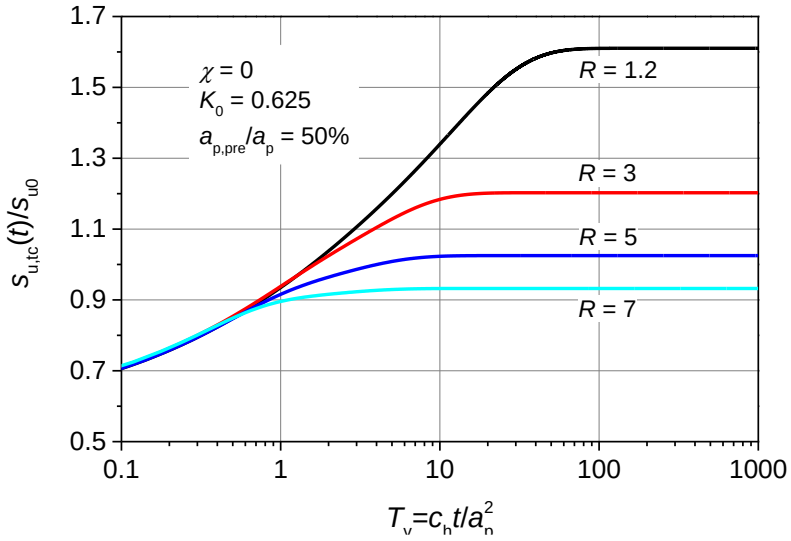

Figure 64. Variation of shear modulus ratio with time factor after pile installation for different overconsolidation ratios

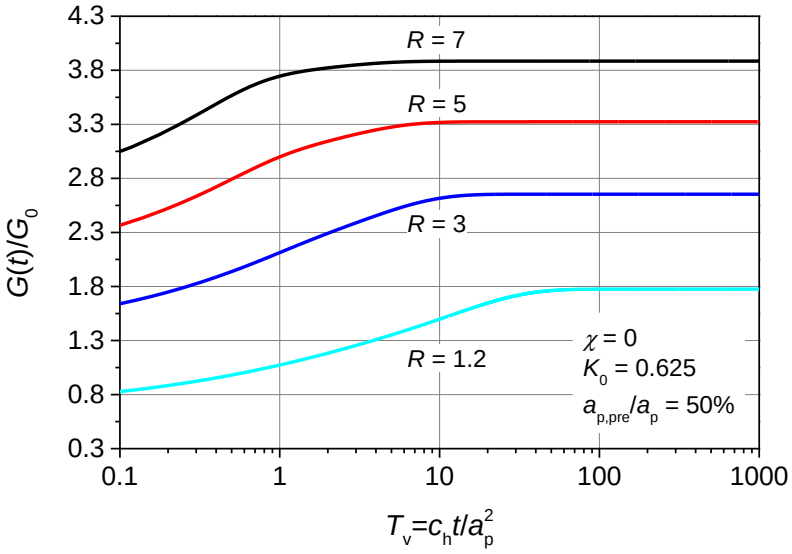

Figure 65. Variation of shaft resistance factor with time factor after pile installation for different overconsolidation ratios

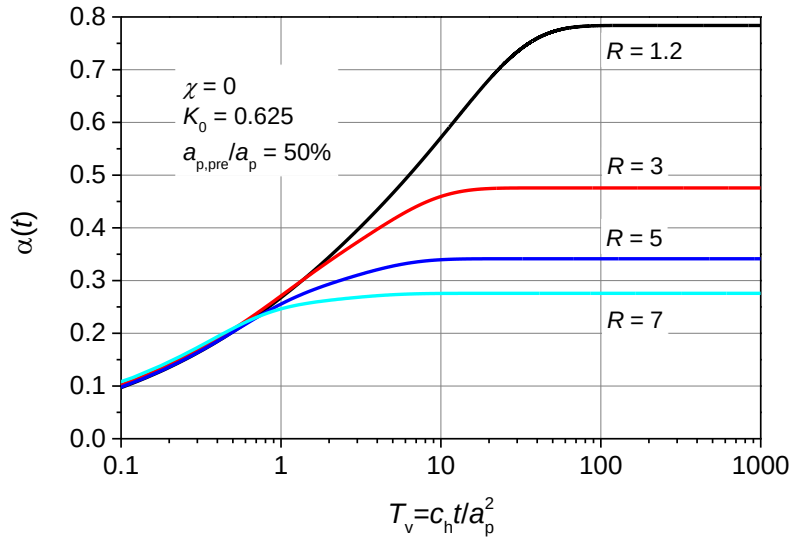

As observed from Figures 62-65, the installation induced excess pore water pressure increases with the increase of the overconsolidation ratio but the time required for full dissipation of the excess pore water pressure decreases as the overconsolidation ratio increases due to the higher gradient of the excess pore-water pressure. Although higher excess pore water pressure is generated in the soil with larger value of overconsolidation

ratio, the setup of the undrained shear strength and the shaft resistance factor decrease as the overconsolidation ratio increases. This indicates that the pile installed in the soil with smaller overconsolidation ratio exhibits more significant setup of shaft resistance. However, it should be emphasized that the long-term undrained shear strength and shaft resistance in fact are still larger for the soil with larger overconsolidation ratio, as the undrained shear strength is normalized with the in situ undrained shear strength that increases more significantly with the increases of the overconsolidation ratio. It is also interesting to note that the shear modulus immediately after installation is higher than the in situ values for the cases $R = 3, 5, 7$, while smaller than the in situ value for the case $R = 1.2$. This is because mean effective stress increases in the overconsolidated soil while decreases in the normally consolidated soil during the expansion phase of pile installation.

Effects of Coefficient of Earth Pressure at Rest. Figures 66-69 show the variations of the normalized excess pore water pressure $\Delta u/p_0'$, the normalized undrained shear strength $s_{\mathrm{u,tc}}(t)/s_{\mathrm{u0}}$, the normalized shear modulus $G(t)/G_0$ and the shaft resistance $\alpha(t)$ with the normalized time factor after pile installation for different coefficients of earth pressure at rest. $a_{\mathrm{p,pre}}/a_{\mathrm{p}} = 50\%$ and $R = 3$ are used in the analysis. As seen in the figure, an increase of the coefficient of earth pressure at rest results in an increase of the excess pore water pressure immediately after installation. As a consequence, the setup effects and the long-term shear strength, shear modulus and shaft resistance factor increase with the increase of the coefficient of earth pressure at rest. However, compared with the effects of the size of the pre-drilled hole and the overconsolidation ratio, the effect of the coefficient of earth pressure at rest is not very obvious, although it more or less impacts the setup effects and the long-term shear strength, shear modulus and shaft resistance factor.

Figure 66. Dissipation of excess pore water pressure after pile installation for different coefficients of earth pressure at rest

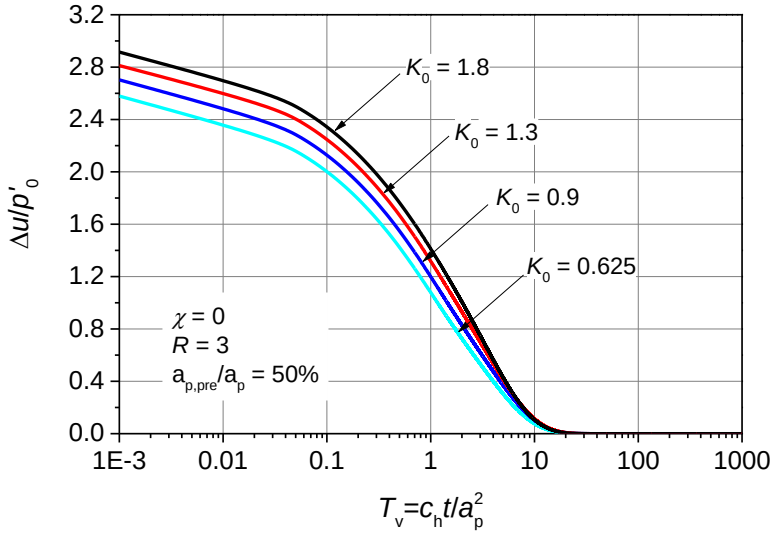

Figure 67. Variation of undrained shear strength ratio with time factor after pile installation for different coefficients of earth pressure at rest

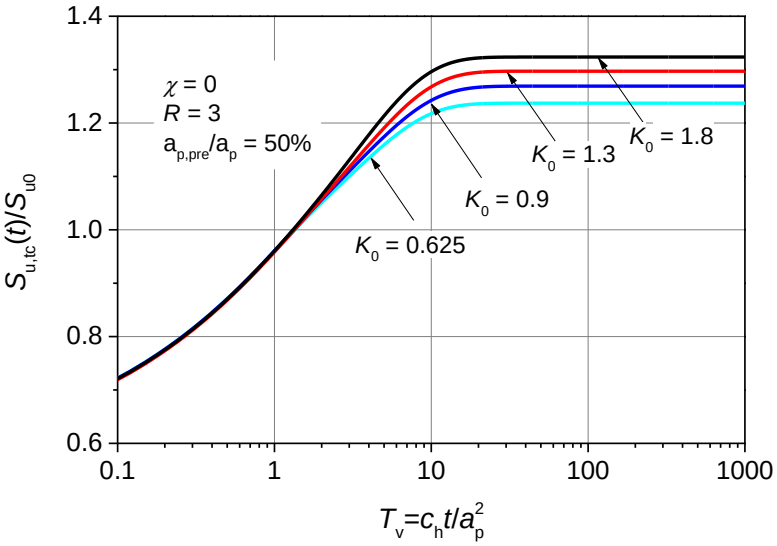

Figure 68. Variation of shear modulus ratio with time factor after pile installation for different coefficients of earth pressure at rest

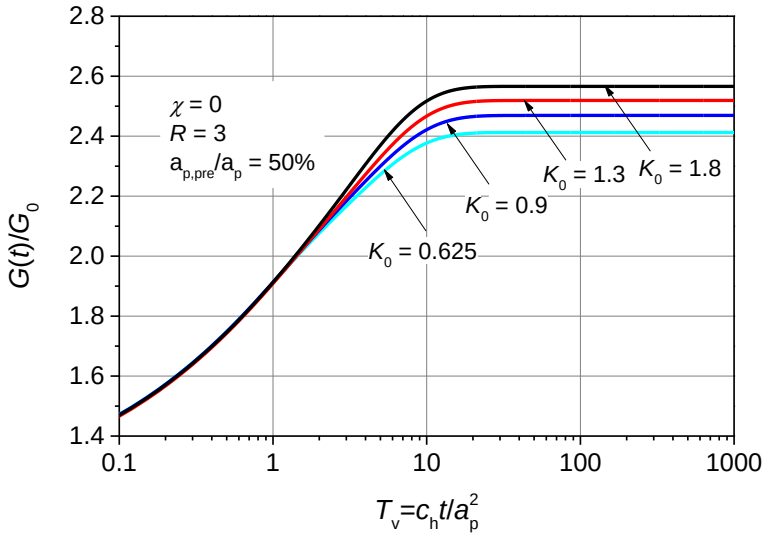

Figure 69. Variation of shaft resistance factor with time factor after pile installation for different coefficients of earth pressure at rest

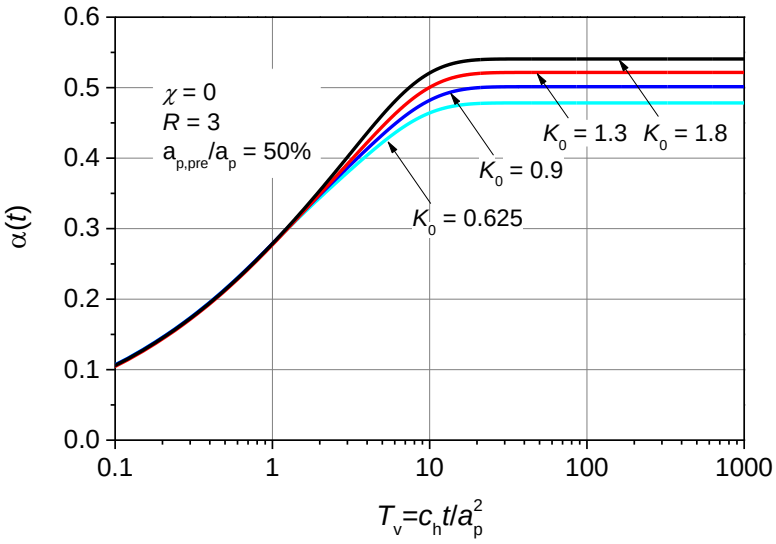

Figures 70 and 71 plot the variations of the long term shaft resistance factor and shaft resistance reduction factor, respectively, with the size of the pre-drilled hole for different coefficients of earth pressure at rest. Note $R = 1.2$ is used to draw the figures. Due to the stronger horizontal restriction effects, more significant squeezing effect will be induced by pile installation in the soil with larger coefficient of earth pressure at rest, which will

enhance the density and improve the stress state of the soil after consolidation. Hence it can be seen in Figure 70 that the long-term shaft resistance factor increases as the coefficient of earth pressure at rest increases. It is also interesting to see from Figure 71 that the reduction factor almost keeps unchanged with the increases of the coefficient of earth pressure at rest, which means the coefficient of earth pressure at rest has a negligible effect on the shaft resistance reduction factor, although it slightly impacts the setup and long-term shaft resistance of the pre-bored pile.

Figure 70. Long-term shaft resistance factor for different coefficients of earth pressure at rest

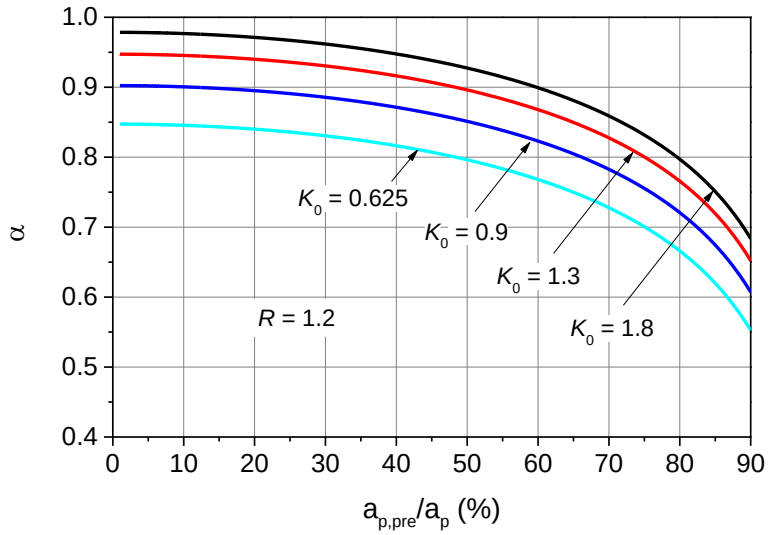

Figure 71. Shaft resistance reduction factor for different coefficients of earth pressure at rest

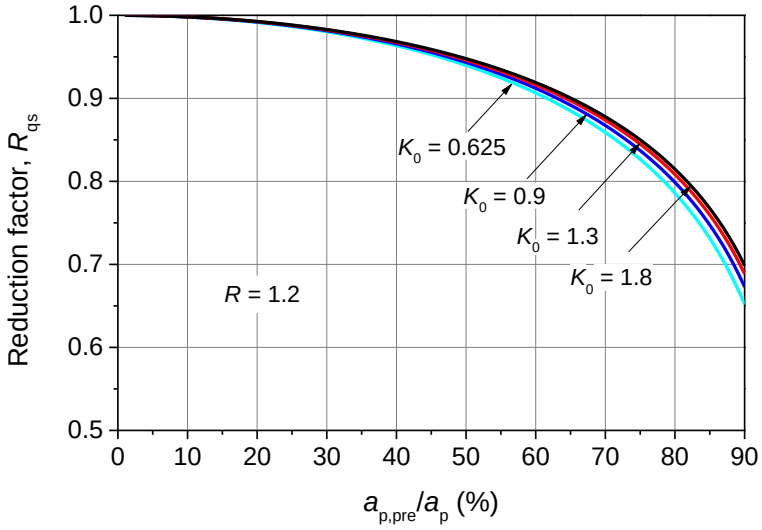

Since the expansion effects of pile installation is modeled by undrained cavity expansion in this report, the numerical model and the practical design formulas are in fact developed for the precast circular driven piles. However, the square precast prestressed concrete driven pile is the most common pile type used in Louisiana. Hence, before applying the developed numerical model and the proposed design formulas to square precast concrete pile, the diameter of the square pile should first be equivalent to the circular driven piles based on the volume equivalent principle. For a square precast concrete pile with side length of b, the corresponding equivalent diameter of circular pile, D_{eq}, can be given as follows:

$$D_{\mathrm{eq}} = \frac{2b}{\sqrt{\pi}} \qquad (59)$$

Take advantage of equation (62), the numerical model, the practical design formulas as well as the results presented in this report can be applied for the square precast concrete pile. However, it should be noted from Eq. (62) that a pre-boring diameter 80% (maximum value of $a_{\mathrm{p,pre}}/a_{\mathrm{p}}$ recommended by LADOTD) of the square pile side dimension is nearly the same as 70% of the equivalent diameter of a circular pile, while pre-boring 80% of the diagonal dimension is the same as 100% of the equivalent diameter of a circular pile. Since pre-boring 100% of the equivalent diameter of a circular pile would result in a total reduction of the side resistance in the prebored zone, this indicates that the side dimension instead of the diagonal dimension should be considered

to determine pre-bore diameter (with the use of reduction factor proposed in this report), if the resistance in that zone is relied upon to meet the required nominal resistance.

Conclusions

Pre-boring is a routine practice used to aid large displacement pile installation in hard/stiff cohesive soils. However, the design of pre-bored piles primarily relies on the local experiences at present as the effects of pre-boring on the driving force, the setup and long-term shaft resistance of the pile are still unclear. Quantifying the impacts of pre-boring on the drivability and long-term load carrying capacity of the pile will greatly help geotechnical design engineers to understand the interactions among the factors of pre-boring, pile size, soil conditions, pile driving, etc. and improve the design and construction qualities of pile foundations in hard/dense soils. However, it is impractical to conduct large number of fully instrumented pile load tests due to the significant cost involved. As an alternative to the field experimentation, numerical simulation and analytical analysis are conducted in this report to investigate the impacts of the size of pre-drilled hole on the driving force reduction, the setup and the long-term load carrying capacity of pre-bored piles. From the numerical analysis and analytical study, the major conclusions can be draw as follows:

- Pre-boring significantly impacts the magnitude and the distribution range of the excess pore water pressure, which is the primary cause that influences the long-term behaviours of the piles with different sizes of pre-bored hole.
- Both the mean effective stresses and the radial effective stresses are significantly higher than their in-situ values after full consolidation of the surrounding soils. The effective stresses around the pile with larger size of pre-bored hole are smaller than that around the pile with smaller size of pre-bored hole after consolidation.
- The pile with smaller pre-bored hole not only exhibits stiffer response during loading, but also yields larger ultimate side resistance. The reduction in side resistance decreases with the increase of overconsolidation ratio, while K_0 has an insignificant effect on the reduction factor.
- The driving force reduction is irrelevant to the shaft resistance as the soil immediately reaches the critical state once the pre-drilled hole expands. The reduction of the pile tip resistance due to pre-boring is the primary cause for the driving force reduction.

- Pre-boring not only reduces the driving force required for pile installation, but also results in a loss of setup and a reduction in long-term shaft resistance and the reduction effects increases with the size of the pre-drilled hole.
- The driving force reduction effect decreases with increases of the overconsolidation ratio, residual friction angle, ratio of length to diameter. The coefficient of static earth pressure has a negligible impact on the driving force reduction.
- The setup effects and long-term shaft resistance factor decrease significantly with the increase of the overconsolidation ratio. However, the long-term shaft resistance of the pre-drilled pile increases as the overconsolidation ratio increases.
- The coefficient of earth pressure at rest slightly impacts the driving force, the setup and long-term shaft resistance of pre-bored piles but has negligible effects on the driving force reduction factor and the shaft resistance reduction factor.
- The shaft resistance reduction factor R_{qs} and the shaft resistance factors α and β decrease significantly when $a_{\mathrm{p,pre}}/a_{\mathrm{p}} > 50\%$, while decrease insignificantly in the range of $0 < a_{\mathrm{p,pre}}/a_{\mathrm{p}} < 50\%$. This means the long-term load carrying capacity will be reduced greatly if the size of the pre-bored hole is larger than 50% of the pile radius.
- For the hole size $a_{\mathrm{p,pre}}/a_{\mathrm{p}} = 80\%$ proposed by LTRC [21], the shaft reduction factor R_{qs} falls in the range of $0.50-0.78$ for the typical Louisiana soils, which indicates the side resistance of a pile with a pre-bored size of 80% is about $50\%-78\%$ the side resistance of a full-displacement pile in typical Louisiana soils.
- According to the volume equivalent principle, the diameter of a pre-drilled hole with diameter of 80% of the side dimension of a square pile is equal to 70% of the diameter of an equivalent cylindrical pile, i.e., $a_{\mathrm{p,pre}}/a_{\mathrm{p}} = 70\%$ in terms of a cylindrical pile. For $a_{\mathrm{p,pre}}/a_{\mathrm{p}} = 70\%$, the shaft reduction factor R_{qs} falls in the range of 0.63-0.85 for the typical Louisiana soils investigated.
- The 2016 edition of the *Louisiana Standard Specifications for Roads and Bridges* (LSSRB) does not specify a limit for pre-bored hole diameter. It does require that any pre-boring below the scour elevation be approved by the Engineer of Record. Previous editions of the specification used a prebored hole

diameter of 80% of the pile diameter. This limitation is still commonly used in practice. The results of this study indicate that an 80% diameter prebored hole can result in long-term side resistance that is 50% to 78% of that of a non-prebored pile. This result indicates that when the 80% criterion is applied the effect on side resistance should be carefully considered.

- For square concrete piles, a pre-boring diameter 80% of the pile side dimension is nearly the same as 70% of the equivalent diameter of a circular pile, while pre-boring 80% of the diagonal dimension is the same as 100% of the equivalent diameter of a circular pile. Pre-boring 100% of the equivalent diameter of a circular pile would result in a total reduction of the side resistance in the prebored zone. This indicates that the diagonal dimension should not be used to determine pre-bore diameter if the resistance in that zone is relied upon to meet the required nominal resistance.

Recommendations

A reasonable design of the size of the pre-bored hole should balance the cost of pile installation and the long-term load carrying capacity to achieve the goal of reducing number of piles, shortening pile lengths, and reducing pile cross-sectional area as well as reducing the size of driving equipment. The results presented in this report show that the shaft resistance increases more significantly than the driving force when the size of the pre-drilled hole increases. The shaft resistance increases about 10%–18% at the expense of increase of 4%–6% driving force for a wide range of soils when $a_{\mathrm{p,pre}}/a_{\mathrm{p}}$ decreases from 80% to 70%. Hence, it is recommended that $a_{\mathrm{p,pre}}/a_{\mathrm{p}} = 70\%$ or slightly smaller size of pre-drilled hole should be considered for pre-piles in Louisiana in order to reduce the total cost of the pile, if the drivability allows. Of course, the proposed design formulas and the reduction factors generated from the numerical model still need to be validated/calibrated with the field test results, before they can be recommended for use in evaluating the drivability and long-term capacities of real world pre-bore piles. Hence, the researchers have the following recommendations for the future instrumented field tests

- The site selection for the intended pile load tests is critical, which shall reflect the typical field conditions that require the pre-boring to be used for pile installation. The typical soil profiles at the north of Louisiana, which mainly consists of a firm to stiff clay of 20 ft. thickness, and an underlying stiff to very stiff clay layer extending to the elevation of 200 ft. is recommended for the future field pile tests.
- The pile is recommended to be instrumented with stress transducer, pore pressure transducers, and the vibrating wire strain gauges to record the driving force, the soil pressure, the pore water pressure and the strain of the pile during the test. The quick test procedure suggested by ASTM standard D1143 [82] is recommended for the static loading tests.
- Given the fact that the reduction factor decreases significantly when $a_{\mathrm{p,pre}}/a_{\mathrm{p}} > 50\%$, the instrumented pile tests are recommend to investigate four different sizes of pre-bored hole, $a_{\mathrm{p,pre}}/a_{\mathrm{p}} = 60\%,\ 70\%,\ 80\%$ and 90% as well as the case of without pre-boring

- The field data gathered from the pile load tests should be compared with the numerical results and the proposed design formulas. Whenever necessary, some correction factors may be introduced to better fit the measured data and to improve the accuracy of the numerical model and practical design formulas for predicting the side friction of pre-bored piles.

Acronyms, Abbreviations, and Symbols

Term	Description
$\bar{C}_{\mathrm{h}}$	Generalized coefficient of consolidation
$\Delta\sigma'_{h\mathrm{i}}$	Horizontal stress change induced by pile installation
$\Delta\sigma'_{hc}$	Stress change due to subsequent soil consolidation
$\Delta\sigma'_{hl}$	Stress change during the loading process
σ'_{rf}, $\sigma'_{\theta\mathrm{f}}$, σ'_{zf}	Radial, tangential and vertical effective stresses in the critical state zone, respectively
σ'_a	Cavity pressure
A_b	Area of pile base
A_n	Integration constants
A_{pp}	Prebored area
A_{tp}	Total pile area
C_F	Correction factor for K_δ when δ' is not equal to frictional angle of soil
C_d	Perimeter of pile
F_d	Total driving force of full displacement piles
F_{pre}	Total driving force of pre-bored piles
$F_{s,pre}$, $F_{b,pre}$	Force provided by pile shaft resistance and pile tip resistance
G_0	Initial shear modulus
J_0, J_1	First kind Bessel functions of zero-order and first-order, respectively
K_0	Coefficient of lateral earth pressure at rest
K_{0nc}	Coefficient of lateral earth pressure for normally consolidated soil
K_s	Ratio of vertical effective stress to local effective radial stress at failure
K_δ	Coefficient of lateral earth stress at certain depth
P_u, P_{u0}	Pile loading capacity with and without pre-boring, respectively
Q_b	Ultimate base resistance
Q_s	Ultimate shaft resistance
Q_s	Total shaft resistance
Q_u	Total pile bearing capacity

Term	Description
R_{p}	Radius beyond which the excess pore water pressure remains zero
R_{qs}	Shaft resistance reduction factor
$R_{d,pre}$	Reduction factor for driving force
U_{r}	Radial displacement
Y_0, Y_1	Second kind Bessel functions of zero-order and first-order, respectively
$a_{\mathrm{p,pre}}$	Size of pre-bored hole
a_{p}	Pile diameter
$f_{\mathrm{s,I}}$	Shear stress at the pile shaft
$f_{\mathrm{s,L}}(t)$	Ultimate shaft resistance after pile installation
$f_{\mathrm{s,pre}}(t)$	Shaft resistance of pre-bored piles after installation
f_{sr}	Residual shaft resistance
k_0	Initial coefficient of permeability
k_{h}	Horizontal permeability coefficient.
p', q	Two stress parameters used in the Cam-clay model
p_0', p_f'	Mean effective stress at the in-situ and failure conditions,
p_{f}', q_{f}	Mean effective stress and the deviatoric stress at the critical state
p_c'	Isotropic preconsolidation pressure
q_b	Ultimate unit point resistance
q_s	Ultimate skin resistance per unit area of shaft
$s_{\mathrm{u,ps}}$	Undrained shear strength of the soil under plane strain condition
$s_{\mathrm{u,tc}}$	Undrained shear strength under triaxial compression
s_u	Original undrained shear strength
γ_{w}	Unit weight of pore water
δ'	Peak mobilized angle of friction acting parallel to the pile shaft
η_0	Initial stress ratio
λ_{k}	Slope of $e-\ln k$ curve,
λ_n	Eigenvalues of the Bessel function;
σ_{h0}'	In-situ horizontal stress
σ_{hf}'	Local effective radial stress at failure

Term	Description
σ'_{rp}	Radial effective stress at elastic-plastic boundary
σ'_r, σ'_θ, σ'_z	Radial, tangential and vertical effective stresses, respectively
σ'_{v0}	In-situ vertical effective stress
v_0	Initial value of the specific volume
v_{cs}	Specific volume at unit p' on the critical state line
φ'	Effective friction angle of the soil.
$\phi'_{\mathrm{triaxial}}$	Effective friction angle under triaxial condition
CIUC	Isotropically consolidated undrained triaxial compression
DFI	Deep Foundation Institute
DOTD	Louisiana Department of Transportation and Development
EOID	End of initial driving
E-P	Elastic-plastic
FEM	Finite element model
G	Shear modulus
IADC	International Association of Drilling Contractors
LADOTD	Louisiana Department of Transportation and Development
LSSRB	Louisiana Standard Specifications for Roads and Bridges
LTRC	Louisiana Department of Transportation and Development Center
LTRC	Louisiana Transportation Research Center
M	Slope of the critical state line
MPC	Multi-point constraints
OCR	Conventional definition of overconsolidation ratio
PDCA	Pile Driving Contractors Association
TRB	Transportation Research Board
TRIS	Transportation Research Information Services
α	Shaft resistance factor in terms of total stress method
β	Shaft resistance factor in terms of effective stress method
L	Pile length
R	Overconsolidation ratio in Cam Clay model
e	Void ratio

Term	Description
k	Coefficient of permeability
v	Poisson's ratio
Δu	Excess pore water pressure
Λ	Plastic volumetric strain ratio
δu_v, δu_{r}	Increments of vertical and horizontal displacements, respectively
θ	Apex angle of the pile tip
λ, κ	Slopes of the virgin consolidation line and swelling line, respectively
ω	Angle of pile taper from vertical

References

[1] Chen, S. L., and Abousleiman, Y. N. (2012). Exact undrained elasto-plastic solution for cylindrical cavity expansion in modified Cam Clay soil. *Géotechnique* 62(5), 447–456.

[2] Ghose-Hajra, M., and Tavera, E. (2016). Testing protocol for predicting driven pile behavior within pre-bored soil. Louisiana Transportation Research Center Final Report, No. 546.

[3] LADOTD (2016). *Standard Specifications for Roads and Bridges*. 2016 edition.

[4] Randolph, M. F., and Wroth, C. P. (1979). An analytical solution for the consolidation around a driven pile. *International Journal for Numerical and Analytical Methods in Geomechanics*, 3, 217–229.

[5] Randolph, M. F., Carter, J. P., and Wroth, C. P. (1979). Driven piles in clay-the effects of installation and subsequent consolidation. *Géotechnique* 29(4), 361–393.

[6] Skov, R., and Denver, H. (1988). "Time dependence of bearing capacity of piles." Proceedings of 3rd International Conference. Application of Stress-Wave Theory to Piles, B. H. Fellenius, ed., BiTech, Ottawa, 879–888.

[7] Potts, D. M., and Martins, J. P. (1982). The shaft resistance of axially loaded piles in clay. *Géotechnique* 32(4), 369–386.

[8] Konrad, J. M., and Roy, M. (1987). Bearing capacity of friction piles in marine clay. *Géotechnique*, 37(2), 163–175.

[9] Ng, K. W., Roling, M., AbdelSalam, S. S., Suleiman, M. T., and Sritharan, S. (2012a). Pile setup in cohesive soil. I: experimental investigation. *Journal of Geotechnical and Geoenvironmental Engineering*, 139(2), 199–209.

[10] Ng, K. W., Suleiman, M. T., and Sritharan, S. (2012b). Pile setup in cohesive soil. II: analytical quantifications and design recommendations. *Journal of Geotechnical and Geoenvironmental Engineering*, 139(2), 210–222.

[11] Basu, P., Prezzi, M., and Salgado, R. (2014). Modeling of installation and quantification of shaft resistance of drilled-displacement piles in sand. *International Journal of Geomechanics* 14(2), 214–229.

[12] Abufarsakh, M., Rosti, F., Souri, A., and Ahmad, S. (2015). Evaluating pile installation and subsequent thixotropic and consolidation effects on setup by numerical simulation for full-scale pile load tests. *Canadian Geotechnical Journal*, 52(11), 1734–1746.

[13] Haque, M. N., Abu-Farsakh, M. Y., Tsai, C., and Zhang, Z. (2016). Load-Testing Program to Evaluate Pile-Setup Behavior for Individual Soil Layers and Correlation of Setup with Soil Properties. *Journal of Geotechnical and Geoenvironmental Engineering*, 143(4), 04016109.

[14] McClelland, B., Focht Jr, J. A., and Emrich, W. J. (1969). Problems in the design and installation of offshore piles. *Journal of Soil Mechanics and Foundations Div*, 95 (6913 Proceeding).

[15] Poulos, H. G., and Davis, E. H. (1980). Pile foundation analysis and design, John Wiley, New York.

[16] Randolph, M. F., and Gourvenec, S. (2011). Offshore Geotechnical Engineering. Spon Press.

[17] Meyerhof, G. G. (1976). Bearing capacity and settlement of pile foundations. *Journal of Geotechnical Engineering Division*, ASCE 102(3), 195–228.

[18] FHWA (2016). Design and construction of driven pile foundations - Volume 1. Publication No. FHWA-16-009.

[19] Tomlinson, M. J. (1985). Foundation design and construction, Longman Scientific and Technical, Essex, England.

[20] Mascarucci, Y., Miliziano, S., and Mandolini, A. (2014). A numerical approach to estimate shaft friction of bored piles in sands. *Acta Geotechnica* 9, 547–560.

[21] Louisiana Transportation Research Center (2017). Analysis of driven pile capacity within pre-bored soil. Request for Proposals, LTRC No. 18-1GT, SIO No. DOTLT1000208.

[22] Rojas, E. (1993). Static behavior of model friction piles. *Ground Engineering*, May, 26–30.

[23] Lehane, B. M. (1992). Experimental Investigations of pile behaviour using instrumented field piles. PhD Thesis, Imperial College London.

[24] Orrje, O., and Broms, B. (1967). Effects of Pile driving on soil properties. *Journal of the Soil Mechanics and Foundations Division* 93(5), 59–74.

[25] Hageryt, D. J., and Peck, R. B. (1971). Heave and lateral movements due to pile driving. *Journal of the Soil Mechanics and Foundations Division* 97(SM11), 1513–1532.

[26] Azzouz, A. S., and Morrison, M. J. (1988). Field measurements on model pile in two model pile in two clay deposits. *Journal of Geotechnical Engineering* 114(1), 104–121.

[27] Roy, M., Blanchet, R., Tavenas, F., and Rochelle, P. L. (1981). Behaviour of a sensitive clay during pile driving. *Canadian Geotechnical Journal*, 18(1), 67–85.

[28] Fellenius, B. H., Riker, R. E., and O'Brien, A. J. O. (1989). Dynamic and static testing in soil exhibiting setup. *Journal of Geotechnical Engineering* 115(7), 984–1001.

[29] Bond, A. J., and Jardine, R. J. (1991). Effects of installing displacement piles in a high OCR clay. *Géotechnique* 41(3), 341–363.

[30] York, D. L., Brusey, W. G., and Clemente, F. M. (1994). Set-up and relaxation in glacial sand. *Journal of Geotechnical Engineering*, 120(9), 1498–1513.

[31] Long, J. H., Kerrigan, J. A., and Wysockey, M. H. (1999). Measured time effects for axial capacity of driven piling. *Transportation Research Record* 1663(1), 8–15.

[32] Liu, J., Zhang, Z., and Yu, F., et al. (2012). Case history of installing instrumented jacked open ended piles. *Journal of Geotechnical Geoenvironmental and Engineering*, 138(7), 810–820.

[33] Zhang, L., and Wang, H. (2015). Field study of construction effects in jacked and driven steel H-piles. *Géotechnique*, 59(1), 63–69.

[34] Housel, W. S, and Burkey, J. R. (1948). Investigation to determine the driving characteristics of piles in soft clay. In: Proceeding of the 2nd international conference on soil mechanics and foundations in engineering, Rotterdam, The Netherlands, Vol 5, pp. 146–154.

[35] Cummings, A. S., Kerkhoff, G. O., and Peck, R. B. (1950). Effect of Driving Piles in Soft Clay. *Transactions of the American Society of Civil Engineers*, 115(1), 275–285.

[36] Bozozuk, M., Fellenius, B. H., and Samson, L. (1978). Soil disturbance from pile driving in sensitive clay. *Canadian Geotechnical Journal* 15(3), 346–361.

[37] Coop, M. R., and Wroth, C. P. (1989). Field studies of an instrumented model pile in clay. *Géotechnique*, 39(4): 679–696.

[38] Matsumoto, T., Michi, Y., and Hirano, T. (1995). Performance of axially loaded steel pipe piles driven in soft rock. *Journal of Geotechnical and Geoenvironmental Engineering* 121(4), 305–315.

[39] Hwang, J., Liang, N., and Chen, C. (2001). Ground response during pile driving. *Journal of Geotechnical and Geoenvironmental Engineering* 127(11), 939–949.

[40] Haque, M. N., Abufarsakh, M., and Tsai, C. (2016). Field investigation to evaluate the effects of pile installation sequence on pile setup behavior for instrumented test piles. *Geotechnical Testing Journal* 39(5), 769–785.

[41] Chandler, R. J., and Martins, J. P. (1982). An experimental study of skin friction around piles in clay. *Géotechnique* 32(4), 119–132.

[42] Al-Mhaidib, A. I. (2001). Loading rate effect of piles in clay from laboratory model tests. *Journal of King Saud University (Engineering Sciences)* 13(1), 39–55.

[43] Carniero, A., and Jardine, R. (2012). A model study of how pre-drilling affects displacements pile capacity in stiff clays. 7th International Conference on Offshore Site Investigations and Geotechnics. Publisher: Society for Underwater Technology, 473–480.

[44] Shong, L. S., Feng, H. S., and Chuan, V. B. (2013). Pile capacity reduction of Jack-In piles with empty prebored hole at meta-sedimentary formation in peninsular

Malaysia. International Symposium on Advances in Foundation Engineering. pp, 285–290.

[45] Tomlinson, M. J. (1957). The adhesion of piles driven in clay soils. Proceedings of the 4th International Conference on Soil Mechanics and Foundation Engineering, London.

[46] Skempton, A. W. (1959). Cast-in-situ bored piles in London clay. *Géotechnique*, 9(4), 153–173.

[47] Burland, J. B. (1973). Shaft friction of piles in clay-a simple fundamental approach. *Ground Engineering* 6(3), 30–42.

[48] O'Neill, M. W. (2001). Side resistance in piles and drilled shafts. *Journal of Geotechnical and Geoenvironmental Engineering* 127(1), 3–16.

[49] MDSC, Inc. (2016). Driven Piles – user manual.

[50] Nordlund, R. L. (1963). Bearing capacity of piles in cohesionless soils. *Journal of the Soil Mechanics and Foundations Division*, ASCE 89(SM3), 1–35.

[51] Vesic, A. S. (1972). Expansion of cavities in infinite soil mass. *Journal of the Soil Mechanics and Foundations Division*, 98(SM3), 265–290.

[52] Kirby, R. C., and Esrig, M. I. (1979). Further development of a general effective stress method for prediction of axial capacity for driven piles in clay. Proceedings of the conference on recent developments in the design and construction of piles, London, pp. 335–344.

[53] Baligh, M. M. (1985). Strain path method. *Journal of Geotechnical Engineering* 111(9), 1108–1136.

[54] Baligh, M. M. (1986). Undrained deep penetration: II. Pore Pressures. *Géotechnique 36*(4), 487–501.

[55] Carter, J. P, Booker, J. R., and Yeung, S. K. (1986). Cavity expansion in cohesive frictional soils. *Géotechnique* 36(3), 349–353.

[56] Yu, H. S., and Houlsby, G. T. (1991). Finite cavity expansion in dilatants soils: loading analysis. *Géotechnique*, 41(2), 173–183.

[57] Collins, I.F., and Stimpson, J. R. (1994). Similarity solutions for drained and undrained cavity expansion in soils, *Géotechnique* 44(1), 21–34.

[58] Cao, L. F., Teh, C. I., and Chang, M. F. (2001). Undrained cavity expansion in modified Cam clay I: theoretical analysis. *Géotechnique* 51(4), 323–334.

[59] Randolph, M. F. (2003). Science and empiricism in pile foundation design. *Géotechnique*, 53(10), 847–875.

[60] Soderberg, L. O. (1962). Consolidation theory applied to foundation pile time effects. *Géotechnique*, 12(3), 217–25.

[61] Heydinger, A. G., and O'Neill, M. W. (1986). Analysis of axial pile-soil interaction in clay. *International Journal for Numerical and Analytical Methods in Geomechanics* 10(4), 367–381.

[62] Guo, W. D. (2000). Visco-elastic consolidation subsequent to pile installation. *Computers and Geotechnics*, 26(2), 113–144.

[63] Zheng, J. J., Lu, Y. E., Yin, J. H., and Guo, J. (2010). Radial consolidation with variable compressibility and permeability following pile installation. *Computers and Geotechnics*, 37(3), 408–412.

[64] Gong, W. B., Li, J. P., and Li, L. (2017). Evolution of mechanical properties of soils subsequent to a pile jacked in natural saturated clays. *Ocean Engineering* 136, 209–217.

[65] Wang, J., Verma, N., and Steward, E. (2009). Estimating setup of driven piles into Louisiana clayey soils. FHWA/LA.09/463, LTRC Project No. 04-1GT, State Project No. 736-99-1359.

[66] Potts, D. M. (2002). Numerical analysis: a virtual dream or practical reality? *Géotechnique* 52(6), 535–573.

[67] Mabsout, M., and Sadek, S. (2003). A study of the effect of driving on pre-bored piles. *International Journal for Numerical and Analytical Methods in Geomechanics* 27(2), 133–146.

[68] Dijkstra, J., Broere, W., and Heeres, O. M. (2011). Numerical simulation of pile installation. *Computers and Geotechnics* 38(5), 612–622.

[69] Qiu, G., and Grabe, J. (2012). Numerical investigation of bearing capacity due to spudcan penetration in sand overlying clay. *Canadian Geotechnical Journal*, 49(12), 1393–1407.

[70] Fakharian, K., Attar, I. H., and Haddad, H. (2013). Contributing factors on setup and the effects on pile design parameter. In Proceedings of the 18th International Conference on Soil Mechanics and Geotechnical Engineering, Paris.

[71] Basu, P., Prezzi, M., Salgado, R., and Chakraborty, T. (2013). Shaft resistance and setup factors for piles jacked in clay. *Journal of Geotechnical and Geoenvironmental Engineering*, 140(3), 04013026.

[72] Carter, J. P., Randolph, M. F., and Wroth, C. P. (1979). Stress and pore pressure changes in clay during and after the expansion of a cylindrical cavity. *International Journal for Numerical and Analytical Methods in Geomechanics* 3, 305–322.

[73] Yu, H. S. (2000). Cavity expansion methods in geomechancis. Dordrecht: Kluwer Academic Publishers.

[74] Abu-Farsakh, M., Haque, N., and Chen, Q. M. (2016). Field instrumentation and testing to study set-up phenomenon of piles driven into Louisiana clayey soils. FHWA/LA.15/562, LTRC No. 11-2GT, State Project No. 736-99-1732.

[75] Mabsout, M., Reese, L. C., Tassoulas, J. L. (1995). Study of pile driving by finite element method. *Journal of Geotechnical Engineering* 121(7), 535–543.

[76] ABAQUS (2017). ABAQUS user's manual. Hibbitt, Karlsson and Sorensen, Inc.

[77] Lin, H., and Penumadu, D. (2006). Strain localization in combined axialtorsional testing on Kaolin clay. *Journal of Engineering Mechanics*, 10.1061/(ASCE) 0733-9399(2006)132:5(555), 555–564.

[78] Cooke, R. W., Price, G., and Tarr, K. (1980). Jacked piles in London clay: interaction and group behaviour under working conditions. *Géotechnique* 30(2), 97–136.

[79] Roscoe, K. H., and Burland, J. B. (1968). On the generalized stress-strain behaviour of 'wet' clay. Engineering Plasticity, Cambridge University Press.

[80] Muir Wood, D. (1990). Soil behaviour and critical state soil mechanics. Cambridge, UK: Cambridge University Press.

[81] Haque, M. N., Abu-Farsakh, M. Y., Chen, Q., and Zhang, Z. (2014). Case study on instrumenting and testing full-scale test piles for evaluating setup phenomenon. *Transportation Research Record*, 2462(1), 37-47.

[82] ASTM International. (2013). Standard test method for deep foundations under static axial compressive load. ASTM International.

[83] Randolph, M. F., and Wroth, C. P. (1981). Application of the failure state in undrained simple shear to the shaft capacity of driven piles. *Géotechnique*, 31(1), 143–157.

[84] McClelland, B. (1974). Design of deep penetration piles for ocean structures. *Journal of Geotechnical and Geoenvironmental Engineering*, 100, 709–747.

[85] Collins, I. F., Pender, M. J., and Wang, Y. (1992). Cavity expansion in sands under drained loading conditions. *International Journal for Numerical and Analytical Methods in Geomechanics* 16, 3–23.

This public document is published at a total cost of $250
42 copies of this public document were published in this first printing at a cost of $250. The total cost of all printings of this document including reprints is $250. This document was published by Louisiana Transportation Research Center to report and publish research findings as required in R.S. 48:105. This material was duplicated in accordance with standards for printing by state agencies established pursuant to R.S. 43:31. Printing of this material was purchased in accordance with the provisions of Title 43 of the Louisiana Revised Statutes.